Modeling 2010 in Massachusetts Bay using the unstructured grid Bays Eutrophication Model

Massachusetts Water Resources Authority
Environmental Quality Department
Report 2011-09

Citation:

Zhao LZ ,Tian RC, Xue P, Chen C, , Leo WS, Mickelson MJ. 2011. **Modeling 2010 in Massachusetts Bay using the unstructured-grid Bays Eutrophication Model**. Boston: Massachusetts Water Resources Authority. Report 2011-09. 118p.

Key word acronyms and definitions

ECOM-si	Estuarine and Coastal Ocean Model-semi-implicit. A structured-grid hydrodynamic model.
FVCOM	Finite-Volume Coastal Ocean Model: An unstructured-grid hydrodynamic model.
GoM/GB FVCOM	FVCOM applied to the Gulf of Maine/Georges Bank.
RCA	Row Column Advanced (RCA) ecological systems operating program: a water quality model.
UG-RCA	Unstructured-grid version of RCA.
MB	Massachusetts Bay.
BEM	Massachusetts Bays Eutrophication Model: a coupled water quality and hydrodynamics model system.
BH	Boston Harbor
WRF	Weather Research and Forecast Model

Modeling 2010 in Massachusetts Bay using the unstructured-grid Bays Eutrophication Model

Submitted to

Massachusetts Water Resources Authority
Environmental Quality Department
100 First Avenue
Charlestown Navy Yard
Boston, MA 02129
(617) 242-6000

Prepared by
Liuzhi Zhao, Rucheng Tian, Pengfei Xue and Changsheng Chen
School for Marine Science and Technology
University of Massachusetts-Dartmouth
New Bedford, MA 02744

And

Wendy S. Leo and Michael J. Mickelson
Environmental Quality Department
Massachusetts Water Resources Authority
Boston, MA 02129

December 2011

EXECUTIVE SUMMARY

The Massachusetts Water Resources Authority (MWRA) contracted the Marine Ecosystem Dynamics Modeling (MEDM) laboratory of University of Massachusetts at Dartmouth (UMASSD) to simulate currents, temperature, salinity, dissolved oxygen, and other water quality parameters in Massachusetts Bay for the calendar year 2010 using the unstructured-grid water quality model (UG-RCA). This report presents the simulation, validation, and interpretation for the hydrodynamic model and the water quality model. Projection of the impact of the MWRA effluent on water quality parameters such as algal development and dissolved oxygen level is presented as well.

We first conducted a hydrodynamic simulation using the Finite-Volume Coastal Ocean Model (FVCOM) which was then used to drive the UG-RCA water quality simulation. The simulation was conducted in a nesting mode within a regional domain covering the entire Gulf of Maine and Georges Bank and a local domain for Massachusetts Bay (MB). Surface forcing including solar radiation, heat flux and wind was simulated using the Weather Research and Forecast model (WRF). For the regional model, 33 rivers were included of which 13 were located in the local domain. Five major tidal constituents were included at the open boundary of the regional domain; the local model was forced by the output of the regional model at the boundary. Data assimilation was conducted with the data from the MWRA monitoring program and all other available data in the region. The model successfully reproduced field observations in terms of temperature and salinity.

The water quality simulation using UG-RCA reproduced most of the observed magnitudes and seasonal cycles of water quality variables. The 2010 chlorophyll simulation did not show a dominant spring phytoplankton bloom such as has been observed in most years. Instead, multiple peaks of chlorophyll concentration were simulated from spring through fall, with limited amplitudes and durations, particularly at the near-field stations. The cause of this unusual seasonal pattern is not understood, but nutrients might be a limiting factor in spring in the 2010 simulation. Relatively low nutrient concentration was observed at the open boundary area, particularly in the deep layers; inflow from the open boundary constitutes an essential nutrient source for MB. Dissolved oxygen (DO) concentration reached an annual peak during the spring as a result of

photosynthetic production, but remained at a lower level in fall. DO dynamics are controlled by multiple factors including high consumption by increased remineralization and low solubility under the high temperatures characteristic of late summer and early fall. Horizontal advection and characteristics of the open boundary inflow can also influence the local DO level.

Based on our projection analysis removing the MWRA outfall from the simulation, the outfall plume was mostly restricted to a local area about 20 km wide. However, consistent with other studies, long-distance dispersal of nutrients at very low levels as far as Cape Cod Bay was predicted under certain circumstances in January and December 2010. Except very close to the outfall, the nutrients from the effluent discharge are a small percentage of the natural background levels. In the vertical dimension, the plume was basically constrained within the bottom 10 m during the stratified season in summer and early fall. In winter and late fall when stratification is weak, the outfall effluent plume can reach to the surface layer, as predicted by earlier models and as observed in field monitoring. However, no substantial bay-wide influence was observed on chlorophyll or DO levels. As the plume surfacing and long-distance dispersal occurred during winter when light intensity limits phytoplankton growth, effluent nutrients were not effectively taken up and translated into phytoplankton biomass and subsequent biogeochemical cycles during that period of time.

Table of Contents

List of Figures

List of Tables

1. Introduction

1.1 *Project overview*

The Massachusetts Water Resources Authority (MWRA) has established a long-term monitoring program to evaluate the impact of MWRA sewage treatment plant effluent on the ecosystem function and water quality in the Massachusetts Bay system (MBS) including Boston Harbor (BH), Massachusetts Bay (MB) and Cape Cod Bay (CCB). The monitoring program primarily consists of an array of field observations, but is complemented by water quality modeling as required by the MWRA permit for effluent discharge into MB. Up to 2007, the water quality model RCA (Row-Column Advanced Ecological Systems Operating Program) developed by HydroQual was applied to MBS by HydroQual (1994-1999), University of Massachusetts Boston (2000-2005) and University of Massachusetts Dartmouth (2006-2007) (HydroQual, 2000; HydroQual, 2003; Jiang and Zhou, 2004a, b, 2006a, b, 2008; Tian et al. 2009). RCA was driven by the structured-grid hydrodynamic model ECOM-si (HydroQual and Signell, 2001). For the 2008 water quality simulation, we upgraded RCA to the unstructured-grid UG-RCA driven by the Finite-Volume Coastal Ocean Model FVCOM (Chen et al., 2010). Two major updates were included in this upgrade. First, the newly developed RCA version 3 was adapted to MBS whereas an older version was used prior to the 2008 simulations. RCA-v3 is a modular system which has more options and greater flexibility than the previously used version. Secondly, the unstructured-grid finite-volume algorithms well-suited to resolve the complex coastline and bottom topography in MBS were adapted from FVCOM. We tested the newly developed system for the case of 2006 and applied it for the 2008 simulation, which showed that UG-RCA can be successfully applied to MBS. We used this system for the 2009 and 2010 simulations. This report presents the details of data treatment, model setup, model-data comparison and interpretation of the simulated results. Following the 2009 simulation report (Tian et al., 2010), the figures in this report make use of new color scales suggested by MWRA.

1.2 *Physical background*

The MBS comprises the Boston Harbor in the west, Cape Cod Bay in the south and Massachusetts Bay in the central region (**Figure 1.1**). It is a semi-enclosed coastal embayment with a length of approximately 100 km and a width of 50 km. The water depth averages about 35 m, with the maximum depth of 90 m in Stellwagen Basin, shoaling to 20 m on Stellwagen Bank.

Stellwagen Bank, located on the east side of MB, limits deep-water exchange between MB and the Gulf of Maine (GoM). Deep water exchange occurs mainly through the North Passage off Cape Ann and the South Passage off Race Point.

The hydrodynamic circulation in MBS is subject to both local forcing such as wind and remote forcing by tides and intrusion of the Western Maine Coastal Current (WMCC) (Bigelow, 1927; Butman et al., 2002). The general circulation pattern within MBS is counterclockwise with inflow through the North Passage and outflow through the South Passage. The inflow is primarily determined by (a) the WMCC which bifurcates near Cape Ann with one branch flowing into MBS (Bigelow, 1927; Lynch et al., 1996) and (b) Gulf of Maine coastal freshwater discharges, particularly from the Merrimack River located north of the bay (Butman, 1976). Driven by buoyancy and the Coriolis force, a considerable portion the Merrimack River freshwater discharge often enters into Massachusetts Bay. Manohar-Maharaj (1973) estimated that in May, up to 90% of the freshwater found in Massachusetts Bay originated from the Merrimack River. However, the amount of fresh water intrusion into Mass Bay varies depending on the path of the WMCC and on the wind forcing. Local wind forcing can significantly alter the current pattern and velocity (Geyer et al., 1992; Butman et al., 2002; Jiang and Zhou, 2004a). Wind-induced upwelling and downwelling were observed and simulated in previous studies (e.g., Geyer et al., 1992; HydroQual and Signell, 2001; Jiang and Zhou, 2004a; Tian et al., 2009). However, the water column stratification is primarily controlled by seasonal variations in net surface heat flux and freshwater discharge. Water stratification starts in spring due to increased insolation and freshwater discharge, intensifies in summer due to surface heating, and erodes in fall due to surface cooling and increased wind stress, following which the water column becomes well mixed again in winter.

1.3 *Biological background*

Phytoplankton in the MBS generally shows seasonal cycles typical of temperate regions due to the seasonality in solar radiation, water column stratification and nutrient availability (Libby et al., 1999; Libby et al., 2000). During winter when the water column is well-mixed and solar radiation is weak, phytoplankton growth is restricted due to limited light exposure in most of the MBS. Phytoplankton usually bloom in spring following the establishment of water column stratification and increases in solar radiation. However, spatial differences and interannual variations in the timing of the phytoplankton spring bloom can occur due to local forcing and the physical

environment. For example, the spring phytoplankton bloom often develops earlier in CCB than in Stellwagen Basin due to CCB's shallow water depth. During the post-bloom season in summer, phytoplankton biomass is low in most of the MBS due to nutrient limitation, but local phytoplankton growth can still occur due to, for example, wind-driven upwelling activity and river discharge. The fall bloom in MBS usually occurs in late September and early October when increased wind stress and cooling at the sea surface erode the stratification, increasing vertical mixing and replenishing nutrients from the deeper layer to the euphotic zone. With further increases in vertical mixing and decreases in solar radiation, phytoplankton growth is limited again, leading to high nutrient concentrations and low phytoplankton abundance in winter.

The seasonal cycle of phytoplankton production is accompanied by succession in phytoplankton species. Diatoms dominate the spring phytoplankton bloom under nutrient-replete conditions, particularly with high silicate concentrations, although in recent years the haptophyte *Phaeocystis pouchetti* has become dominant in spring (Libby et al. 2009, 2010). On the other hand, phytoflagellate species prevail during the summer stratified season under nutrient-depleted conditions. With the replenishment of surface nutrients in fall, a phytoplankton assemblage of different sizes and species develops. Phytoplankton seasonal succession results in variations in biological parameter values and carbon: chlorophyll ratio. The seasonality in phytoplankton production and biomass is reflected in the secondary production level as variations in zooplankton abundance and species through bottom-up control (Turner, 1994; Libby et al., 2000).

Benthic biological and biogeochemical dynamics directly affect nutrient supply and oxygen demand and thus the water quality of MBS. BH, CCB and Stellwagen Basin are characterized by a soft sea floor with fine sediment and high organic matter content, whereas the coastal regions are mostly covered by coarse sediment and rocks (Kropp et al., 2001; Kropp et al., 2002; Maciolek et al., 2003). In regions of soft floor with fine sediments, sediment oxygen demand (SOD) is higher than that in the hard-floor region. In BH, for example, high values of SOD and nutrient flux have been observed. Outside of the harbor in MB and CCB, physical processes significantly affect benthic biogeochemical processes in these relatively well-oxygenated sediments (Maciolek et al., 2003; Tucker et al., 2002; Jiang and Zhou, 2008). Most of these biological and biogeochemical processes are parameterized in the BEM.

1.4 *Modeling updates*

The modeling project has played a valuable role in both scientific investigation and decision making for the MWRA outfall design and monitoring program. Before the relocation of the outfall from Boston Harbor to its new offshore position in September 2000, Signell et al. (2000) conducted a series of simulations to analyze the impact of the relocation. They found that the effluent concentration decreased by ten-fold in the harbor, while only slightly elevated effluent concentration was predicted only within several kilometers around the offshore outfall, due to dilution and dispersal in the larger water body. During the summer stratified season, the effluent was more highly concentrated around the outfall as compared to the winter season when dispersal and dilution dominated. Previous modeling work also showed that the outfall effluent discharge did not have considerable bay-wide effect on the function of the bay ecosystem (Jiang and Zhou, 2006b and 2008; Tian et al., 2009).

The reliability of model predictions depends on the correctness of the parameterization and the robustness of the simulation. Over the years, efforts have been continuously made to improve the modeling system. For example, HydroQual and Signell (2001) found that the parameterization of short-wave radiation in the water column is of primary importance to the simulation of temperature variation and distribution. Shortwave radiation energy was initially introduced to the first sigma layer in the physical ECOM-si model, which led to an overheating in surface waters. An exponential decay function with depth was then implemented in the model which considerably improved temperature predictions. Chen et al. (2009) and Tian et al. (2009) found that wind forcing plays a key role in both physical and biological simulations. A spatially-resolved wind field improved model-data comparison and increased DO level in the bottom layer by 9-18% for the case of 2007 as compared with runs driven by uniform wind forcing. The improvement is particularly notable during storm events and front passage. HydroQual (2001a) conducted a sensitivity analysis on the impact of boundary conditions on the simulation of water quality variables. They found that certain variables such as DO in the interior of the bay are correlated with values at the open boundary, particularly at the north-northeast region of Mass Bay. Certain variations in bottom DO were directly caused by the boundary conditions. To improve the open boundary condition, Jiang and Zhou (2004b) introduced the objective analysis (OA) method of interpolating boundary conditions based on field observations, which has been used up to the present (Jiang and Zhou, 2008; Tian et al., 2009; Chen et al., 2010 and the present study). HydroQual (2001b) found that the

Bays Eutrophication Model with two phytoplankton groups failed to reproduce observed fall chlorophyll levels in 1993. The addition of a third group notably improved the model prediction. The major characteristic of the third “fall” phytoplankton group is the lower carbon-to-chlorophyll ratio than that in the previous two groups, winter/spring and summer phytoplankton groups. As shown by HydroQual (2002), the chlorophyll simulation could be improved on an annual basis by altering parameter values, but seasonal deviation such as that observed in the fall of 1993 was better resolved by adding the additional fall phytoplankton group, compared to sensitivity runs using the two original phytoplankton groups.

Massachusetts Bay (MB) is a complex embayment. First, its varying coastline and bottom topography can induce complex hydrodynamic features such as mesoscale eddies, filaments and coastal jets (Jiang and Zhou, 2006a and b). Second, the Western Maine Coastal Current bifurcates at Cape Ann, with one branch intruding into MB, which represents an external forcing for both physical and biochemical dynamics. Third, wind forcing, combined with the coastline and bottom topography, can generate upwelling and downwelling. Fourth, river discharges further complicate hydrodynamics and nutrient loadings. All of these features are a challenge for the modeling community to get right in the modeling dynamics and setup. Improvements have been continuously made over the years as described above; one major step was the introduction of the Finite-Volume Coastal Ocean Model (FVCOM) and the development of the unstructured-grid water quality model driven by FVCOM (Chen et al., 2009 and 2010). FVCOM is one of the models most suitable to resolve complex coastline and bottom topography. The nesting setup of FVCOM can ensure mass conservation and continuity in physical forcing at the open boundary (Chen et al., 2010).

Prior to 2008 the water quality model used was RCA-v2 (Hydroqual, 2003, Chen et al. 2010). With the use of FVCOM for the hydrodynamic model, we upgraded the water quality model to an unstructured-grid water quality model UG-RCA, which is based on RCA-v3 (Hydroqual, 2004) As described in more detail in Chen et al. 2010 and Tian et al. 2010, UG-RCA has the same basic model structure and biological dynamics of RCA-v2, but has more model parameters, uses photosynthetically active radiance (PAR) to drive phytoplankton growth rather than total solar radiation, and does not require recalculating salinity as a check on transport – salinity and transport are derived directly from FVCOM.

2. Methods

This section consists of six subsections. The first briefly describes the Finite-Volume Coastal Ocean Model used to simulate the physical fields to drive the water quality model. Next we describe the structure and functionality of the unstructured-grid water quality model used for the 2010 simulation. The third section describes the unstructured triangular grids including the nesting domain and the vertical coordinate. The section on forcing describes both the meteorological forcing for FVCOM and surface forcing for UG-RCA. The fifth section, "Nutrient loadings," describes most of the nutrient and organic matter sources including the MWRA outfall. The final section describes how the open boundary condition of the UG-RCA state variables was determined, and describes the data set used for open boundary conditions.

2.1 *FVCOM*

The unstructured-grid, finite volume, 3D, free surface primitive equation Coastal Ocean Model (FVCOM) was developed originally by Chen et al. (2003). FVCOM is a message-passaging interface parallelized model updated by a team of scientists at the University of Massachusetts-Dartmouth (UMASSD) and Woods Hole Oceanographic Institution (WHOI) (Chen et al., 2006a, b). In the horizontal, FVCOM uses a non-overlapping unstructured triangular grid, which is particularly suitable for resolving the complex coastal geometry of Massachusetts Bay. In the vertical, FVCOM is discretized by layers using the generalized terrain-following hybrid coordinate (Pietrzak et al., 2002). This vertical coordinate system allows for vertical layers of uniform thickness near the surface and bottom over the slope with a smooth transition to topography-following layers in the inner shelf and estuaries, which is critical to resolving the wind-driven surface mixed layer and sloping bottom boundary layer. FVCOM is solved numerically by the flux calculation in an integral form of the governing equations with options of either mode-split (like the Princeton Ocean Model, or the Regional Ocean Modeling System developed at Rutgers) or semi-implicit (like ECOM-si) schemes. The mode-split option was used for the present study. The flux calculation ensures the conservation of mass and momentum over individual control volumes and thus the whole computational domain. The finite-volume numerical approach combines the advantage of finite-element methods for geometric flexibility and finite-difference methods for simple discrete code structure and computational efficiency.

FVCOM uses the modified MY-2.5 and Smagorinsky turbulent closure schemes for vertical and horizontal mixing, respectively (Mellor and Yamada, 1982; Smagorinsky, 1963). FVCOM provides optional vertical turbulence closure schemes using the General Ocean Turbulence Model (GOTM) developed by Burchard et al., 2002. The present version of FVCOM contains several new modules: non-hydrostatic dynamics (Lai et al., submitted); advanced data Kalman Filter data assimilation packages (Chen et al., 2009); an unstructured-grid surface wave model (FVCOM-SWAVE) (Qi et al., 2008), an unstructured-grid sea ice model (UG-CICE, Gao et al., submitted), a sediment model (FVCOM-SED) and generalized biological model (FVCOM-GEM). An automatic nesting grid system is also implemented in FVCOM, which allows two different FVCOM models to run through the nested boundary without the need of interpolation from one to another.

2.2 *UG-RCA*

UG-RCA adapts the biological dynamics and model structure of RCA, but integrates transport and eddy diffusivity using the finite volume algorithms employed in FVCOM. Briefly, it consists of 26 water quality state variables and 23 sediment variables, including various forms of organic carbon, nitrogen and phosphorus, inorganic nutrients, phytoplankton and dissolved oxygen (Figure 2.2). Dissolved oxygen (DO) is a primary state variable of environmental concern in the simulation system. In the model, DO is computed by the reaeration flux at the sea surface, sediment oxygen demand (SOD) at the bottom and internal biological and biogeochemical dynamics in the water column such as phytoplankton photosynthetic production, respiration consumption, biogeochemical oxygen demand through the mineralization of particulate and dissolved organic matter, and nitrification. Phytoplankton growth is sustained by solar radiation and dissolved inorganic nutrients including ammonium NH_4^+, nitrate NO_3^- and nitrite NO_2^-, phosphate PO_4^{3-} and dissolved silica SiO_3^{2-}. Nutrients are formed through the mineralization of organic substances in the water column and at the sediment-water interface. In the model, organic matter is divided into dissolved and particulate forms with each being further divided into refractory and labile categories. Zooplankton grazing is not explicitly modeled with trophodynamics, but represented by a first order, temperature-dependent rate of transformation of phytoplankton into particulate and dissolved organic matter. Phosphorus, nitrogen, and silicon were parameterized in a similar way as the organic carbon pools. The total number of state variables is 26: salinity, three phytoplankton groups (spring, summer and fall groups), four nutrients (ammonia, nitrate+nitrite, phosphate and dissolved

silica), four organic phosphorus forms, four organic nitrogen pools, seven organic carbon pools (four labile and refractory dissolved and particulate forms plus two reactive and one exudate components), biogenic silica, dissolved and aqueous oxygen.

UG-RCA has 180 parameters in total (Table 2.2). In the present model setup, however, 31 of the total 180 parameters are not used, so that there are effectively 149 parameters. Parameters 1-4 are the "option" parameters that control the model setup. Parameter #1 "AGMOPT" stands for "Algal Growth Model Option", by which users can select different phytoplankton growth functions: "0" to select the standard phytoplankton growth function, "1" to select the Laws-Chalup function. Parameter #2 "ACTALG" defines the number of "Active Algal Groups" effectively simulated in the model. It is assigned a value of 3 for winter-spring, summer and fall phytoplankton groups in Massachusetts Bay. Parameter #3 "KAOPT" defines the choice of reaeration parameterization: 0 for constant, 1 for spatially variable, 2 for current velocity shear dependent, and 3 for wind stress dependent. Parameter "KEOPT" defines the choice of light attenuation function: 0 for constant, 1 for spatially variable, 2 for temporally variable, 3 for 2D spatially and temporally variable, and 4 for 3D spatially and temporally variable. As PAR is used in UG-RCA whereas GoM-WRF predicts total solar radiation, parameter #5 "PAR" defines the PAR fraction or conversion factor from total solar radiation to PAR. Other parameters are defined in Table 2.2 which essentially control biological and biogeochemical rates in the model.

The sediment module in UG-RCA is essentially the same as the model developed by DiToro (2001). It is designed to capture the sinking flux of organic matter from the water column to sediments, sedimentary diagenesis transforming organic matter into inorganic nutrients, nutrient feedback from sediment to the water column, sediment oxygen demand during sedimentary diagenesis, and denitrification which converts nitrate into gaseous nitrogen (N_2) and thus leads to nitrogen loss from the system through outgassing to the atmosphere. For brevity, sediment module parameters are not listed in Table 2.2.

2.3 *Model grid*

FVCOM used for Massachusetts Bay is a sub-grid domain model (hereafter referred to as MB-FVCOM) nested within the Gulf of Maine regional domain model (hereafter referred to as

GoM-FVCOM). The computational domain of MB-FVCOM is configured with 9738 cells and 5472 nodes. The horizontal resolution of this sub-grid domain varies from 290 m near the coast to 5-10 km near the nested boundary (Figure 2.2, upper panel). GoM-FVCOM consists of 27421 cells and 14777 nodes, with the horizontal resolution varying from 10-25 km in the open ocean to 1.0 km near the coast (Figure 2.2, lower panel). GoM-FVCOM uses hybrid terrain-following coordinates with a total number of 30 layers in the vertical. In shallow regions with depth < 60 m, the vertical layers are defined using the σ-coordinate, while in regions with depth ≥ 60 m, the s-coordinate is used. These two coordinates merge on the 60-m isobath at which the water column is divided by uniform layers with a thickness of 2 m. In the σ-coordinate, the layer thickness varies with water depth, with a maximum of 2 m. In the s-coordinate, five uniform layers with a thickness of 2 m are specified in the upper and lower layers adjacent to the surface and bottom, respectively. The remaining mid-depth is divided into 20 layers with thickness varying with water depth. The same vertical coordinate system was used for MB-FVCOM. The GoM regional and Massachusetts Bay sub-domain grids share common triangular cells along the nesting boundary. The model output from GoM-FVCOM at the nested boundary can directly drive MB-FVCOM with no need for any spatial interpolation. This one-way nesting approach ensures volume and mass conservation between the two computational domains.

Both GoM-FVCOM and MB-FVCOM are solved using the mode-split integration scheme. The time step is 12 seconds for the external mode and 120 seconds for the internal mode for GoM-FVCOM, and 5 seconds for the external mode and 50 seconds for the internal mode for MB-FVCOM.

UG-RCA is configured on the same grid as MB-FVCOM, but with a smaller offshore extent (Figure 2.2). It is driven by the hourly MB-FVCOM fields of water temperature, salinity, velocity and turbulence mixing diffusivities. UG-RCA is coded with the flexibility to allow users to select a different time step from the hydrodynamic model. For the Massachusetts Bay modeling project, the time step used to drive UG-RCA is 50 seconds, with 72 time steps per hour.

2.4 *Forcing*

2.4.1 Physical models

Both GoM-FVCOM and MB-FVCOM are driven by surface forcing (wind stress, precipitation, evaporation, surface net heat flux, and short-wave irradiance), river discharges and tidal forcing. Please note that the tidal forcing for MB-FVCOM consists of the GoM-FVCOM prediction of surface elevation at the common boundary. Available hydrographic and satellite sea-surface temperature data were assimilated for both simulations.

The surface forcing data were provided by the data-assimilated fields of the WRF (Weather Research and Forecast) model. WRF is the new-generation mesoscale numerical weather prediction system developed principally by National Center for Atmospheric Research (NCAR) through collaboration with other government agencies (http://wrf-model.org/index.php). WRF uses the hydrostatic North American Mesoscale weather model fields as initial and boundary conditions with two-way nesting capability, and can provide continuous hindcasts and 3-day forecasts. WRF replaced the older MM5 in our GoM weather forecast model system (Chen et al., 2005). GoM-WRF is configured with a "regional" domain (covering the Scotian Shelf, Gulf of Maine, Georges Bank, and the New England Shelf) and a "local" domain (covering Massachusetts coastal waters west to Long Island Sound) with horizontal grid spacing of 9 and 3 km respectively, and 31 sigma levels in the vertical with finer resolution in the Planetary Boundary Layer. All available data from the National Data Buoy Center's Coastal-Marine Automated Network (C-MAN) and meteorological buoys are assimilated. The surface wind stress, air-sea heat flux components, and evaporative flux are computed using GoM-WRF output, with a horizontal resolution of 9 km, the COARE 2.6 bulk algorithm (Fairall et al., 1996, 2003), and satellite sea surface temperature. The surface radiative fluxes are computed using International Satellite Cloud Climatology Project (ISCCP) data. The resulting hindcast data-assimilated surface forcing fields are used to drive both the regional GoM-FVCOM and MB-FVCOM.

GoM-FVCOM includes 33 rivers emptying into the GoM region. Of those, 13 are inside the Massachusetts Bay sub-domain. Those, plus the MWRA outfall discharge, are included in MB-FVCOM. The freshwater discharge data from the rivers were directly downloaded from the US

Geological Survey (USGS) http://waterdata.usgs.gov/ma/nwis. No accurate discharge data are available for the Mystic River, and its discharge was assumed to be proportional to the Charles River discharge by a factor of 0.195. The daily freshwater flow from the MWRA outfall was provided by MWRA.

Tidal forcing used to drive GoM-FVCOM was specified at the open boundary with the real o'clock time. The tidal elevation at the open boundary is calculated based on amplitudes and phases of five major tidal constituents: three semi-diurnal tides (M_2, S_2 and N_2,) and two diurnal tides (K_1 and O_1). In addition to the surface forcing and river discharge, MB-FVCOM is driven by the lateral boundary conditions specified through one-way nesting with the GoM-FVCOM model output. The surface elevation at the nesting node at the boundary is directly given by the GoM-FVCOM.

Wind, heat flux, and Merrimack River discharges in 2010 are exemplified in Figure 2.3 and compared with those of the 16-year (1995-2010) average. Northwest wind prevailed in January and February in both 2010 and the 16-year average, but the wind direction was slightly different between them, with wind more toward the southwest in 2010 than in the 16-year average. North-northeast wind dominated in March 2010 whereas northwest dominated in the average, with wind speed in 2010 almost double that of the average. April was quiet in both years with wind speed < 1 m /s in average. Mostly south wind dominated from April through September. From October through December, north-northwest wind prevailed and in December, the wind speed reached the level observed in January. Surface heat flux was mostly comparable between the 2010 and 16-year average, with high values in summer and low values in winter and late fall. Nevertheless, surface heat flux was visibly higher in May and July in 2010 than in the average. River discharge was particularly high in March and early April 2010 with river flow more than triple that in 16-year average during the same period of time. A dry summer was observed in 2010, with low river discharge from late April through September. During fall from October through December, small, high-frequency discharge events (mostly biweekly) occurred in 2010.

In summary, the physical environment in 2010 is characterized by a wet winter and dry summer as compared to the previous year. Fresh water discharge in winter and early spring have the potential to lead to early stratification and thus change physical and biological dynamics in the

water column, such as the timing and amplitude of the spring phytoplankton bloom. If this freshening event is on a regional scale, changes in the physical and biological dynamics in the Gulf of Maine can affect MB ecosystem function through the open boundary forcing. The extremely dry weather in summer also has the potential to alter physical and biological dynamics in the water column.

2.4.2. UG-RCA surface forcing

UG-RCA is directly driven by the hourly model output field of MB-FVCOM. In addition to the initial and open boundary conditions, UG-RCA requires the surface wind speed and solar radiation as the surface forcing. The wind speed (w) is used to determine the reaeration rate for oxygen exchange at the air-sea interface, which is formulated as:

$$F_{O2} = k\left(DO_{sat} - DO\right) \tag{2.1}$$

$$k = 0.728\sqrt{w} - 0.317w + 0.0372w^2 \tag{2.2}$$

$$DO_{sat} = 14.6244 - 0.36713T + 0.0044972T^2 + 0.0966S + 0.00205S\cdot T + 0.0002739S^2 \tag{2.3}$$

where F_{O2} is the oxygen reaeration flux, DO_{sat} is the dissolved oxygen saturation concentration determined with an empirical function of temperature (T) and salinity (S) (Hyer et al., 1971; HydroQual, 1993), and k is the piston coefficient (also called the piston velocity) of the oxygen air-sea exchange, determined by an empirical function depending on the wind speed (Banks and Herrera, 1977).

The solar radiation is used to compute the phytoplankton growth rate based on the Laws-Chalup function:

$$\mu_{\mathbf{max}} = \frac{G_{pre}\left(1-k_{RG}\right)\left(1-f_{SC}\right)I}{G_{pre}\Big/G_{pr0} + I\left[1+G_{pre}\Big/\left(I_S G_{pr0}\right)\right]}, \tag{2.4}$$

where I is the photosynthetically active radiation PAR (einsteins m^{-2} d^{-1}) and I_s is the half-saturation radiation (Laws and Chalup, 1990). Other parameters are defined in Table 2.2.

Calibrated with satellite-derived shortwave irradiance and available measurement data at the coast, GoM-WRF provides the light intensity at surface required for UG-RCA. The GoM-WRF

predicted total short-wave radiation was then converted into PAR using a conversion factor of 0.437 determined based on decadal SeaWIFs PAR data and GoM-WRF predicted total solar radiation (Chen et al., 2010).

2.5 *Nutrient loadings*

Nutrient and carbon loadings include the MWRA effluent outfall from the Deer Island Treatment Plant (DITP), non-MWRA point sources, non-point sources, river discharge and atmospheric sources. Each source was specified based on recent observed data when available, combined with historical observations and estimates.

MWRA conducts daily measurements of treated sewage flow in millions of gallons per day and daily or weekly concentration of various pollutants in mg l^{-1}. The data for NO_3^-, NO_2^-, NH_4^+ and PO_4^{3-} were directly used to drive UG-RCA, while the bulk-parameter data of Carbonaceous Biochemical Oxygen Demand (CBOD), Total Kjeldahl Nitrogen (TKN) and Total Phosphorus (TP) were first converted and partitioned into model variables (Tables 2.3 and 2.4). For example, CBOD was converted into total organic carbon using the function TOC = 0.7CBOD+18 (HydroQual and Normandeau, 1993) and then partitioned to each organic matter pool using the functions listed in Table 2.3. TKN and TP were converted into total organic nitrogen and phosphorus and then partitioned into their respective organic pools. Silicate was not analyzed on a regular basis in the MWRA effluent. To help determine the silicate loading, MWRA collected four samples over the period of May 19-22, 2009. MWRA's Department of Laboratory Services reported an average value for these samples of 90 µM Si. This value was less than one quarter of the value (12.5 mg/L = 446.4 µM Si) suggested by HydroQual (1993; p.3-6) for all RCA simulations. We replaced the previous value used in RCA with the value estimated from the 2009 measurements.

Non-point source loadings comprise the storm drain system-derived runoff and groundwater discharge which are fully based on the most recent available estimates (Menzie-Cura, 1991; Alber and Chan, 1994). For runoff from combined sewer systems, updates were conducted using the total estimated combined sewer overflow (CSO) volume at the Mystic/Chelsea confluences, the upper Inner Harbor, the lower Inner Harbor, Fort Point Channel, North Dorchester Bay, South Dorchester Bay and the Neponset River estuary. Estimated annual outflow at these sites were provided by

MWRA. These data were divided into monthly values following the same monthly variation in freshwater discharge as the Charles River. The Charles River discharge is correlated with the precipitation in the region (Appendix A of Libby et al. 2009). The pollutant concentrations in combined sewage reported by Alber and Chan (1994, their table 2.4) were used to estimate the contaminant loadings for previous BEM simulations and also for the 2009 simulation with UG-RCA. The groundwater discharges and those from other non-MWRA treatment plants were specified using the same value estimated by Menzie-Cura (1991).

The river discharges included in the UG-RCA simulation were the Charles River, Neponset River and Mystic River. The Merrimack River was included in MB-FVCOM, but not in UG-RCA since it was located outside the UG-RCA sub-domain. The model accounts for entry of nutrients from the Merrimack River and other rivers to the north to the extent that they affect the measured open boundary conditions as described in section 2.6.The nutrient concentrations near the mouth of the Boston Harbor tributaries were measured by MWRA as part of its CSO receiving-water monitoring program; the nutrient loading from these rivers were estimated using their monthly averaged values. Measurements were made of inorganic nutrients, organic phosphorus, particulate organic nitrogen (PON) and dissolved organic nitrogen (DON). The river loadings were estimated by multiplying the river discharge rate with the nutrient concentration. The measured inorganic nutrients can be directly used, whereas the total organic phosphorus must be converted into model variables using the functions listed in Table 2.3. PON and DON measured in rivers were equally split into refractory and labile pools for RPON, LPON, RDON and LDON, respectively; because standard aquatic measurements of nutrients and carbon do not determine how much is refractory, labile, or very labile (reactive), the coefficients in Table 2.4 are used to partition the measured amounts into the model state variables (HydroQual and Normandeau, 1993.)

The atmospheric loadings were provided using the values estimated by Menzie-Cura (1991). These values were used in the previous BEM simulations (HydroQual and Normandeau, 1995; HydroQual, 2000; HydroQual, 2003; Jiang and Zhou, 2004a; Tian et al., 2009, 2010). The loadings included both dry-fall and wet-fall inorganic and organic nitrogen, phosphorus, and carbon.

For nitrogen, by far the major source to Massachusetts Bay is the boundary with the Gulf of Maine, as demonstrated by HydroQual (2000). Only sources within the model domain are considered in this section. For organic carbon loading, non-MWRA sewage treatment plants contributed the largest value in 2010 (31%), followed by the MWRA outfall (23%), atmospheric (17%), non-point sources (15%) and rivers (14%) (Figure 2.4). The carbon effluent discharge from the MWRA outfall was comparable to that of the previous years from 2006 to 2009. Only in 2007 was the carbon effluent discharge slightly lower than that in the other years. For nitrogen loading, the MWRA outfall represented the largest input (48%), followed by the atmospheric flux (28%), non-MWRA point sources (13%), non-point sources (7%) and river discharge (4%). The 2010 nitrogen effluent discharge from the MWRA outfall was mostly comparable with the rest of the other years. For phosphorus loading, the MWRA outfall again contributed the largest portion (49%), followed by the non-MWRA point sources (28%), non-point sources (15%), river discharge (5%) and atmospheric flux (3%). In contrast to nitrogen effluent, the phosphorous discharge from the MWRA outfall decreased by 15% as compared to the average load from 2006 to 2009.

2.6 *Open boundary conditions for UG-RCA*

The UG-RCA simulation requires the open boundary conditions of water quality state variables. Following the previous BEM simulation approach, bi-weekly open boundary conditions were specified by using the objective analysis (OA) procedure to interpolate the MWRA field data onto the boundary nodes. The field measurements were made approximately monthly at 7 stations near the MWRA outfall (called "near-field" stations indicated by "N") and bimonthly at 24 far-field stations indicated by "F" (Figure 2.5). Three additional cruises were conducted for the *Alexandrium* red tide monitoring program on April 26, May 4 and 21 (noted as AF stations in Figure 2.5).

The data included 14 variables: Chlorophyll, DO, NH_4^+, NO_3^-, PO_4^{3-}, SiO_3^{2-}, DON, DOC, DOP, PON, POC, POP, Biogenic silica and salinity. DON was estimated by the difference between the total dissolved nitrogen (TDN) and total dissolved inorganic nitrogen (NO_3^-, NO_2^-, NH_4^+). DOP was estimated by the difference between total dissolved phosphorus (TDP) and dissolved phosphate (PO_4^{3+}). Particulate phosphorus (PARTP) was used as POP. DON and PON were split equally into labile and refractory pools. The partition coefficients for organic carbon and phosphorus are listed in Table 2.4. It should be pointed out that nutrient concentration in the deep layer during the winter

season was relatively lower in 2010 than that observed in the previous years at the stations F26 and F27 (Figure 2.6). At Station F26, for example, nitrate concentration in the deep layer during winter ranged around 11-12 μM in 2008 and 2009 whereas it was only ca. 7 μM in 2010. At Station F27, nitrate concentration ranged from 11 to 13 μM in the deep layer in winter 2008 and 2009, but only 7-9 μM in 2010. These two stations are close to the open boundary in the North Passage and thus have the potential to influence the open boundary condition determined through data OA mapping.

The OA-mapped chlorophyll field at the open boundary was partitioned to the three phytoplankton groups using the partition coefficients listed in Table 2.5. The fraction of the phytoplankton community represented by each group changes over time along the open boundary, and over time and space in the interior. The coefficients in Table 2.5 are the partitions imposed at the open boundary during each season of the year. From January to April, the chlorophyll along the boundary was considered as entirely comprised of the winter-spring phytoplankton group with a zero partition coefficient for the other two phytoplankton groups. May was considered as a transition period with boundary chlorophyll being equally split into winter-spring and summer phytoplankton groups. In June and July, the boundary chlorophyll belonged to the summer phytoplankton group. August was another transitional period with boundary chlorophyll being split into the summer and fall phytoplankton groups. Chlorophyll on the boundary consisted of only fall phytoplankton in September and October and was split into winter-spring and fall phytoplankton groups in December. The carbon to chlorophyll ratios of phytoplankton were 40, 65 and 15 for winter-spring, summer and fall phytoplankton, respectively (HydroQual, 2000; HydroQual, 2003; Jiang and Zhou, 2004a; Tian et al., 2009).

The OA analysis was done using the OA software called OAX. This software was developed by Bedford Institute of Oceanography (Hendry and He, 1996). We used this method in the 2006-2009 BEM simulations (Tian et al., 2009, Chen et al., 2010, Tian et al., 2010). In the OAX, the covariance function (R) between data and estimation site is based on their pseudo-distance (r) determined as:

$$R(r) = (1 + r + \frac{r^3}{3})e^{-r} \tag{2.5}$$

$$r = \sqrt{\left(\frac{x_d - x_m}{a}\right)^2 + \left(\frac{y_d - y_m}{b}\right)^2 + \left(\frac{z_d - z_m}{c}\right)^2 + \left(\frac{t_d - t_m}{T}\right)^2} \quad (2.6)$$

where x, y, z, and t are the four spatial and temporal coordinates; the subscripts d and m indicate data and model positions, respectively; and parameters a, b, c, and T are the de-correlation scales for their corresponding coordinate. Given the fact that the measurement sites were away from the open boundary and measurements were made on a monthly or bi-monthly basis, the OA analysis was done with relatively large de-correlation scales: 30 km in the horizontal, 15 m in the vertical and 45 days in time.

Examples of the OA-mapping results on the open boundary for April 15 and August 15 are presented in Figure 2.7. Given the low frequency of field observations and the large distance between the open boundary and the observation sites, particularly for the Southern Passage, the OA-mapped results should be interpreted with caution. Briefly, chlorophyll concentration was higher in April than in August and a slight subsurface chlorophyll maximum was observed on the April transect. Nutrients showed high concentrations in the deeper channel and low values in the surface layer, but ammonium showed higher values in mid-depth on the April transect. Ammonium was very low in August so that no variation was visible on the August transect. Similar to chlorophyll, DO concentration was higher in April than in August. In general, particulate organic substances were more abundant in surface layers than in deeper layers and slightly higher in the South Passage than in the North Passage. Dissolved organic substances displayed a similar distribution pattern to particular organic matter at the open boundary, higher in the surface layers and low in the bottom layers with a north-south gradient.

As observed nutrient concentration during the winter season was considerably lower in 2010 than that observed in the previous years, particularly in the deep layers close to the open boundary, the open boundary condition determined based on these data resulted in lower nutrient concentration as well. As an example, nitrate concentration at the open boundary determined through OA mapping was illustrated in Figure 2.8 for the years 2010 and 2009 as a comparison. On the boundary transect of Jan. 30, nitrate concentration mostly varied around 7-9 μM in the deep portion of the North Passage, whereas it ranged from 9 to 11 μM in 2009. Similar pattern and difference were observed on the March 1 transect, with nitrate concentration varying between 7 and

8 µM in 2010 whereas from 10 to 12 µM in 2009. As the North Passage is the major pathway for Gulf of Maine water flowing into MB, the low nutrient concentration at the open boundary can affect nutrient supply to MB in winter and thus have the potential to influence phytoplankton development during the spring bloom season through nutrient limitation.

3. Results

3.1 *Physical Fields*

3.1.1 Model-data comparisons

The BEM is designed to assess the water quality of Massachusetts Bay (MB). Since this system is highly controlled by the physical environment, available data were assimilated into the physical model MB-FVCOM to provide the best known physical fields for the water quality model. These data included the satellite-derived sea-surface temperature (SST) and all available hydrographic data. The model-data comparisons described here demonstrate how well MB-FVCOM, with these assimilated data, provides realistic physical fields.

Figures 3.1 and 3.2 show the comparison between model-predicted and observed temperature and salinity at selected MWRA monitoring stations F26, F27, F29, F31, N01 and N10. Stations F26 and 27 are located in the northern part of the study area close to the UG-RCA open boundary. Station F29 is located in the southern part of the study area close to the open boundary. Stations N01 and N10 are located in the central MB and F31 is within Boston Harbor. Assimilation of SST and hydrographic data made the model-predicted temperature and salinity match the observations well, but in several cases, data assimilation caused rapid adjustments in the simulated results.

Near the open boundary area (Stations F26, F27 and F29) and in central MB (N01 and N10), the water column was stratified from spring to early fall, with large temperature and salinity differences between the surface and bottom. At the harbor station F31, however, the water column was fully mixed through the entire year. High-frequency (weekly) fluctuations in temperature were observed at the selected stations.

Salinity displayed larger fluctuations near the surface than near the bottom. The variation was particularly high at Stations F26 and F27, signaling the impact of the freshwater discharge from the Merrimack River just north of MB.

Figure 3.3 shows the comparison between modeled surface temperature, salinity and currents, and data collected at Buoy 44013 near station N07 and about 8.5 km southeast of the outfall. Surface temperature compares well between the data and simulation. Salinity data at the buoy are available only from June 1, 2010. A drop in surface salinity was observed in early June at the beginning of the data set, which was not reproduced by the model. The model predicted salinity compared relatively well with data thereafter. The buoy data showed weak current, mostly smaller than 10 cm s^{-1}. Given the limited data set, it is not conclusive to assess the overall robustness of the simulation in the whole simulation domain. As shown later, mesocale eddies are dominant current features in MBS. The timing and location of these eddies can cause deterioration in the model-data comparison at a fixed point.

Figures 3.4-3.8 compare the near-surface distributions of temperature and salinity. Note that the plots of observed data gathered all the observations for the month. The plot for February includes the early February and the later February survey. Observations in the other months span at least three days, the shortest time it takes to complete a survey. The model plots gathered model results for the same time as each observed data point. After the observed data and modeled results were gathered for the month, they were contoured. The assimilation worked well to reproduce observed fields of temperature and salinity. In February, there was a mostly homogeneous distribution of both temperature and salinity (Figure 3.4). Only a slight inshore-offshore gradient was observed, but within a range of 1 °C and 1 psu, respectively. In April, temperature mostly showed a homogeneous distribution, whereas salinity displayed an inshore-offshore gradient in both the observed and modeled fields (Figure 3.5). In June, the temperature showed an offshore-inshore gradient with low temperature in the offshore region and high temperature in the inshore region (Figure 3.6). In contrast, salinity displayed an opposite gradient, with high values in the offshore region and low values in the inshore region and Boston Harbor (Figure 3.6). Temperature was considerably higher in June (ranging from 14 to 16 °C) than in April (4-6 °C). In August, the surface temperature reached 20 °C, but with little spatial distribution pattern (Figure 3.7). Although the surface temperature was slightly higher in the southern end of the domain than in the southern part of the bay, the difference remained < 0.5 °C. The difference between the model prediction and observation was also smaller than 0.5 °C. Salinity, on the other hand, displayed a notable inshore-offshore gradient, with particularly low values in the northwestern part of the simulation domain

and high values in the offshore region. In October, the surface temperature decreased to below 13 °C, but no notable spatial distribution pattern is discernable with the color scales used for mapping (Figure 3.8).

3.1.2 Monthly surface sub-tidal currents, temperature and salinity

The surface monthly sub-tidal current field from January through April was characterized by four major features (Figure 3.9):

(1) Offshore coastal current flowing south-southeastward from the Western Gulf of Maine Coast toward Cape Cod. This current was strong in January and weakened gradually through April;

(2) Current bifurcation at the North Passage entrance, with one branch flowing south-southeastward and the other entering MB. The bifurcation was the most evident in March among the four months depicted in Figure 3.9 and weakest in April;

(3) General counter-clockwise circulation in MB with inflow through North Passage and outflow in Southern Passage. This counterclockwise circulation was also the strongest in March and weakest in April, similar to the offshore coastal current;

(4) Mesoscale eddies that change in space and time.

Eddies were barely discernible in January and February, well-developed in March and weaker again in April. The surface current pattern in May persisted into June, with a combination of a baywide counterclockwise circulation pattern and smaller-scale eddies. In July and August, however, the current pattern was essentially dominated by eddies rather than a baywidecirculation pattern (Figure 3.10). Four eddies were identified in July: one in the offshore region, one in the North Passage, another in the northwestern corner of the simulation domain and the other one in Cape Cod Bay to the southern end of the simulation domain. In August, the offshore current pattern showed a reversed pattern as compared with that in the first half of the year. Large eddies, for example, can modify the current pattern on a local scale. From September through December, the currentsgradually returned to the winter-spring patter, with the offshore coastal current and the counterclockwise circulation within the bay intensified and mesoscale eddies diminished (Figure 3.11).

To examine the seasonal variability of water properties, we present in Figures 3.12-3.17 the model-predicted temperature and salinity field near the surface at the end of each month. In section

3.1.1, we showed that the water is seasonally well-stratified in Massachusetts Bay except in the shallow area of Boston Harbor. The monthly fields show that water temperature was not spatially uniform in the Bay. The surface temperature was the coldest in January and February, with temperature ranging from 2 °C within the bay, particularly in Cape Cod Bay to 4 °C in the offshore region (Figure 3.12). Surface temperature started to rise in March, ranging from 3 to 5 °C, but a gradient formed with warmer water in the southern part of the domain and cooler water in the northern end of the domain. In April, surface temperature rose to 7–9 °C. The surface water temperature distribution in May and June was characterized by high temperature in Cape Cod Bay and much of MB where temperature reached 16 °C in May and 20 °C in June (Figure 3.13). In July and August, the surface layer in the whole simulation domain was occupied by warm water with temperature reaching 20 °C everywhere except along the coast north of Cape Ann. Surface temperature decreased to below 15 °C in September and 13 °C in October, without notable spatial variation within the simulation domain (Figure 3.14). This cooling trend continued in November when the temperature dropped below 11 °C and below 9 °C in December. An inshore-offshore gradient formed in December with colder water in the inshore region and higher temperature in the offshore region.

Salinity in January and February showed little spatial variation (Figure 3.15). Low salinity surface waters were perceptible only near the mouth of the Merrimack River and in Boston Harbor. In March, the lower salinity water extended to a great part of the Bay while forming an inshore-offshore gradient and in April, fresher waters extended further offshore. Surface salinity started to increase in May in the offshore region and in June, high-salinity waters expanded to most of MB (Figure 3.16). In July and August, however, a tongue of relatively low salinity waters was observed offshore Cape Cod, which signaled an offshore perturbation instead of a local event within the Bay. Surface salinity increased again in the offshore region in September and October and the high-salinity water extended into the Bay in November and December, forming a spatial distribution at the end of the year similar to that observed in January (Figure 3.17).

3.1.3 Comparison with previous years simulations

As a comparison with the previous year, difference of monthly surface current, temperature and salinity were exemplified for April and September (Figures 3.18-3.20). As mentioned early, the coastal current in the offshore region from MB was well developed in April 2010, but much weaker as compared with that in 2009 (Figure 3.18). This is reflected by a strong northwestward current in the difference between the two years, which was calculated by subtracting the 2009 flow field from that of 2010. The basin-wide anticlockwise circulation in MB was also weaker in 2010 than in 2009, demonstrated by a clockwise circulation in the difference between the two years. Also, two eddies near the North Passage were well developed in 2009, which were mostly absent in 2010. For the case of September, the major difference in the surface current field was the eddies that developed in 2009 near the North Passage and the South Passage, which were mostly absent or weak in the 2010 simulation.

As for the temperature comparison, surface waters were considerably warmer in 2010 than in 2009 (Figure 3.19). In April 2010, the surface water temperature was 1.5-3 °C higher in 2010 than in 2009. The difference was particularly large in Cape Cod Bay. The surface water temperature was also higher in September 2010 than in 2009, but with a much smaller difference between the two years. The temperature difference was mostly around 1 °C in MB in September while it had reached above 3 °C in April. On the other hand, surface waters were considerably fresher in April 2010 than during the same period in 2009 (Figure 3.20). The difference reached up to 3 psu at the northeast end of the simulation domain and above 1 psu in the MB. It should be pointed out that this freshening event coincides with the high river discharge observed in early spring 2010. In September, however, surface salinity was higher in 2010 than in 2009 (Figure 3.20). The difference was particularly high at the north end of the MB where the surface salinity was about 1 psu higher in 2010 than in 2009. September 2010 is also within the dry summer in 2010 that we previously noted (Figure 3.19), while summer 2009 was quite wet (Libby et al., 2010). Only in the offshore region was the surface salinity slightly lower in 2010 than in 2009, with the difference less than 0.5 psu.

3.2 *Water quality fields*

3.2.1 Model-data comparisons

Data-model correlation analyses of key variables are presented in Figure 3.21, including surface chlorophyll, NO_3, SiO_3, NH_4, and bottom DO and DO saturation. Good correlations were found between the modeled and observed results for NO_3^- near the surface and DO near the bottom. The correlation coefficient reached 0.86 for surface nitrate and 0.95 for bottom DO. For the near-surface chlorophyll and silicate, the correlation was not as good as that for nitrate and DO. Basically the model tended to overestimate chlorophyll at low concentrations, underestimate chlorophyll at high concentrations and underestimate silicate at the high concentration ranges as well. Ammonium data were relatively more scattered than other variables. Unlike the dissolved oxygen concentration, for which a good correlation was found between the model prediction and observation, the model tended to underestimate the saturation of dissolved oxygen. The saturation of dissolved oxygen was not directly modeled, rather it is calculated based on temperature, salinity and DO data. Biases in the simulation of these different parameters could all influence the accuracy of DO saturation estimates.

Annual cycles of key variables were plotted with the observational data for visual comparison (Figures 3.22-3.36). Chlorophyll concentration was broadly similar between the simulation and observation, but higher values observed at certain stations were not reproduced by the model, (Figures 3.22 - 3.24). The absence of dominating bloom events was the common feature in the 2010 simulation in most of the near-field stations (Figure 3.22). Peaks of chlorophyll concentration can be observed in spring and fall, but the low amplitudes and short duration do not constitute dominant blooms. Instead, multiple peaks of chlorophyll concentration of short durations with relatively small amplitudes were predicted from spring through fall at most of the near-field stations. This simulation result was substantiated by observation data at some stations such as N18 and N01, but high values were observed in spring and fall at other stations such as at Station F22, N04 and N07. Particularly high values of chlorophyll concentration were reported near the end of the year in November 2010, whereas the fall bloom typically occurs in October in other years. The spring bloom was slightly better developed at some far-field stations (e.g., F29 and F01), but essentially absent at others (e.g., stations F10 and F15) (Figure 3.23). The data did not show a typical dominating bloom at these stations either. At the Harbor stations, neither the model nor the

data revealed dominating bloom events (Figure 3.24). Basically, chlorophyll concentration stayed at the relatively high level during a long period of time from spring through fall. As mentioned in Tian et al. (2009), the shallow depth and multiple anthropogenic and natural nutrient sources contribute to the sustained high primary production in the harbor during the summer. Taylor et al. (2010) did a comparison of multi-year averaged seasonal cycles of major water quality variables. They found that even though chlorophyll levels remain relatively high during the summer season in Boston Harbor, chlorophyll decreased after the diversion of the MWRA outfall from the Harbor to the offshore location.

At most of the monitoring stations, model-estimated and observed dissolved inorganic nitrogen (DIN) showed similar seasonal variation both near the bottom and at the surface (Figures 3.25 and 3.26). Typically, DIN was replenished during the winter mixing season. DIN depletion in surface waters was observed in March and April when DIN concentration decreased to a very low level due to the consumption by spring phytoplankton development. DIN remained at a low level through summer and early fall and replenished again in late fall and winter. In contrast to surface waters, DIN in the bottom layer stayed at a relatively high level all through the summer and fall seasons, indicating a stratification in DIN concentration at most of the monitoring stations. At some far-field stations and particularly at Station F01, the model tended to underestimate nutrient concentration in the bottom layer (Figure 3.26). The model predicted similar DIN concentration in both the surface and bottom layers at a low concentration level, the high concentration up to 10 μM was reported. This station is located in Cape Cod Bay with a depth about 27 m. This depth would be expected to be within the euphotic zone and nutrients should be taken up within the reasonable period of time. As such, there might be local nutrient sources that are not captured by the model. One possible nutrient input is through groundwater (Becker, 1992, Jiang et al. 2007). Although groundwater sources were considered in the actual UG-RCA setup, the configuration was based historical estimates without spatial structure. Another possible source is through horizontal advection. As we will show later in the report, the dispersion of the MWRA outfall effluents are mostly restricted to local domain during the summer stratified season. Only during mixing season in winter was the dispersion found down to Cape Cod Bay, as for the 2009 model projection (Tian et al., 2010). At most of the harbor stations including the far-field station F23 off the harbor mouth, similar magnitudes and seasonal cycles were observed and simulated, indicating nutrient depletion in the

whole water column without stratification in nutrient concentration (Figure 27). Only at the stations 024 and 124 was slightly higher DIN concentration found in the bottom layer than in the surface layer. Station 024 is located in the Charles River mouth and Station 124 is located in southeastern corner of the inner bay where freshwater discharge and local events can modify nutrient concentration on a local scale.

Model-simulated primary production was depicted at three monitoring stations where field observations were conducted (Figure 3.28). Except perhaps for station N04 in 2009, modeled primary production did not show typical peaks for spring and fall blooms, but rather remained at a relatively high level throughout the summer season. Primary production at the near-field station N18 close to the MWRA outfall was not particularly higher than that at other stations. At all three stations, modeled primary production increased gradually in spring and dropped abruptly in late fall.

Most of the DON and PON data were reproduced by the model (Figures 3.29-3.32) except for particularly high observed DON values (e.g., DON at Station F22 and N07 in Figure 3.29) and some of the lower PON values (e.g., PON in the bottom layer at Station F13 and F06). DON showed very little seasonal variation, in contrast to PON which manifested relatively high values from spring through fall and low values during the winter mixing season. Approximately following the chlorophyll distribution, predicted PON did not display dominant bloom events, rather short-term fluctuations with limited amplitudes. No anomalous signal was found near the outfall in either DON or PON, showing that the organic nitrogen pools are essentially controlled by internal dynamics within the water column and the outfall effluent did not noticeably alter their distribution. POC displayed high frequency variations without dominant seasonal events (Figures 3.33 and 3.34). POC was relatively low in winter and high during all other seasons. At most of the near-field stations and at Station F22 as well (Figure 3.33), the model tended to overestimate the concentration of POC, particularly in the bottom layer. Model-data comparison appeared to be better at certain far-field stations in terms of magnitude, but both the data and simulation are characterized by high frequency variations with relatively little seasonal pattern.

Relatively good comparison of DO has been obtained between simulation and observation (Figures 3.35 and 3. 36). DO displayed high values during the spring, but stayed at a low level

during the summer and fall season. The model slightly underestimated the DO level during the spring peak DO concentration period, but the difference remained minimal compared to the total concentration. As pointed out by Tian et al. (2009), the high DO values in spring reflected photosynthesis production through phytoplankton growth, whereas remineralization of organic substances occurred in summer and fall so that DO stayed low during that period of time. Water mass inflow through the open boundary and horizontal advection can also alter bottom DO concentration in the region (Libby et al., 2008).

Time-series of key variables (temperature, DIN, chlorophyll and DO) throughout the water column are shown in Figures 3.37-3.41. In general, the model reproduced the observed homogeneous water column in winter and stratification in summer and early fall in the temperature profile. The lowest temperature of about 2-4 °C was reached in February and temperature stratification started around early April. The strongest stratification occurred in July with a mixed layer depth ranging from 5-10 m. Destratification took place at the end of October throughout MB, and a homogeneous water column continued through November and December. Seasonal cycles of temperature were not well captured by the data in some cases due to limited sampling, particularly at the end of the year. At Station F23, for example, summer stratification and fall cooling were not observed in the data, but the model predicted these events.

DIN displayed a similar seasonal cycle between the model and the data: replenished in winter throughout the whole water column, depleted fully in spring and early summer, regenerated through remineralization and input from the sediment to the bottom layer, and vertically mixed again in late fall and winter. The model seemed to underestimate DIN in the bottom layer in summer at station F02. This station is located in Cape Cod Bay. As mentioned earlier, local nutrient input in Cape Cod Bay might have occurred that was not included in the model nutrient loadings.

Certain discrepancies appeared in the chlorophyll time series. A dominant phytoplankton bloom indicated by chlorophyll concentration was observed at stations F23 (Figure 3.37) and F06 (Figure 3.40) in spring. The model, on the other hand, did not predict particularly high concentration during that period of time. Instead, the model predicted small peaks of chlorophyll concentration with short durations and limited amplitudes. At stations N18 and N01, the data revealed short period of

elevated chlorophyll concentration during spring in April and chlorophyll subsurface maximum in summer, but the model tended to underestimate these events (Figures 3.38 and 3.39). Extrapolating the observational data through the end of the year gives high values of chlorophyll in December at Station N01, but one must keep in mind that there were no measurements made after mid-November. At Station F02, high chlorophyll concentration was observed in early February during winter; in contrast, the model predicted a small spring bloom in April (Figure 3.41). As mentioned above, the model predicted multiple peaks of chlorophyll concentration with short duration and limited amplitudes that differed from typical phytoplankton bloom events. On the other hand, the data showed quite high values in February during the winter season. These unusual phenomena in both the simulation and data resulted in relatively large discrepancies in the model-data comparison. DO matched well in general between the model and observation in terms of seasonal cycle and magnitude. The highest values of DO were observed and modeled during the spring season and the lowest values appeared in the bottom layer in summer when remineralization consumption and sediment oxygen demand were highest within an annual cycle.

Sediment nutrient fluxes and oxygen demand (SOD) were observed (Tucker et al., 2010) at three stations in BH (BH02, BH03 and BH08A) and three stations in Massachusetts Bay (MB01, MB03 and MB05) (Figure 2.5). At the bay stations shown at the right side of the figure, the model-data comparison of ammonium flux was reasonably good, with little seasonal variation (Figures 3.42). In contrast, nutrient fluxes were substantially higher during summer and early fall at the harbor stations as compared with the bay stations, indicating that remineralization contributed a substantial share to the increased nutrient supplies in summer in BH. Similar pattern was observed for SOD, with low flux at bay stations and high flux in the Harbor. Differing from nutrient, SOD fluxes was notably higher during late summer and fall than during the first half of the year, whereas no considerable seasonal variation was observed for nutrient fluxes. The model computed results compared relatively well with the observations for most sediment fluxes in both the Harbor and in the Bay in general, but tended to underestimate nutrient and SOD fluxes at Station BH02 and BH03 during the summer season.

In summary, the UG-RCA 2010 simulation reproduced most of the observed magnitudes and seasonal variations of an array of parameters. For some specific cases, however, model-data

deviation was observed, such as the underestimation of chlorophyll concentration during the winter and spring seasons.

3.2.2 Comparison with previous years simulations

In this section we compare the UG-RCA simulations of 2008, 2009 and 2010. Indicated by the chlorophyll concentration, 2008 was characterized by a large spring phytoplankton bloom. The bloom approximately started early March, reached the peak at end March and early April and terminated around mid May. A dominant spring bloom also occurred in 2009, but later by approximately one month, with peak concentration reached near the end of April. In 2010, however, there was only a small short bloom that started in early April and terminated near the end of the same month. The timing of the bloom was between those in 2008 and 2009, with peak concentration reached in early April, but amplitude considerably lower than that in the previous two years. In the fall, a large phytoplankton bloom was observed in 2008, with peak values of 5 μg l^{-1} chlorophyll in mid October. In 2009, however, the fall bloom was mostly absent in the simulation without a typical peak of chlorophyll concentration. In 2010, an earlier, small bloom was predicted with a peak concentration around the end of September and early October. Only near the outfall did the chlorophyll concentration reach to a similar level of the 2008 fall bloom. The DIN seasonal cycle was generally similar among the three years, with high values in winter, low values in summer and replenishment in late fall (Figure 3.45). Nonetheless, slight differences can be seen from year to year. DIN concentration was high in winter 2008 and 2009, but relatively lower in 2010.

For bottom DO, no substantial difference was observed between the three years (Figure 3.46). DO displayed high values during the spring phytoplankton bloom season and low values in late summer and early fall over all three years. The DO level was quite similar at the end of the annual simulation in 2008 and 2010, but relatively lower at the end of 2009.

4. Projection Experiments

We conducted a model run without MWRA effluent to assess the potential influence of the MWRA outfall on the water quality and ecosystem function in Massachusetts Bay. In this section, we refer the initial run with the MWRA outfall as the "control run" and the sensitivity-analysis run as the "non-sewage" run. We compared the chlorophyll concentration, dissolved inorganic nitrogen and DO between the two simulations. The results are similar to those of "no sewage" projection runs conducted for other years in past model studies (HydroQual and Normandeau, 1995; Jiang and Zhou, 2006b; Tian et al., 2009; Chen et al., 2010; Tian et al. 2010.) In field observations we can only compare "prediversion" with "postdiversion", and except in the immediate area of the outfall no changes have been observed. In contrast, the BEM allows us to isolate effects of the discharge that may be seen some distance away, even though those effects are too small to have any ecological significance.

The intensities and seasonal variations of the chlorophyll concentration for these two runs were almost identical (Figure 4.1). Even though the two simulation lines were not fully superposed on each other, the difference between them remained negligible throughout the year. The seasonal cycle of DIN near the surface was also similar between the two simulations (Figure 4.2). The results were almost the same in summer. A noticeable difference was found in winter, during which the "non-sewage" run predicted lower DIN concentration than the control run with the MWRA outfall. Near the bottom, the non-sewage run predicted a notably lower DIN concentration than the control run near the outfall, while the two predictions were more comparable at other stations (Figure 4.3). This result is consistent with field measurements that show elevated levels of DIN near the outfall (Libby et al 2009). The DO results were practically identical between the two simulations, indicating that the MWRA outfall does not have notable influence on the DO level in the simulation domain (Figure 4.4).

However, in the bottom layers of the model, we do find a notable difference between the two runs in terms of ammonium, which is the most abundant nutrient in the outfall sewage discharge (Figures 4.5-4.7). This is consistent with field observations of dissolved inorganic nitrogen concentrations (Libby et al. 2009) and with nitrogen stable isotope studies (Tucker and Giblin,

2002; Tucker et al. 1999.) In January, ammonium from the outfall was spread along the coast down to Cape Cod Bay (CCB), but limited to the coastal region (Figure 4.5). This was also the pattern predicted when the outfall was located in Boston Harbor (Fitzpatrick and Isleib, 2003, Signell et al. 2000). The projection results show that some ammonium levels from the effluent discharged at the outfall disperses back into Boston Harbor. However, since local sources to the harbor have decreased so much (Taylor 2006b), the ammonium levels in Boston Harbor have dropped significantly since the outfall was moved offshore (Taylor 2006a.) . In February, the effluent signal retreated to the middle of MB, and in March and April, the effluent ammonium was mostly restricted to a local domain. Restricted effluent dispersion continued through the summer and early fall until November when effluent ammonium dispersal extended again along the coast toward CCB (Figures 4.6 and 4.7). This seasonal variation is consistent with results from nitrogen stable isotope studies (Montoya et al., 2003) which show the effects of sewage derived nitrogen on the food web confined to areas relatively near the outfall in summer, but occurring in Cape Cod Bay in winter months. At the end of December, a patch of effluent ammonium of low concentration was predicted in CCB, but it was not discernible near the MWRA outfall. If this ammonium in CCB is derived from the outfall, it could be remaining from earlier discharges, since the predicted concentrations of ammonium near the MWRA outfall are low near the end of December. Geyer et al. (1992) noted that the residence time of Cape Cod Bay is long during periods when there is little freshwater inflow into the MBS.

Effluent ammonium concentration at the MWRA outfall was the highest in June and October and lowest in December. Certainly, effluent dispersal is controlled by stratification and by the currents, which can vary over time subject to wind forcing and cold water intrusion from the Western Maine Coastal Current. If we consider ammonium as a semi-conservative tracer of effluent, the two long-distance dispersions in 2010 occurred in January and December, when the stratification was weak or absent. In summary, the effluent is in most cases restricted horizontally within a local domain of about 20 km wide around the outfall location. However, based on the model prediction, long-distance dispersion can occur under particular circumstances, with nutrients transported as far as CCB. This dispersion has been previously shown (Fitzpatrick and Isleib, 2003) to be insensitive to the location of the outfall in Boston Harbor vs. Massachusetts Bay.

We plotted data along a west-east transect across the outfall for the end of each month (Figures 4.8 and 4.9). The height of the effluent plume, as inferred from the ammonium concentration, varied from month to month. In January and February, the outfall plume reached to the surface (Figure 4.8). From March through September, however, the plume was mostly restricted to the bottom 10 m or so. Only in April did the effluent ammonium plume reach the surface in the coastal region. This projection of effluent plume rise is in approximate agreement with the rise height of 5-15 m predicted by Blumberg et al. (1996) using near-field and far-field models. The core of the plume remained contained within the bottom layers from October to November, but its influence was perceptible up to the surface (Figure 4.9). As the plume spreads along the slope of the topography toward the coast, the absolute depth of the plume changes from place to place. Surfacing of the plume occurred during months of weak stratification, indicating that the vertical mixing basically controls the upward spread of the effluent. As mentioned earlier, the model did not predict effluent ammonium on this transect at the end of December in 2010 (Figure 4.9).

Libby et al. (2009) did a comparison between data collected before and after the September 6 2000 diversion of the MWRA outfall from Boston Harbor to the MB. Higher ammonium concentration after the diversion was found at the near-field stations. Although field measurements are are consistent with the model projection shown here, they are not directly comparable. Field measurements before the diversion were conducted when the outfall was located in Boston Harbor, while the non-sewage run here was configured without any effluent discharge into the system. A comparison of data collected before and after the relocation of the outfall shows the real-world changes resulting from diverting the discharge offshore.In contrast, the model is used here to show the direct influence of the outfall on effluent concentration and distribution . Also, the data comparison in Libby et al. (2009) was based on the ammonium averaged over depth, region, and season, while here we output the instantaneous difference in the bottom layer, which represents the maximum difference predicted by the model.

As shown at the beginning of this section, no anomaly was observed in either chlorophyll or DO level corresponding to the ammonium distribution around the outfall. In fact, during the stratified season when light is available, the effluent was basically trapped within the bottom layers around the outfall. During the well-mixed season when effluent could effectively reach the surface,

both light and vertical mixing were unfavorable to phytoplankton growth. As a result, the nutrient discharge from the outfall is not projected to result in differences in biomass and DO.

5. Summary

The 2010 simulation was conducted using MB-FVCOM/UG-RCA. The surface forcing was essentially based on meteorological data collected at Buoy 44013 and weather model predictions; nutrient loadings were based on the MWRA monitoring data and river discharges; and open boundary conditions were established from the data collected during the MWRA monitoring program.

The UG-RCA 2010 simulation reproduced most of the magnitudes and seasonal variations of the observations. For some specific cases, a deviation between simulation and data was observed, such as underestimation of chlorophyll at high-concentration ranges and overestimation at low-concentration range. The seasonal variation of model-predicted water quality variables was dominated by multiple small phytoplankton blooms during relatively short periods of time, particularly at near-field stations as compared to the previous years. Nutrient concentration in winter 2010 was also notably lower than in the previous year, which might be the reason why no dominant spring bloom was predicted. Low nutrient concentrations were also observed near the end of the year as compared with other years. DO showed high values during the spring phytoplankton bloom, but remained at a low levels in fall, kept low by high DO consumption and low DO solubility under high temperatures.

Based on our projection analysis removing the MWRA outfall from the simulation, we determined the horizontal and vertical extent of the outfall effluent plume using ammonium as a proxy. In the horizontal scale, the plume was mostly restricted to a local area around the outfall within about 20 km. However, long-distance effluent dispersal as far as Cape Cod Bay was predicted under certain circumstances in January and December 2010. In the vertical, the height of the plume was essentially controlled by vertical dynamics and mixing in the water column. In winter and late fall when the vertical mixing was strong, the outfall effluent plume can reach to the surface layer. During the stratified season in summer and early fall, the ammonium plume was basically constrained within the bottom 10 m. However, no substantial bay-wide influence was observed in chlorophyll or DO. We believe that the timing of the effluent spreading influences its effect on the ecosystem. As the upward mixing and long-distance dispersal occurred during winter

and late fall when light intensity limits phytoplankton growth, effluent nutrients were not effectively taken up and translated into phytoplankton biomass and subsequent biogeochemical cycles.

6. References

Alber M. and Chan A. 1994. Sources of contaminants to Boston Harbor: revised loading estimates. Boston: Massachusetts Water Resources Authority. Report 1994-01, 113pp.

Banks R.B. and Herrera F.F. 1977. Effect of wind and rain on surface reaeration. *J. Envir. Engr. Div., ASCE*. **103**: 489-504.

Becker, S. 1992. The seasonal distribution of nutrients in Massachusetts and Cape Cod Bays. Masters Thesis, University of New Hampshire, Durham. 127pp.

Bigelow H.B. 1927. Physical oceanography of the Gulf of Maine (Part II). *Bulletin of the Bureau of Fisheries*, **40**: 511-1027.

Blumberg A., Ji Z. and Ziegler C.K., 1996, Modeling outfall plume behavior using a far field model, *J. Hydraulic Engineering*, **112**: 610-616.

Burchard H., Bolding K., Rippeth T.P., Stips A., Simpson J.H. and Sündermann J. 2002. Microstructure of turbulence in the Northern North Sea: a comparative study of observations and model simulations. *J. Sea Res.*, **47**: 223–238.

Butman B. 1976. Hydrography and low frequency currents associated with the spring runoff in Massachusetts Bay. *Memoires. Societe Royale des Sciences de Liege*, **6**: 247-275.

Butman B., Bothner M.H., Lightsom F.L., Gutierrez B.T., Alexander P.S., Martini M.A. and Strahle W.S. 2002. Long-term Oceanographic Observations in Western Massachusetts Bay offshore of Boston, Massachusetts: Data Report for 1989-2000, U.S. Geological Survey Digital Data Series 74.

Chen C., Liu H. and Beardsley R. 2003. An unstructured grid, finite-volume, three dimensional, primitive equations ocean model: Application to coastal ocean and estuaries. *Journal of Atmospheric and Ocean Technology*, **20 (1)**: 159–186.

Chen C.**,** Beardsley R.C., Hu S., Xu Q. and Lin H. 2005. Using MM5 to hindcast the ocean surface forcing fields over the Gulf of Maine and Georges Bank region. *Journal of Atmospheric and Ocean Technology.* **22**: 131-145.

Chen C., Beardsley R.C. and Cowles G. 2006a. An unstructured grid, finite-volume coastal ocean model (FVCOM) system. Special Issue entitled "Advance in Computational Oceanography", *Oceanography*, **19(1)**: 78-89.

Chen C., Beardsley R.C. and Cowles G. 2006b. An unstructured grid, finite-volume coastal ocean model-FVCOM user manual, School for Marine Science and Technology, University of Massachusetts Dartmouth, New Bedford, Second Edition. SMAST/UMASSD Technical Report-06-0602, 318 pp.

Chen C., Malanotte-Rizzoli P., Wei J., Beardsley R.C., Lai Z., Xue P., Lyu S., Xu Q., Qi J. and Cowles G.W. 2009. Application and comparison of Kalman filters for coastal ocean problems: An experiment with FVCOM, *J. Geophys. Res.*, **114**, C05011, doi:10.1029/2007JC004548.

Chen C., Tian R., Beardsley R.C., Qi J. and Xu Q. 2010. Modeling 2008 in Massachusetts Bay using an upgraded unstructured-grid Bays Eutrophication Model. Boston: Massachusetts Water Resources Authority. Report 2010-15. 127p.

Di Toro D.M. 2001. *Sediment Flux Modeling*. Wiley-Interscience, New York, 624 pp.

Fairall C.W., Bradley E.F., Rogers D.P., Edson J.B. and Young G.S. 1996. Bulk parameterization of air–sea fluxes in TOGA COARE. *J. Geophys. Res.*, **101**: 3747–3767.

Fairall C.W., Bradley E.F., Hare J.E.,Grachev A.A. and Edson J.B. 2003. Bulk Parameterization of Air–Sea Fluxes: Updates and Verification for the COARE Algorithm. *Journal of Climate* 2003; **16:** 571-591.

Fitzpatrick, J.J. and Isleib, R. 2003. A post-audit analysis of the impacts of wastewater treatment plant outfall relocation on Boston Harbor, Massachusetts Bay and Cape Cod Bay water quality. Proceedings of the Water Environment Federation, WEFTEC 2003: Session 61 through Session 70, pp. 530-555(26).

Gao G., Chen C., Qi J. and Beardsley R.C. Submitted. Development of Unstructured-grid Version CICE: Validation and Applications, Submitted to *J. Geophys. Res.*

Geyer W.R., Gardner G.B., Brown W.S., Irish J., Butman B., Loder T. and Signell R.P. 1992. Physical oceanographic investigation of Massachusetts and Cape Cod Bays. Boston: Massachusetts Bays Program. MBP-92-03, 497pp.

Hendry R. and He I. 1996. Technical report on objective analysis (OA) project, Bedford Institute of Oceanography, Dartmouth, Nova Scotia, 105pp.

HydroQual, Inc. and Normandeau Associates, Inc. 1993. A water quality model for Massachusetts and Cape Cod Bays. Boston: Massachusetts Water Resources Authority. Report 1993-05, 222pp.

HydroQual, Inc. and Normandeau Associates, Inc. 1995. A water quality model for Massachusetts and Cape Cod Bays: Calibration of the Bay Eutrophication Model (BEM). Boston: Massachusetts Water Resources Authority. Report 1995-08. 402 pp.

HydroQual, Inc. 2000. Bays Eutrophication Model (BEM): modeling analysis for the period 1992-1994. Boston: Massachusetts Water Resources Authority. Report 2000-02, 158pp.

HydroQual, Inc. 2001a. Boundary sensitivity for the Bays Eutrophication Model (BEM). Boston: Massachusetts Water Resources Authority. Report 2001-14. 90pp.

HydroQual. 2001b. Analysis of the addition of a third algal group to the Bays Eutrophication Model (BEM) kinetics. Boston: Massachusetts Water Resources Authority. Report 2001-15. 110 p.

HydroQual, Inc. and Signell R.P. 2001. Calibration of the Massachusetts and Cape Cod Bays Hydrodynamic Model: 1998-1999. Boston: Massachusetts Water Resources Authority. 2001-12, 170pp.

HydroQual. 2002. Sensitivity of the Bays Eutrophication Model (BEM) to changes in algal model coefficients. Boston: Massachusetts Water Resources Authority Report 2002-16. 236 p.

HydroQual, Inc. 2003. Bays Eutrophication Model (BEM): modeling analysis for the period 1998-1999. Boston, Massachusetts Water Resources Authority. Report 2003-03, 318pp.

HydroQual, 2004. “User’s Guide for RCA, Release 3.0”, Hydroqual, Inc, New Jersey.

Hyer P.V., Fang C.S., Ruzeck E.P. and Hargis W.J. 1971. Hydrography and hydrodynamics of Virginia estuaries, studies of the distribution of salinity and dissolved oxygen in the upper York system. Gloucester Point, VA:Virginia Institute of Marine Science.

Jiang M.S. and Zhou M. 2004a. Calibration of the Massachusetts and Cape Cod Bays water quality model: 2000-2001. Boston: Massachusetts Water Resources Authority. Report 2004-09. 90pp.

Jiang M.S. and Zhou M. 2004b. Calibration of the Massachusetts and Cape Cod Bays Hydrodynamic Model: 2000-2001. Boston: Massachusetts Water Resources Authority. Report 2004-08. 71pp.

Jiang M. and Zhou M. 2006a. The Massachusetts and Cape Cod Bays hydrodynamic model: 2002-2004 simulation. Massachusetts Bay Eutrophication Model: 2002-2004 Simulation. Boston: Massachusetts Water Resources Authority. Report 2006-12. 128 p.

Jiang M. and Zhou M. 2006b. Massachusetts Bay Eutrophication Model: 2002-2004 Simulation. Boston: Massachusetts Water Resources Authority. Report 2006-13. 126 p.

Jiang, M., G. T. Wallace, M. Zhou, S. Libby and C. D. Hunt. 2007. Summer formation of a high-nutrient low-oxygen pool in Cape Cod Bay, USA, *J. Geophys. Res*., **112**, C05006, doi:10.1029/2006JC003889.

Jiang M. and Zhou M. 2008. Massachusetts Bay Eutrophication Model: 2005 simulation. Boston: Massachusetts Water Resources Authority. Report 2008-13. 82 p. Report 2008-12., 118pp.

Kropp R.K., Diaz R., Hecker B., Dahlen D., Boyle J.D., Abramson S.L. and Emsbo-Mattingly S. 2001. 2000 Outfall Benthic Monitoring Report. Boston: Massachusetts Water Resources Authority. Report 2001-14, 148pp.

Kropp R.K., Diaz R., Dahlen D., Boyle J.D. and Hunt C.D. 2002. 2001 Harbor Benthic Monitoring Report. Boston: Massachusetts Water Resources Authority. Report 2002-19, 74pp.

Lai Z., Chen C., Cowles G. and Beardsley R.C. Submitted. A Non-Hydrostatic Version of FVCOM, Part I: Validation Experiments (submitted to *J. Geophys. Res.-Oceans*, in revision).

Laws E.A. and Chalup M.S. 1990. A microalgal growth model. *Limnol. Oceanogr*. 35, 597-608.

Libby P.S., Hunt C.D, Geyer W.R., Keller A.A., Oviatt C.A. and Turner J.T. 2000. 1999 Annual Water Column Monitoring Report. Boston: Massachusetts Water Resources Authority. Report 2000-09, 180pp.

Libby P.S., Hunt C.D, McLeod L.A., Geyer W.R., Keller A.A., Borkman D., Oviatt C. A. and Turner J. T. 2001. 2000 Annual Water Column Monitoring Report. Boston: Massachusetts Water Resources Authority. Report 2001-17, 196pp.

Libby P.S., Borkman D.G., Geyer W.R., Keller A.A., Turner J.T., Mickelson M.J., and Oviatt C.A. 2008. Water Column Monitoring in Massachusetts Bay: 1992-2007. Boston: Massachusetts Water Resources Authority. Report 2008-16, 170pp.

Libby P.S., Borkman D., Geyer W.R., Keller A.A., Turner J.T., Mickelson M.J. and Oviatt C.A. 2009. Water column monitoring in Massachusetts Bay 1992-2007: focus on 2007 results. Boston: Massachusetts Water Resources Authority. Report 2009-04. 162 p. (incl. appendices).

Libby P.S., Borkman D.G., Geyer W.R., Turner J.T. 2010**.** 2009 Water Column Monitoring Results. Boston: Massachusetts Water Resources Authority. Report 2010-13. 36p + appendices.

Lynch D.R., Naimie C.E. and Werner F.E. 1996. Comprehensive coastal circulation model with application to the Gulf of Maine. *Cont. Shelf Res.*, 12: 37-64.

Maciolek N. J., Diaz R. J., Dahlen D., Hecker B., Gallagher E. D., Blake J. A., Williams I. P., Emsbo-Mattingly S., Hunt C. and Keay K. E. 2003. 2002 Outfall Benthic Monitoring Report. Boston: Massachusetts Water Resources Authority. Report 2003-13, 166pp.

Manohar-Maharaj V. 1973. Spring run off in to Massachusetts Bay. Masters Thesis, MIT, Cambridge, 97p.

Mellor G. L. and Yamada T. 1982. Development of a turbulence closure model for geophysical fluid problems. *Rev. Geophys. Space Phys.*, **20**: 851-875.

Menzie-Cura. 1991. Sources and loadings of pollutants to Massachusetts Bays. Boston: Massachusetts Bays Program. Report MBP-91-01, 266pp.

Montoya, J.P., Rathbun, K.M., and Mayo, C.S. 2003. Recent nitrogen isotope data from Massachusetts and Cape Cod Bays. Information Briefing for the MWRA Outfall Monitoring Science Advisory Panel, 6 January 2003.

Pietrzak J., Jakobson J.B., Burchard H., Vested H.J. and Peterson O. 2002. A three-dimensional hydrostatic model for coastal and ocean modeling using a generalized topography following coordinate system. *Ocean Modelling* **4**:173–205.

Qi J., Chen C., Beardsley R.C., Perrie W. and Cowles G. 2009. An unstructured-grid finite-volume surface wave model (FVCOM-SWAVE): implementation, validations and applications. *Ocean Modelling*, **28**: 153-166. doi:10.1016/j.ocemod.2009.01.007.

Signell, R.P., Jenter, H.L. and Blumberg, A.F., 2000, Predicting the physical effects of relocating Boston's sewage outfall, *J. Estuarine, Coastal and Shelf Sci*., **50**: 59-72.

Smagorinsky J. 1963. General circulation experiments with the primitive equations, I. The basic experiment. *Monthly Weather Review*, **91**: 99–164.

Taylor D.I. 2006. 5 years after transfer of Deer Island flows offshore: an update of water-quality improvements in Boston Harbor. Boston: Massachusetts Water Resources Authority. Report 2006-16. 77 p.

Taylor D.I. 2006b. Update of patterns of wastewater, river and non-point source loadings to Boston Harbor (1990 - 2005). Boston: Massachusetts Water Resources Authority. Report 2006-22. 77 p.

Taylor D.I., Oviatt C.A. and Borkman D.G. 2010. Non-linear Responses of a Coastal Aquatic Ecosystem to Large Decreases in Nutrient and Organic Loadings. *Estuaries and Coasts*:1-13. DOI 10.1007/s12237-010-9312-3.

Tian, R.C., Chen C.S., Xu Q.C., Xue P.F., Cowles G.W., Beardsley R. and Rothschild B. 2009. Massachusetts Bay Eutrophication Model: 2006-2007 Simulation. Boston: Massachusetts Water Resources Authority. Report 2009-11. 147p.

Tian, R.C., Chen, C., Zhao, L.Z., Xue, P., Leo, W.S., Mickelson M.J. 2010. Modeling 2009 in Massachusetts Bay using the unstructured-grid Bays Eutrophication Model. Boston: Massachusetts Water Resources Authority. Report 2010-22. 100p.

Tucker, J., Sheats, N. Giblin, A.E., Hopkinson, C.S., and Montoya, J.P. 1999. Using stable isotopes to trace sewage-derived material through Boston Harbor and Massachusetts Bay. *Marine Environ. Res.* **48**: 353-375.

Tucker J. and Giblin, A. 2002. Stable Isotope Analyses of Sediment and Invertebrate Samplesfrom Boston Harbor and Massachusetts Bay. Boston: Massachusetts Water Resources Authority.Report ENQUAD 2002-21. 24 p.

Tucker J., Kelsey J., Giblin A. and Hopkinson C. S. 2002. Benthic Metabolism and Nutrient Cycling in Boston Harbor and Massachusetts Bay: Summary of Baseline Data and Observations after One Year of Harbor-to-Bay Diversion of Sewage Effluent. Boston: Massachusetts Water Resources Authority. Report 2002-13. 83pp.

Tucker J., Kelsey S. and Giblin A.E. 2010. 2009 Benthic nutrient flux annual report. Boston: Massachusetts Water Resources Authority. Report 2010-10. 27 p.

Turner J.T. 1994. Planktonic Copepods of Boston Harbor, Massachusetts Bay and Cape Cod Bay, 1992. *Hydrobiologia*, **293**: 405-413.

Table 2. 1 State variable numbers and units in UG-RCA.

Number	Variable	Unit
1	Salinity	ppt
2	Winter/spring phytoplankton	mg C l^{-1}
3	Summer phytoplankton	mg C l^{-1}
4	Fall phytoplankton	mg P l^{-1}
5	Particulate organic phosphorous – refractory component	mg P l^{-1}
6	Particulate organic phosphorous – labile component	mg P l^{-1}
7	Dissolved organic phosphorous – refractory component	mg P l^{-1}
8	Dissolved organic phosphorous – labile component	mg P l^{-1}
9	Total dissolved inorganic phosphorous	mg N l^{-1}
10	Particulate organic nitrogen – refractory component	mg N l^{-1}
11	Particulate organic nitrogen – labile component	mg N l^{-1}
12	Dissolved organic nitrogen – refractory component	mg N l^{-1}
13	Dissolved organic nitrogen – labile component	mg N l^{-1}
14	Total ammonia (ammonia in water and phytoplankton cell)	mg N l^{-1}
15	Nitrite + nitrate	mg Si l^{-1}
16	Biogenic silica	mg Si l^{-1}
17	Total silica – (silica in water and phytoplankton cell)	mg C l^{-1}
18	Particulate organic carbon – refractory component	mg C l^{-1}
19	Particulate organic carbon – labile component	mg C l^{-1}
20	Dissolved organic carbon – refractory component	mg C l^{-1}
21	Dissolved organic carbon – labile component	mg C l^{-1}
22	Dissolved organic carbon – algal exudate	mg C l^{-1}
23	Dissolved organic carbon – reactive component	mg C l^{-1}
24	Particulate organic carbon – reactive component	mg C l^{-1}
25	O2* - aqueous oxygen	mg O_2 l^{-1}
26	Dissolved oxygen	mg O_2 l^{-1}

Table 2. 2 Parameter definition, symbols, values and units in RCA-v3 and UG-RCA, and in RCA-v2. Where values used in RCA differ from those used in UG-RCA, they are shown in parentheses.

Order	Parameter definition	Symbol	Value	Unit
1	MODEL OPTION	AGMOPT	1	
2	Phytoplankton categories	ACTALG	3	
3	REAERATION FORMULATION	KAOPT	3	
4	EXTINCTION COEFFICIENT	KEOPT	1	
5	PAR FRACTION	PAR	0.437	
9	GROWTH TEMPERATURE FOR DIATOMS	TOPT1	8.000	^oC
10	TEMPERATURE CORRECTION EFFECT ON GROWTH RATE BELOW TOPT1	K1BETA1	0.004	$^oC^{-2}$
11	TEMPERATURE CORRECTION EFFECT ON GROWTH RATE ABOVE TOPT1	K1BETA2	0.006	$^oC^{-2}$
12	GROSS PHOTOSYNTHETIC RATE PER UNIT CELL (ASSOCIATED WITH PHOTOSYNTHETIC DARK REACTIONS)	GPRE1	2.5	d^{-1}
13	GROSS PHOTOSYNTHETIC RATE PER UNIT CELL PER UNIT LIGHT INTENSITY UNDER NUTRIENT-SATURATED CONDITIONS AND ZERO IRRADIANCE	GPR01	0.64 (0.28)	m^2 Ein^{-1}
14	SATURATING ALGAL LIGHT INTENSITY	IS1	0.000	Ein m^{-2} d^{-1}
15	HALF SATURATION CONSTANT FOR NITROGEN	KMN1	0.010	mg N l^{-1}
16	HALF SATURATION CONSTANT FOR PHOSPHOROUS	KMP1	0.001	mg P l^{-1}
17	HALF SATURATION CONSTANT FOR SILICA	KMS1	0.020	mg Si l^{-1}
18	BASAL OR RESTING RESPIRATION RATE	K1RB	0.030	d^{-1}
19	TEMPERATURE COEFFICIENT FOR BASAL/ENDOGENOUS RESPIRATION	K1RT	1.0	dimensionless
20	GROWTH-RATE-DEPENDENT RESPIRATION COEFFICIENT	K1RG	0.280	dimensionless
21	DEATH RATE DUE TO GRAZING	K1GRZC	0.100	d^{-1}
22	TEMPERATURE COEFFICIENT	K1GRZT	1.100	dimensionless
23	FRACTION OF C ALLOCATED TO STRUCTURAL PURPOSES	FSC1	0.10	dimensionless
24	CARBON TO CHLOROPHYLL RATIO	WCCHL1	40.0	mg C (mg chl)$^{-1}$
25	CARBON TO PHOSPHORUS RATIO - NON-P LIMITED	WCP1	40.0	mg C (mg P)$^{-1}$
26	CARBON TO NITROGEN RATIO - NON-N LIMITED	WCN1	5.0	mg C (mg N)$^{-1}$
27	CARBON TO SILICA RATIO - NON-SI LIMITED	WCS1	2.500	mg C (mg Si)$^{-1}$
28	QUOTIENT OF NUTRIENT-LIMITED NUTRIENT:C RATIOS AT RELATIVE GROWTH RATES OF 0 AND 1	QF1	0.85	
29	CHLOROPHYLL SELF-SHADING EXTINCTION COEFFICIENT FOR ALGAL GROUP 1	XKC1	0.017	m^2 (mg chl) $^{-1}$
30	BASE ALGAL SETTLING RATE - GROUP 1	VSBAS1	0.500	m d^{-1}
31	NUTRIENT STRESSED ALGAL SETTLING RATE - GROUP 1	VSNTR1	1.000	m d^{-1}
	Algal Group 2			

Order	Parameter definition	Symbol	Value	Unit
41	OPTIMAL GROWTH TEMPERATURE FOR SUMMER GROUP 2	TOPT2	18.000	^oC
42	TEMPERATURE CORRECTION EFFECT ON GROWTH RATE BELOW TOPT2	K2BETA1	0.004	$^oC^{-2}$
43	TEMPERATURE CORRECTION EFFECT ON GROWTH RATE ABOVE TOPT2	K2BETA2	0.006	$^oC^{-2}$
44	GROSS PHOTOSYNTHETIC RATE PER UNIT CELL (ASSOCIATED WITH PHOTOSYNTHETIC DARK REACTIONS)	GPRE2	3.0	d^{-1}
45	PHOTOSYNTHETIC RATE PER UNIT CELL PER UNIT LIGHT INTENSITY UNDER NUTRIENT-SATURATED CONDITIONS AND ZERO IRRADIANCE	GPR02	0.64 (0.28)	m^2 Ein^{-1}
46	SATURATING ALGAL LIGHT INTENSITY	IS2	000.0	Ein m^{-2} d^{-1}
47	HALF SATURATION CONSTANT FOR NITROGEN	KMN2	0.010	mg N l^{-1}
48	HALF SATURATION CONSTANT FOR PHOSPHOROUS	KMP2	0.001	mg P l^{-1}
49	HALF SATURATION CONSTANT FOR SILICA	KMS2	0.005	mg Si l^{-1}
50	BASAL OR RESTING RESPIRATION RATE	K2RB	0.036	d^{-1}
51	TEMPERATURE COEFFICIENT FOR BASAL/ENDOGENOUS RESPIRATION	K2RT	1.0	
52	GROWTH-RATE-DEPENDENT RESPIRATION COEFFICIENT	K2RG	0.280	
53	DEATH RATE DUE TO GRAZING	K2GRZC	0.100	d^{-1}
54	TEMPERATURE COEFFICIENT	K2GRZT	1.100	
55	FRACTION OF C ALLOCATED TO STRUCTURAL PURPOSES	FSC2	0.10	
56	CARBON TO CHLOROPHYLL RATIO	WCCHL2	65.0	mg C (mg chl)$^{-1}$
57	CARBON TO PHOSPHORUS RATIO - NON-P LIMITED	WCP2	40.000	mg C (mg P)$^{-1}$
58	CARBON TO NITROGEN RATIO - NON-N LIMITED	WCN2	5.670	mg C (mg N)$^{-1}$
59	CARBON TO SILICA RATIO - NON-SI LIMITED	WCS2	7.000	mg C (mg Si)$^{-1}$
60	QUOTIENT OF NUTRIENT-LIMITED NUTRIENT:C RATIOS AT RELATIVE GROWTH RATES OF 0 AND 1	QF2	0.85	
61	CHLOROPHYLL SELF-SHADING EXTINCTION COEFFICIENT FOR ALGAL GROUP 2	XKC2	0.017	m^2 (mg chl) $^{-1}$
62	BASE ALGAL SETTLING RATE - GROUP 2	VSBAS2	0.300	m d^{-1}
63	NUTRIENT STRESSED ALGAL SETTLING RATE - GROUP 2	VSNTR2	0.700	m d^{-1}
	Algal Group 3			
73	OPTIMAL GROWTH TEMPERATURE FOR DIATOMS	TOPT3	14.0	^oC
74	TEMPERATURE CORRECTION EFFECT ON GROWTH RATE BELOW TOPT3	K3BETA1	0.004	$^oC^{-2}$
75	TEMPERATURE CORRECTION EFFECT ON GROWTH RATE ABOVE TOPT3	K3BETA2	0.006	$^oC^{-2}$
76	GROSS PHOTOSYNTHETIC RATE PER UNIT CELL (ASSOCIATED WITH PHOTOSYNTHETIC DARK REACTIONS)	GPRE3	2.5	d^{-1}

Order	Parameter definition	Symbol	Value	Unit
77	GROSS PHOTOSYNTHETIC RATE PER UNIT CELL PER UNIT LIGHT INTENSITY UNDER NUTRIENT-SATURATED CONDITIONS AND ZERO IRRADIANCE	GPR03	0.64 (0.28)	m^2 Ein^{-1}
78	SATURATING ALGAL LIGHT INTENSITY	IS3	000.0	Ein m^{-2} d^{-1}
79	HALF SATURATION CONSTANT FOR NITROGEN	KMN3	0.005	mg N l^{-1}
80	HALF SATURATION CONSTANT FOR PHOSPHOROUS	KMP3	0.001	mg P l^{-1}
81	HALF SATURATION CONSTANT FOR SILICA	KMS3	0.040	mg Si l^{-1}
82	BASAL OR RESTING RESPIRATION RATE	K3RB	0.030	d^{-1}
83	TEMPERATURE COEFFICIENT FOR BASAL/ENDOGENOUS RESPIRATION	K3RT	1.0	dimensionless
84	GROWTH-RATE-DEPENDENT RESPIRATION COEFFICIENT	K3RG	0.280	dimensionless
85	DEATH RATE DUE TO GRAZING	K3GRZC	0.100	d^{-1}
86	TEMPERATURE COEFFICIENT	K3GRZT	1.100	dimensionless
87	FRACTION OF C ALLOCATED TO STRUCTURAL PURPOSES	FSC3	0.10	dimensionless
88	CARBON TO CHLOROPHYLL RATIO	WCCHL3	15.0	mg C (mg chl)$^{-1}$
89	CARBON TO PHOSPHORUS RATIO - NON-P LIMITED	WCP3	40.000	mg C (mg P)$^{-1}$
90	CARBON TO NITROGEN RATIO - NON-N LIMITED	WCN3	5.670	mg C (mg N)$^{-1}$
91	CARBON TO SILICA RATIO - NON-SI LIMITED	WCS3	2.500	mg C (mg Si)$^{-1}$
92	QUOTIENT OF NUTRIENT-LIMITED NUTRIENT:C RATIOS AT RELATIVE GROWTH RATES OF 0 AND 1	QF3	0.85	
93	CHLOROPHYLL SELF-SHADING EXTINCTION COEFFICIENT FOR ALGAL GROUP 3	XKC3	0.017	m^2 (mg chl) $^{-1}$
94	BASE ALGAL SETTLING RATE - GROUP 3	VSBAS3	0.300	m d^{-1}
95	NUTRIENT STRESSED ALGAL SETTLING RATE - GROUP 3	VSNTR3	1.000	m d^{-1}
	Biogeochemical parameters			
105	HALF SATURATION CONSTANT FOR PHYTOPLANKTON RECYCLE FRACTIONS MG C/L	KMPHYT	0.050	mg C l^{-1}
106	REFRACTORY PARTICULATE ORGANIC PHOSPHOROUS	FRPOP	0.150	
107	LABILE PARTICULATE ORGANIC PHOSPHOROUS	FLPOP	0.300	
108	REFRACTORY DISSOLVED ORGANIC PHOSPHOROUS	FRDOP	0.100	
109	LABILE DISSOLVED ORGANIC PHOSPHOROUS	FLDOP	0.150	
110	DISSOLVED INORGANIC PHOSPHOROUS	FPO4	0.300	
111	REFRACTORY PARTICULATE ORGANIC NITROGEN	FRPON	0.150	
112	LABILE PARTICULATE ORGANIC NITROGEN	FLPON	0.325	
113	REFRACTORY DISSOLVED ORGANIC NITROGEN	FRDON	0.150	
114	LABILE DISSOLVED ORGANIC NITROGEN	FLDON	0.175	
115	AMMONIA	FNH4	0.200	
116	REFRACTORY PARTICULATE ORGANIC CARBON	FRPOC	0.150	
117	LABILE PARTICULATE ORGANIC CARBON	FLPOC	0.350	
118	REFRACTORY DISSOLVED ORGANIC CARBON	FRDOC	0.100	

Order	Parameter definition	Symbol	Value	Unit
119	LABILE DISSOLVED ORGANIC CARBON PHOSPHORUS	FLDOC	0.400	
120	HYDROLYSIS RATE OF RPOP TO RDOP	K57C	0.010	d^{-1}
121	TEMPERATURE COEFFICIENT	K57T	1.080	
122	HYDROLYSIS RATE OF LPOP TO LDOP	K68C	0.050	d^{-1}
123	TEMPERATURE COEFFICIENT	K68T	1.080	
124	MINERALIZATION RATE OF RDOP TO PO4	K79C	0.010	d^{-1}
125	TEMPERATURE COEFFICIENT	K79T	1.080	
126	MINERALIZATION RATE OF LDOP TO PO4	K89C	0.100	d^{-1}
127	TEMPERATURE COEFFICIENT NITROGEN	K89T	1.080	
128	HYDROLYSIS RATE OF RPON TO RDON	K1012C	0.008	d^{-1}
129	TEMPERATURE COEFFICIENT	K1012T	1.080	
130	HYDROLYSIS RATE OF LPON TO LDON	K1113C	0.050	d^{-1}
131	TEMPERATURE COEFFICIENT	K1113T	1.080	
132	MINERALIZATION RATE of RDON TO NH4	K1214C	0.008	d^{-1}
133	TEMPERATURE COEFFICIENT	K1214T	1.080	
134	MINERALIZATION RATE OF LDON TO NH4	K1314C	0.050	d^{-1}
135	TEMPERATURE COEFFICIENT NITRIFICATION/DENITRIFICATION RATES	K1314T	1.080	
136	NITRIFICATION RATE AT 20 DEG C	K1415C	0.100	d^{-1}
137	TEMPERATURE COEFFICIENT	K1415T	1.080	
138	HALF SATURATION CONSTANT FOR NITRIF- ICATION OXYGEN LIMITATION	KNIT	1.000	mg O_2 l^{-1}
139	DENITRIFICATION RATE AT 20 DEG C	K150C	0.050	d^{-1}
140	TEMPERATURE COEFFICIENT	K150T	1.045	
141	MICHAELIS CONSTANT FOR DENITRIFICATION OXYGEN LIMITATION SILICA MINERALIZATION RATES AT 20 DEG C	KNO3	0.100	mg O_2 l^{-1}
142	MINERALIZATION RATE OF BIOGENIC SI TO AVAIL SI	K1617C	0.080	d^{-1}
143	TEMPERATURE COEFFICIENT CARBON HYDROLYSIS/OXIDATION RATES AT 20 DEG C	K1617T	1.080	
144	HYDROLYSIS RATE OF RPOC TO RDOC	K1820C	0.010	d^{-1}
145	TEMPERATURE COEFFICIENT	K1820T	1.080	
146	HYDROLYSIS RATE OF LPOC TO LDOC	K1921C	0.070	d^{-1}
147	TEMPERATURE COEFFICIENT	K1921T	1.080	
148	OXIDATION RATE OF RDOC	K200C	0.008	d^{-1}
149	TEMPERATURE COEFFICIENT	K200T	1.080	
150	OXIDATION RATE OF LDOC	K210C	0.100	d^{-1}
151	TEMPERATURE COEFFICIENT	K210T	1.080	
152	MICHAELIS CONSTANT FOR LDOC	KMLDOC	0.100	mg C l^{-1}
153	HALF SATURATION CONSTANT FOR ORG CARBON	KDOC	0.200	mg O_2 l^{-1}
154	ALGAL EXUDATE DOC OXIDATION RATE	K220C	0.300	d^{-1}
155	TEMPERATURE COEFFICIENT	K220T	1.047	
156	FRACTION OF PRIMARY PRODUCTIVITY GOING TO LABILE ORGANIC CARBON VIA EXUDATION REPOC/REDOC ARE ASSOCIATED WITH SANITARY/CSO SOLIDS	FLOCEX	0.100	
157	HYDROLYSIS RATE OF REPOC TO REDOC	K2324C	0.01	d^{-1}
158	TEMPERATURE COEFFICIENT	K2324T	1.0	
159	REACTIVE DOC OXIDATION RATE	K240C	0.150	d^{-1}
160	TEMPERATURE COEFFICIENT	K240T	1.047	

Order	Parameter definition	Symbol	Value	Unit
161	CARBON TO PHOSPHORUS RATIO OF CSO SOLIDS	CTOPCSO	0.0	
162	CARBON TO NITROGEN RATIO OF CSO SOLIDS	CTONCSO	0.0	
163	OXIDATION RATE FOR AQUEOUS SOD	K250C	0.150	d^{-1}
164	TEMPERATURE COEFFICIENT	K250T	1.080	
165	HALF SATURATION CONSTANT FOR O2*	KO2EQ	0.100	mg O_2 l^{-1}
166	MINIMUM VALUE FOR KL	KLMIN	0.0	m d^{-1}
167	DIFFUSIVITY OF OXYGEN ACROSS THE AIR-WATER INTERFACE	DIFUS	0.0	m^2 d^{-1}
168	TEMPERATURE CORRECTION COEFFICIENT FOR ATMOSPHERIC REAERATION	KAT	1.024	
169	TEMPERATURE CORRECTION	VSBAST	1.027	
170	PARTICULATE ORGANIC MATTER SETTLING RATE	VSPOM	1.000	m d^{-1}
171	TEMPERATURE CORRECTION	VSPMT	1.027	
172	TEMPERATURE CORRECTION FOR DEPOSITION TO SEDIMENT	VSSEDT	1.027	
173	POWER COEFF. FOR CSO SOLID SETTLING RATE (>=1	BVCSO	1.0	dimensionless
174	CRITICAL REPOC CONC. FOR CSO SETTLING FUNCTION	CRCSO	1.0	mg C l^{-1}
175	MINIMUM SETTLING RATE FOR CSO SOLIDS Vcso = VMINCSO+(VMAXCSO-VMINCSO)*(REPOC/CRCSO)**BVCSO)	VMINCSO	0.0	m d^{-1}
176	MAXIMUM SETTLING RATE FOR CSO SOLIDS	VMAXCSO	0.0	m d^{-1}
177	PARTITION COEFFICIENT FOR SORBED PHOSPHORUS	KADPO4	6.0	l mg SS^{-1}
178	PARTITION COEFFICIENT FOR SORBED SILICA	KADSI	6.0	l mg SS^{-1}
179	SETTLING RATE FOR PHOSPHORUS/SILICA SORBED TO SUSPENDED SOLIDS	VSPIM	0.0	m d^{-1}
180	BASE (CHL-A CORRECTED) EXTINCTION COEFFICIENT (USED WHEN KEOPT=0,2)	KECONST	0.001	m^{-1}

Table 2. 3 Data-model conversion for the MWRA effluent, rivers, and other sources.

	Model		**Conversion**	**Data**	
Variable	Definition	Units	Function	Variable	Units
Flow	Sewage flow	L day^{-1}	3.785mflow	mflow	gallon d^{-1}
TOC	Total organic C	mg C d^{-1}	0.7CBOD+18	CBOD	mg O d^{-1}
RPOC	Refractory POC	mg C d^{-1}	9	CBOD	mg O d^{-1}
LPOC	Labile POC	mg C d^{-1}	0.198CBOD	CBOD	mg O d^{-1}
RDOC	Refractory DOC	mg C d^{-1}	9	CBOD	mg O d^{-1}
LDOC	Labile DOC	mg C d^{-1}	0.132CBOD	CBOD	mg O d^{-1}
REDOC	Reactive DOC	mg C d^{-1}	0.37CBOD	CBOD	mg O d^{-1}
TON	Total organic N	mg N d^{-1}	(TKN-NH4)/1000	TKN	μg N d^{-1}
RPON	Refractory PON	mg N d^{-1}	0.4(TKN-NH4)/1000	TKN	μg N d^{-1}
LPON	Labile PON	mg N d^{-1}	0.4(TKN-NH4)/1000	TKN	μg N d^{-1}
RDON	Refractory DON	mg N d^{-1}	0.1(TKN-NH4)/1000	TKN	μg N d^{-1}
LDON	Labile DON	mg N d^{-1}	0.1(TKN-NH4)/1000	TKN	μg N d^{-1}
TOP	Total organic P	mg P d^{-1}	(TP-PO4)/1000	TP	μg P d^{-1}
RPOP	Refractory POP	mg P d^{-1}	0.3(TP-PO4)/1000	TP	μg P d^{-1}
LPOP	Labile POP	mg P d^{-1}	0.55(TP-PO4)/1000	TP	μg P d^{-1}
RDOP	Refractory DOP	mg P d^{-1}	0.05(TP-PO4)/1000	TP	μg P d^{-1}
LDOP	Labile DOP	mg P d^{-1}	0.1(TP-PO4)/1000	TP	μg P d^{-1}

Table 2. 4 Partition coefficients for organic substances in seawater and river water.

		Labile	Refractory	Reactive	Exudate
Nitrogen	PON	0.5	0.5		
	DON	0.5	0.5		
Phosphorus	POP	0.647	0.353		
	DOP	0.66	0.33		
Carbon	POC	0.4	0.6	-	-
	DOC	0.2	0.7	0.05	0.05

Table 2. 5 Partition coefficients of chlorophyll to phytoplankton groups at the open boundary.

	Winter-spring group	Summer group	Fall group
January-April	1.0	0	0
May	0.5	0.5	0
June-July	0	1.0	0
August	0	0.5	0.5
September-November	0	0	1.0
December	0.5	0	0.5

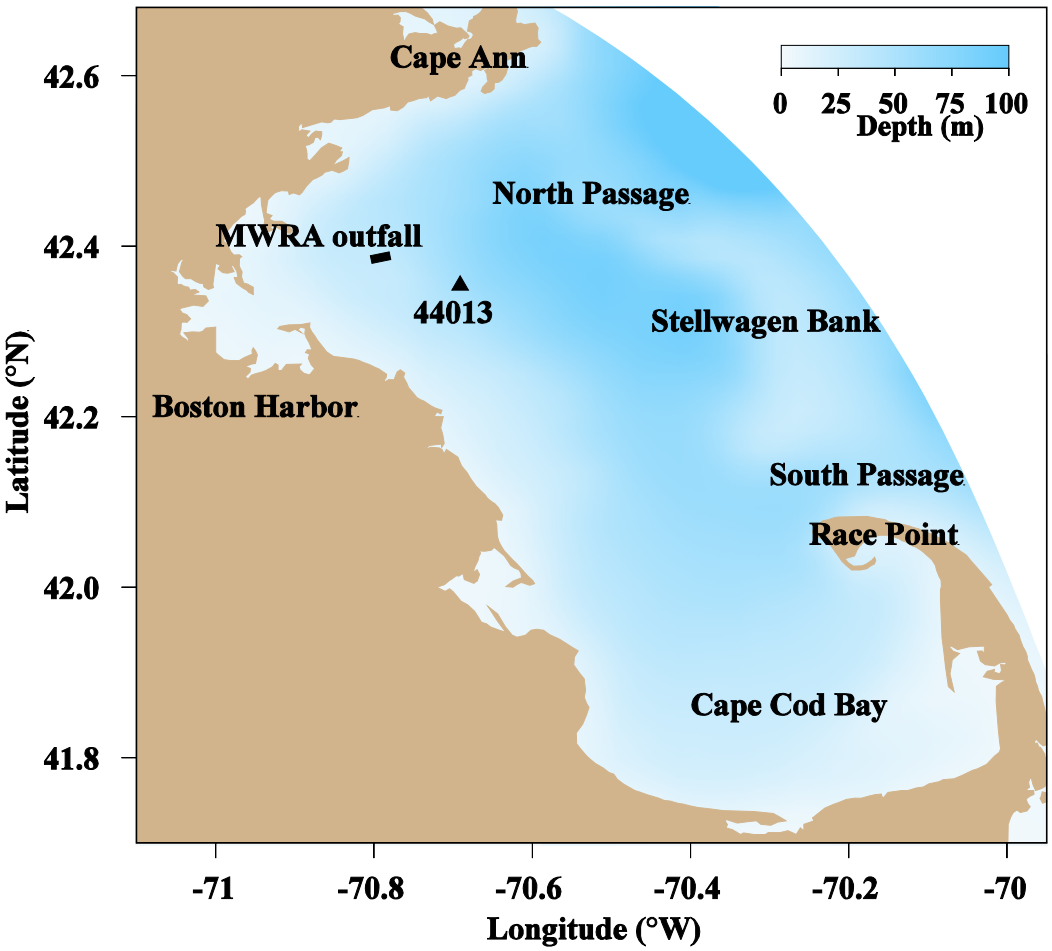

Figure 1. 1 The Massachusetts Bay system (MBS) and location of the MWRA outfall and Buoy 44013.

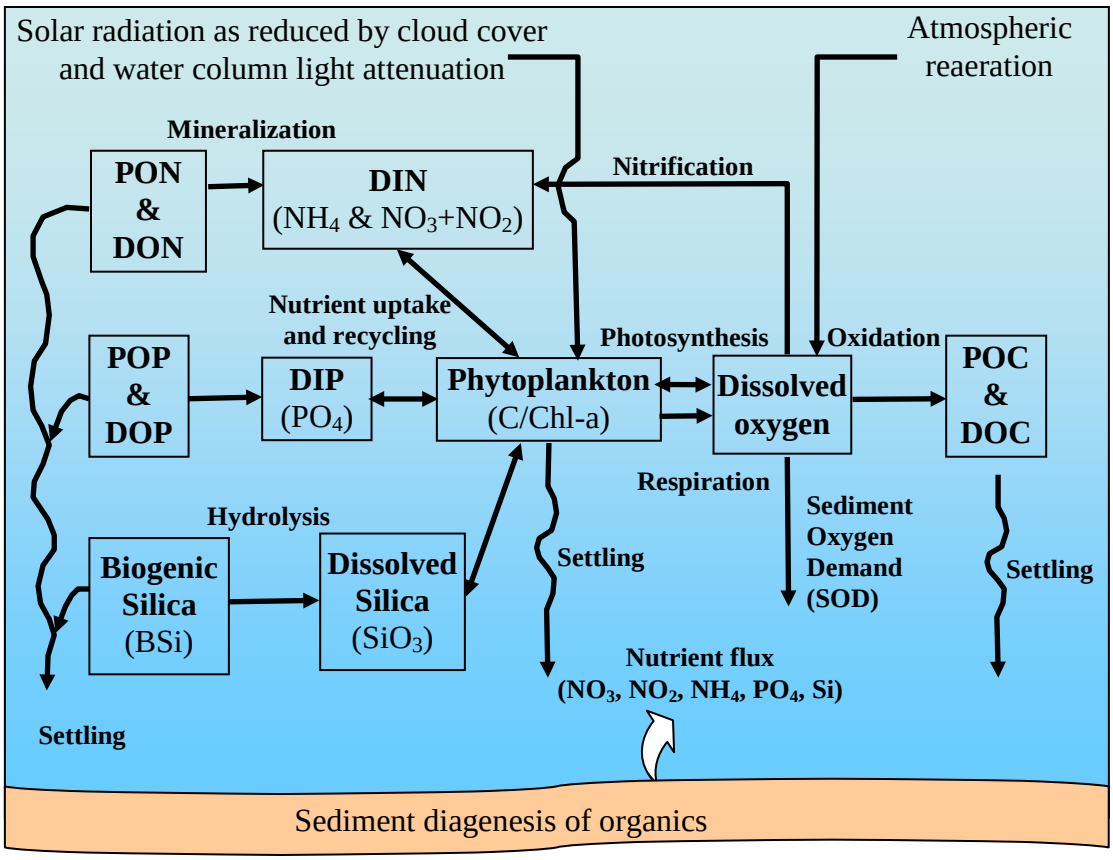

Figure 2. 1 The UG-RCA water quality model (reproduced from HydroQual, 2004).

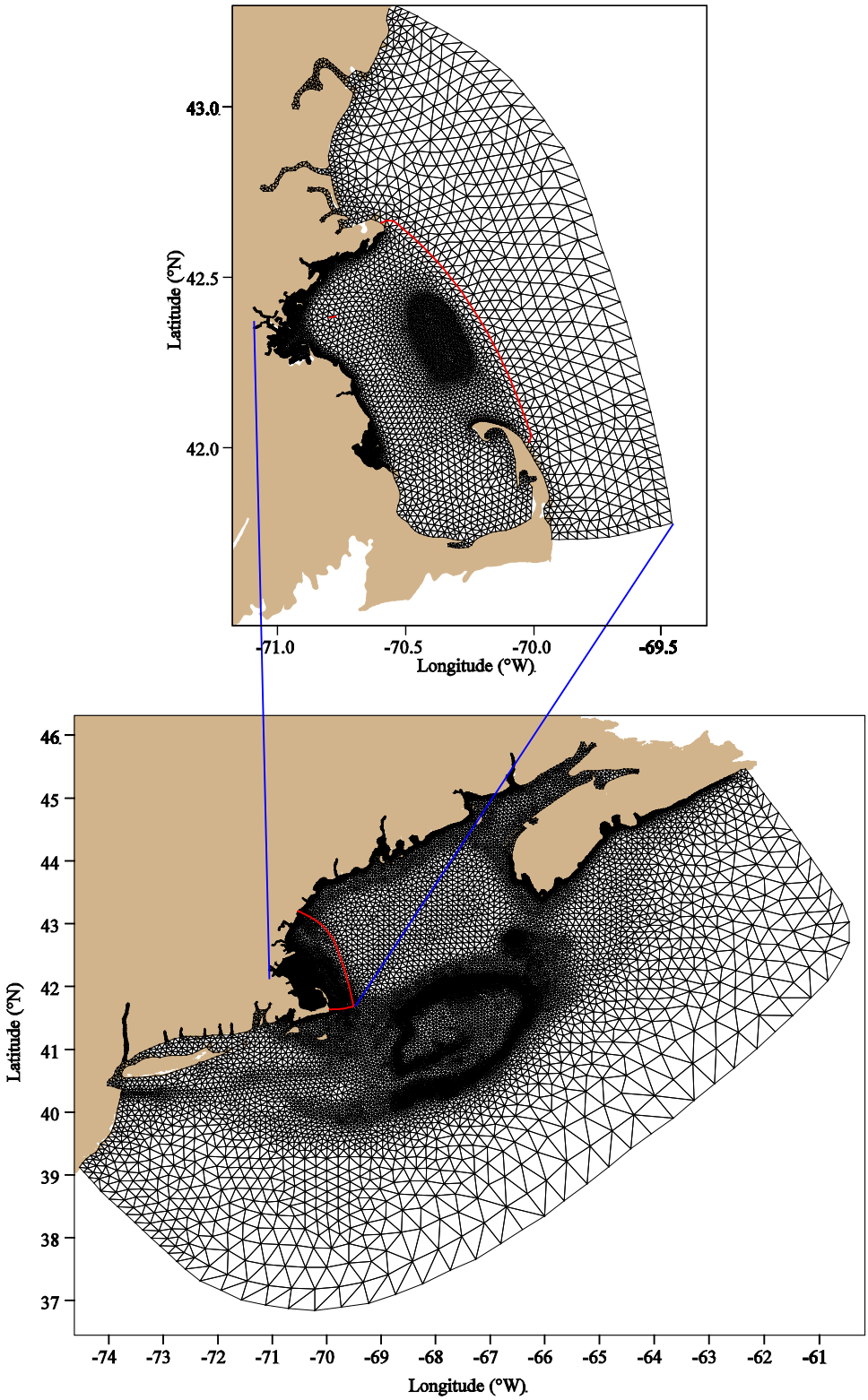

Figure 2. 2 Grid for Gulf-of-Maine FVCOM (lower panel); the red line shows the nested domain of Massachusetts Bay FVCOM. The upper panel shows the higher-resolution grid for MB-FVCOM; the red line shows the domain of the water quality model UG-RCA.

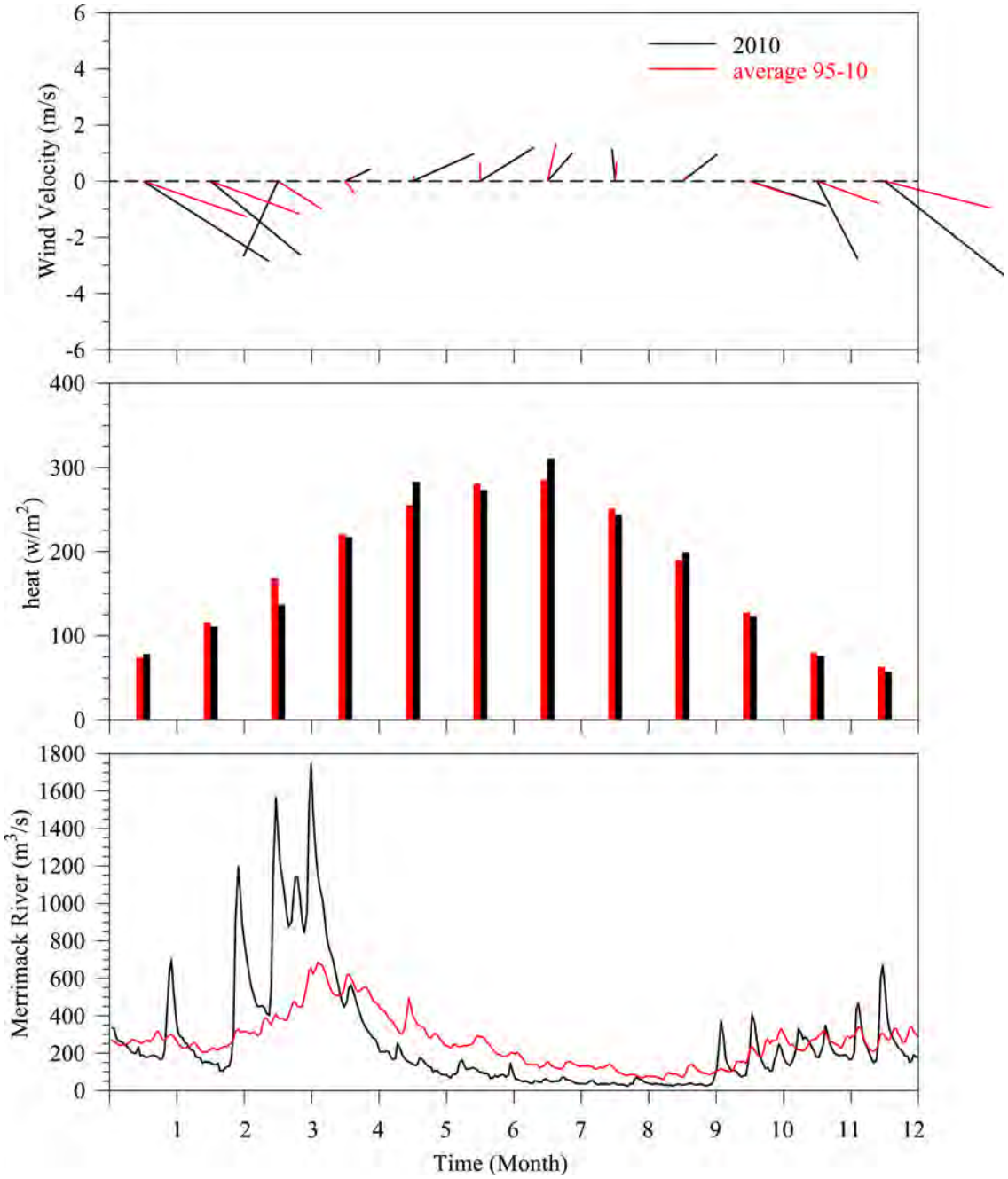

Figure 2. 3 Monthly-averaged wind (upper panel) and heat flux (mid panel) and daily-averaged discharge from Merrimack River in 2010 (black) and **the 16-year (1995-2010) average** (red).

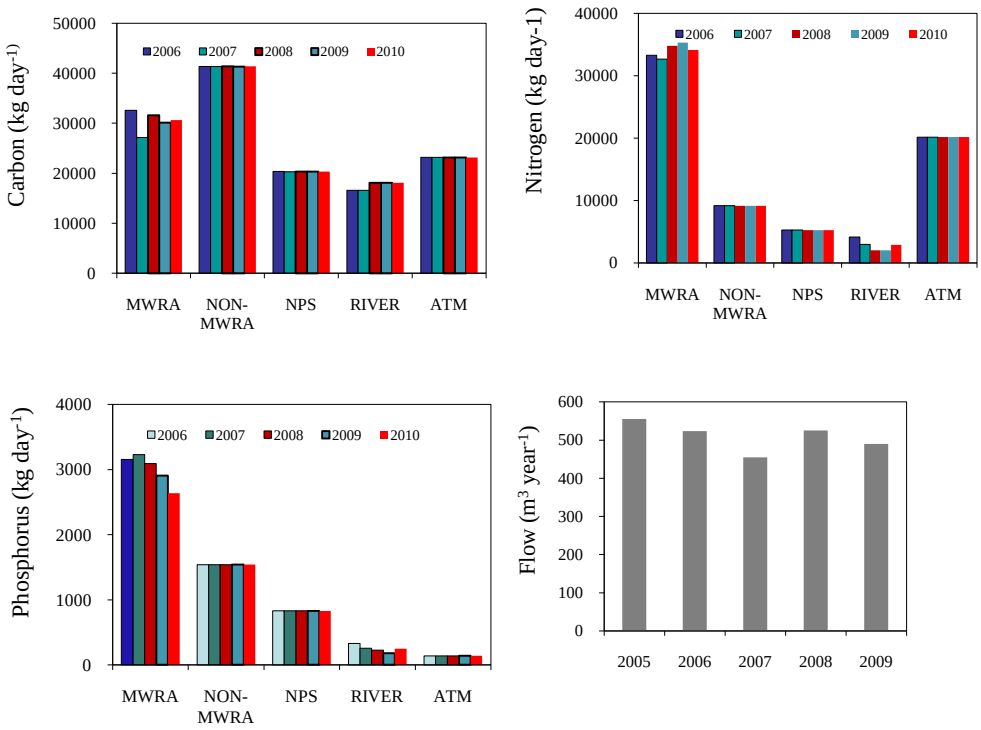

Figure 2. 4 Mean daily loads of carbon, nitrogen and phosphorus from different anthropogenic sources within Massachusetts Bay (does not include loads from cross-boundary fluxes). MWRA: MWRA outfall; Non-MWRA: Non MWRA point sources; NPS: Non-point sources; River: River loadings; ATM: Atmospheric input. The last panel depicts the total flow of the MWRA outfall.

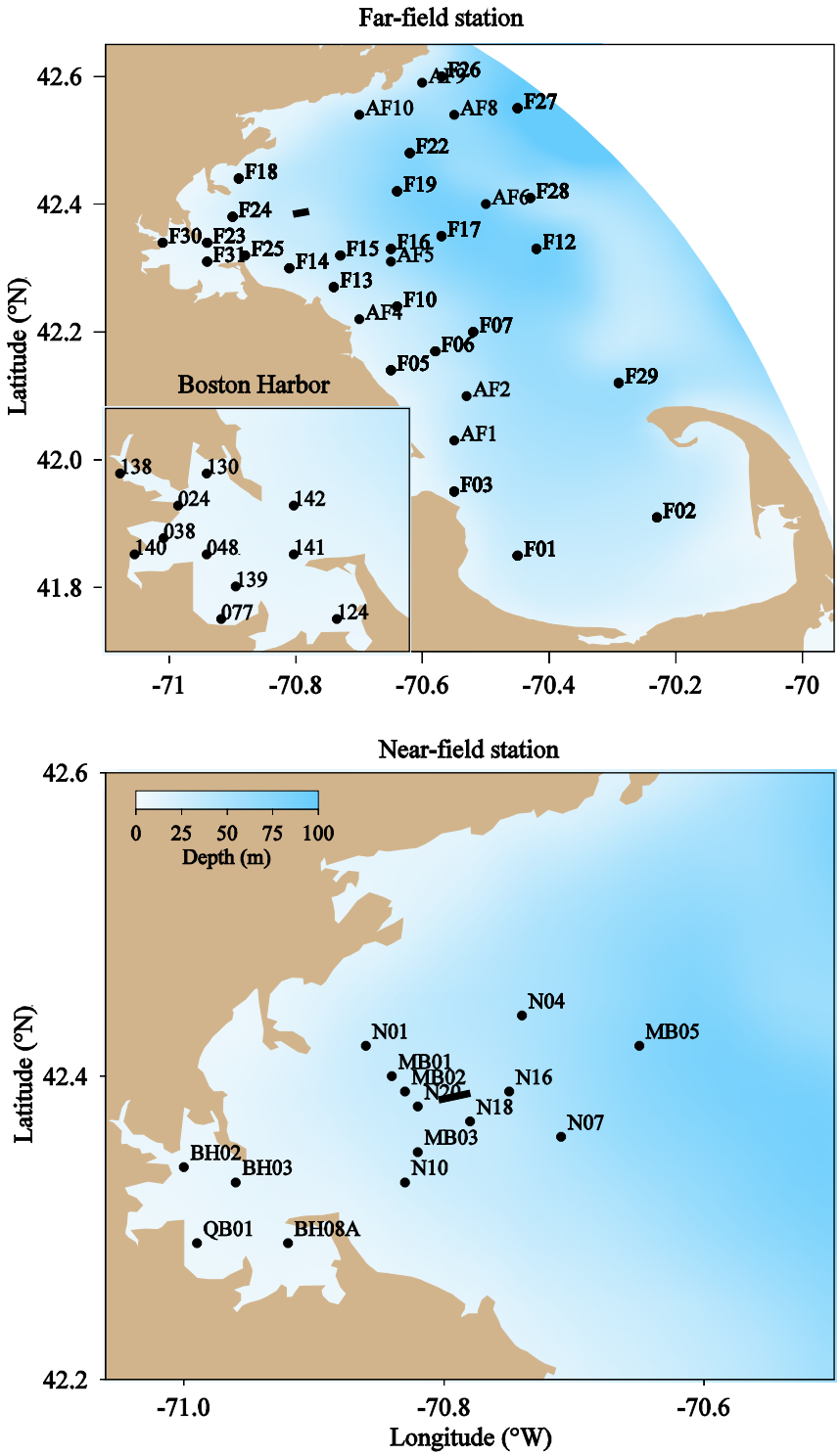

Figure 2. 5 Station locations: far-field (denoted with "F"), *Alexandrium* Rapid Response Study (denoted with "AF") and harbor stations in the upper panel, and near-field (denoted with "N"), harbor sediment flux (denoted with "BH" and "QB") and Massachusetts Bay sediment flux (denoted with "MB") stations in the lower panel. The bold line represents the location of the MWRA outfall.

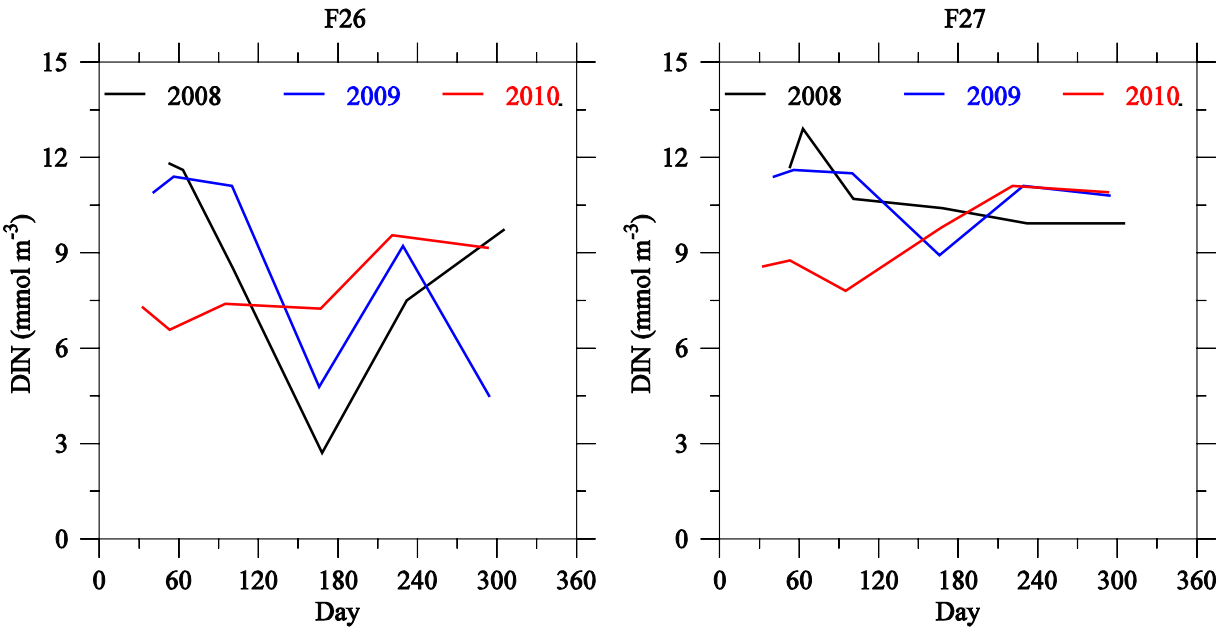

Figure 2. 6. Comparison of observed DIN concentration in the deep layer in 2008 (black line), 2009 (blue line) and 2010 (red line) at the two open boundary stations F26 and F27.

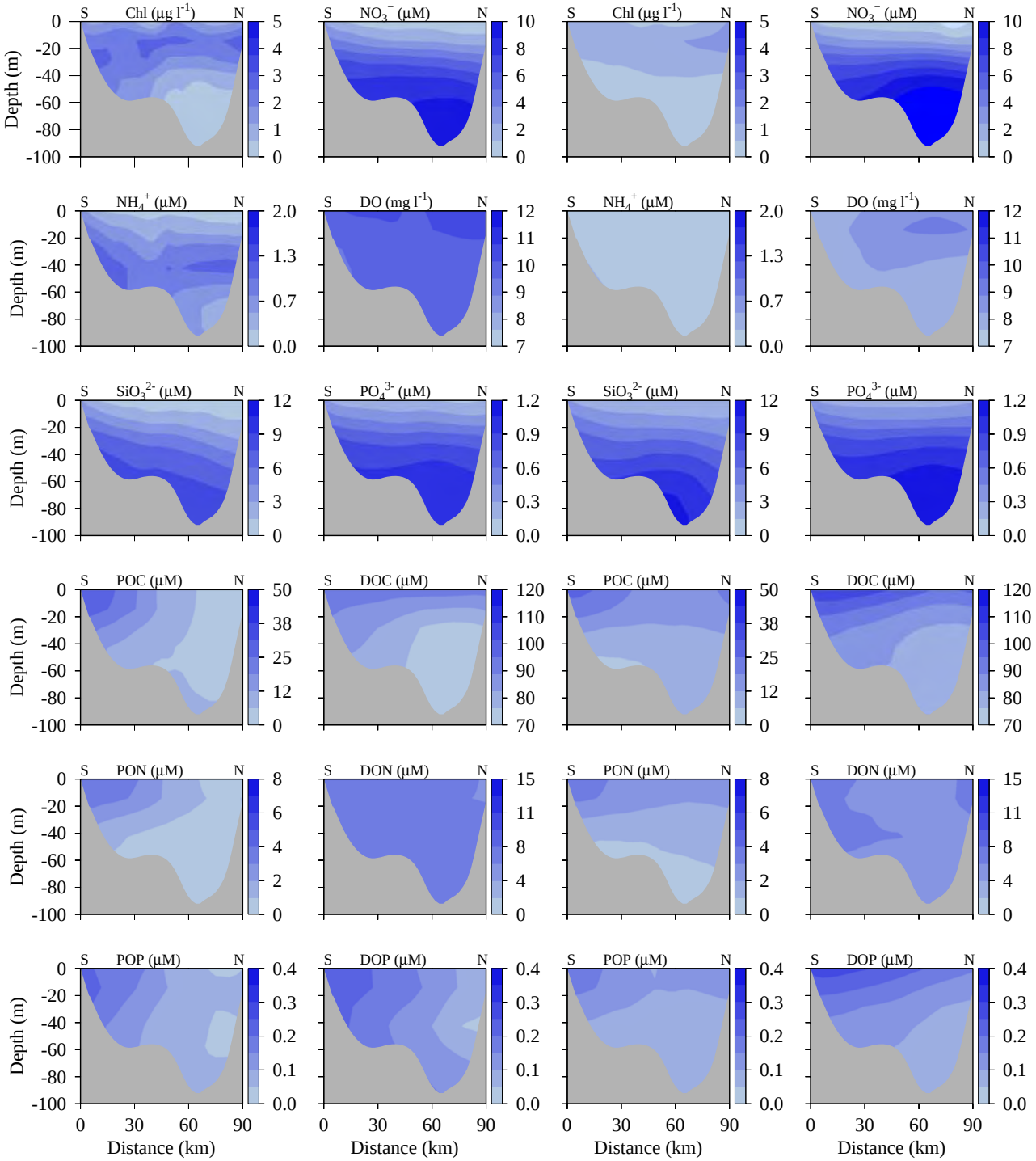

Figure 2. 7 Open boundary condition transects from Cape Cod (south S) to Cape Ann (north N) of chlorophyll, nutrients, DO and organic components on April 15 (left 12 panels) and August 15 (right 12 panels), 2010.

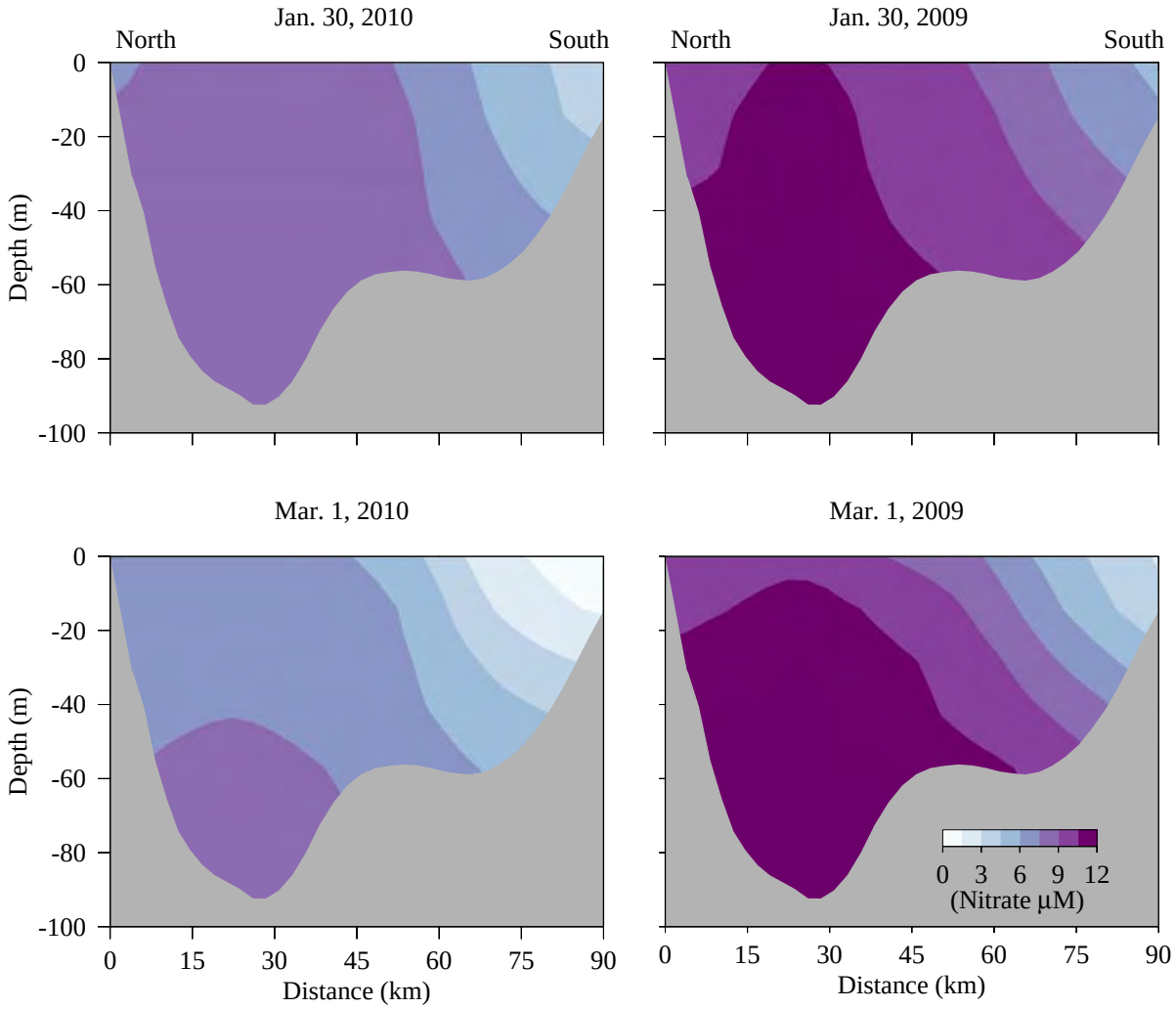

Figure 2. 8. Comparison of nitrate open boundary condition between 2010 (left panels) and 2009 (right panels) in winter on Jan. 30 (upper panels) and Mar. 1 (lower panels).

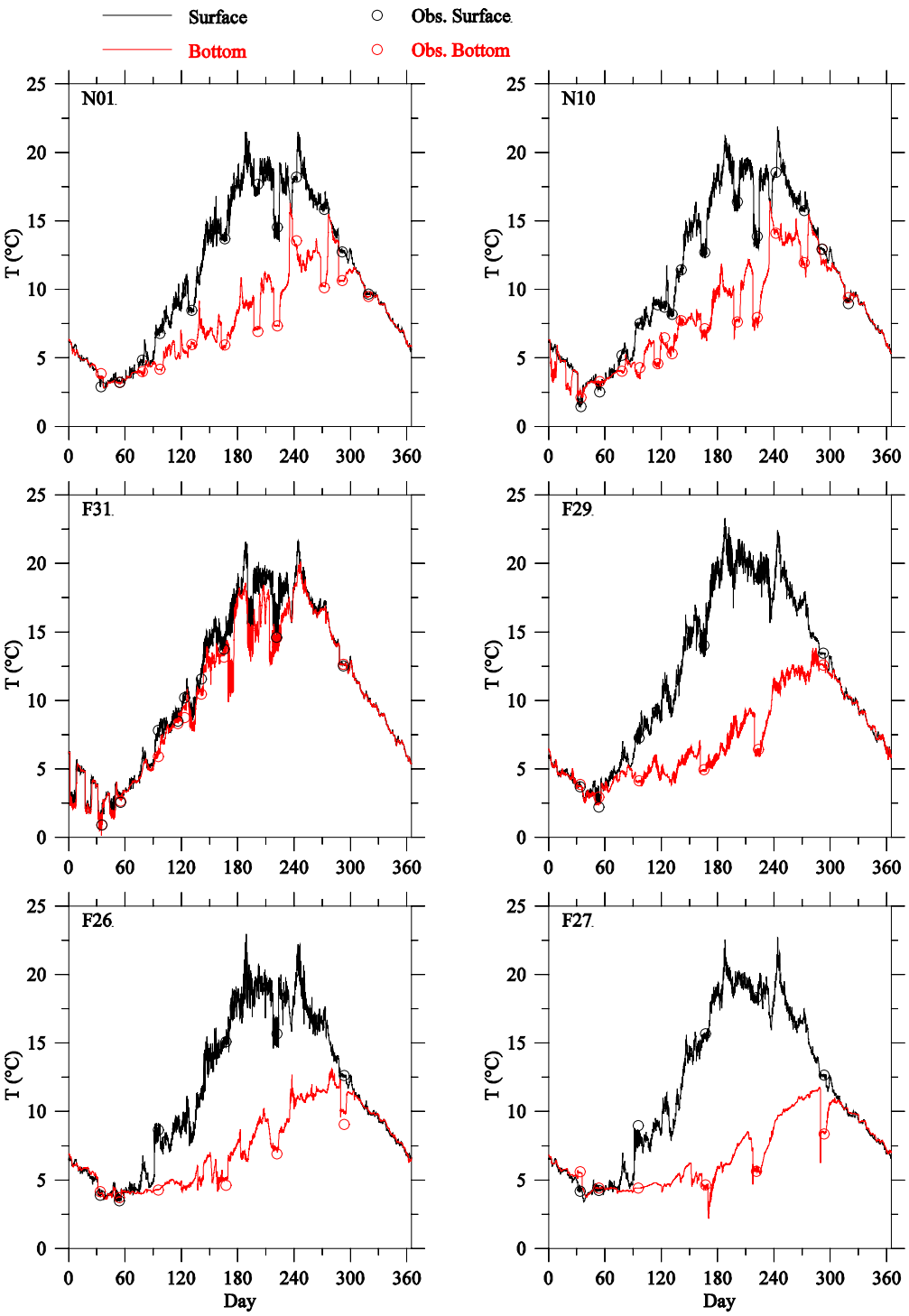

Figure 3. 1 Comparison of temperature observed (circles) and modeled (lines) time series at selected Massachusetts Bay monitoring stations in 2010.

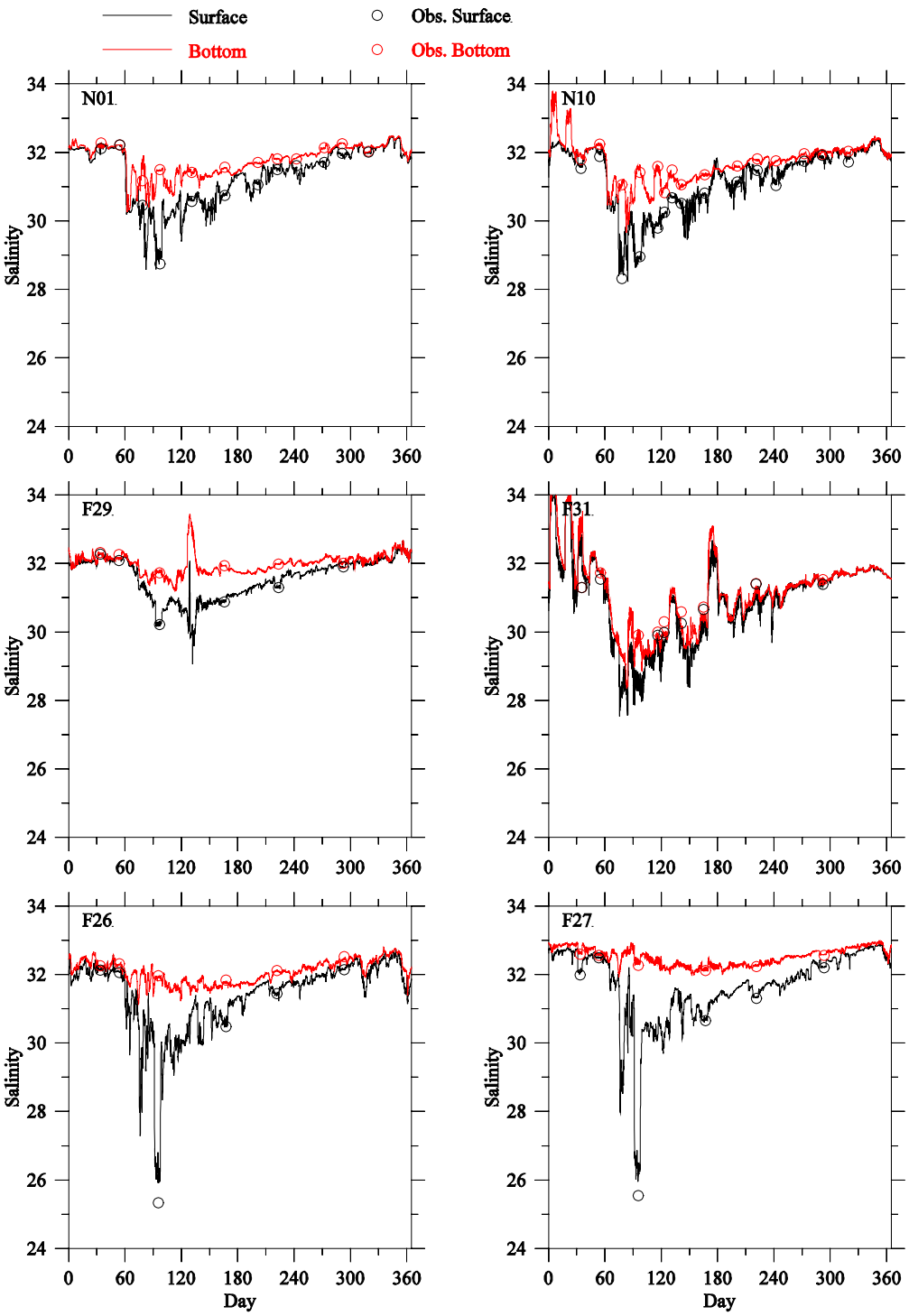

Figure 3. 2 Comparison of salinity observed (circles) and modeled (lines) time-series at selected Massachusetts Bay monitoring stations in 2010.

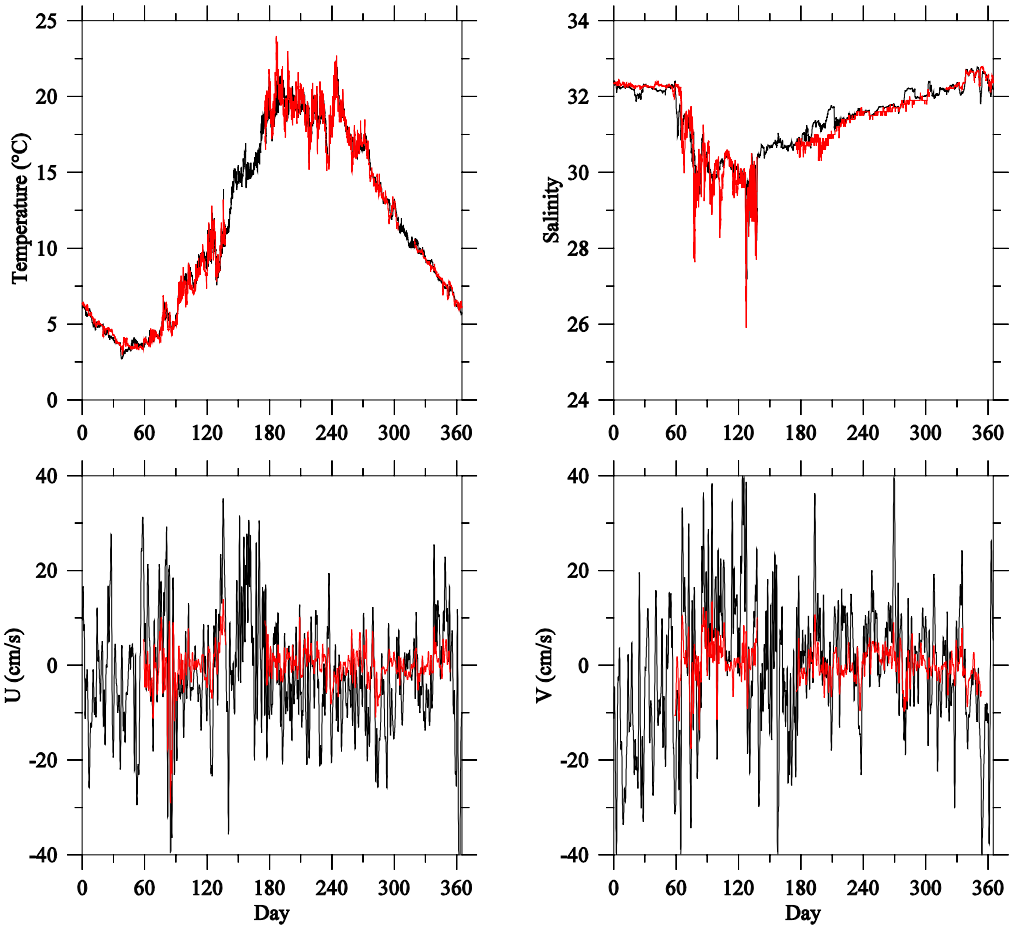

Figure 3. 3 Comparison of observed (red lines) and modeled (black lines) surface temperature, salinity and subtidal current U (west-east direction) and V (south-north direction) time series at Buoy 44013 in 2010. The buoy location is shown on Figure 1.1.

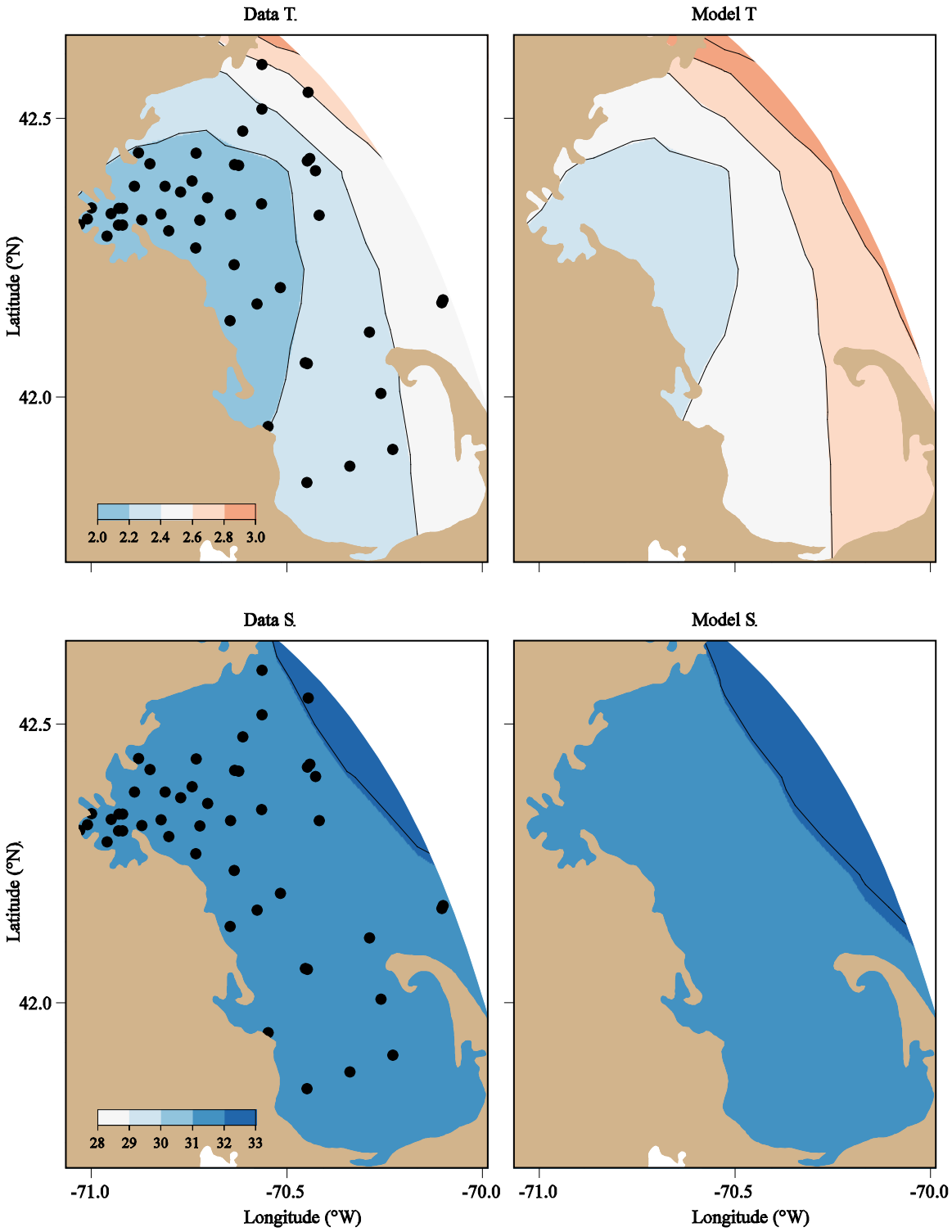

Figure 3. 4 Comparison between observed (left) and model-computed (right) near-surface temperatures (upper panels) and salinities (lower panels) in February 2010.

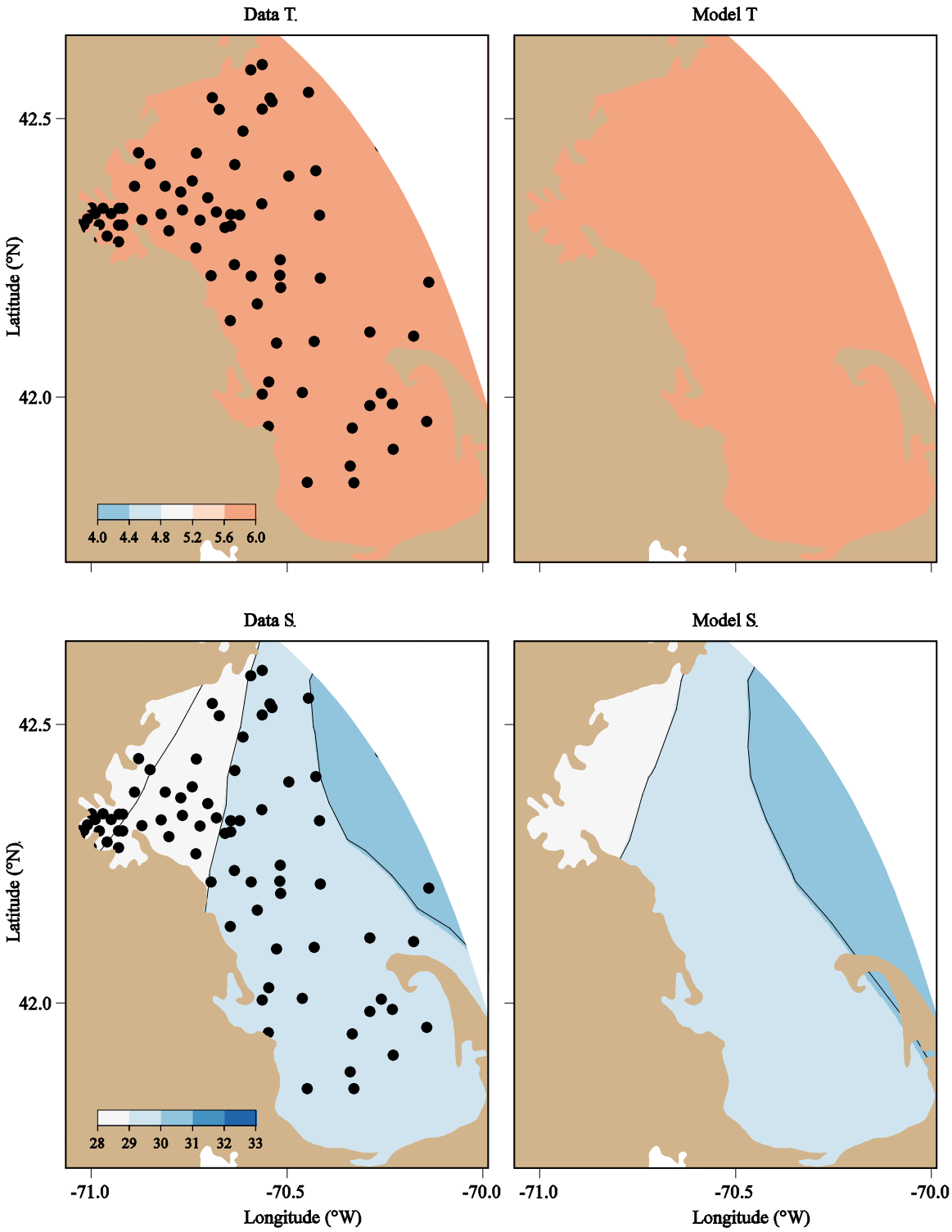

Figure 3. 5 Comparison between observed (left) and model-computed (right) near-surface temperatures (upper panels) and salinities (lower panels) in April 2010.

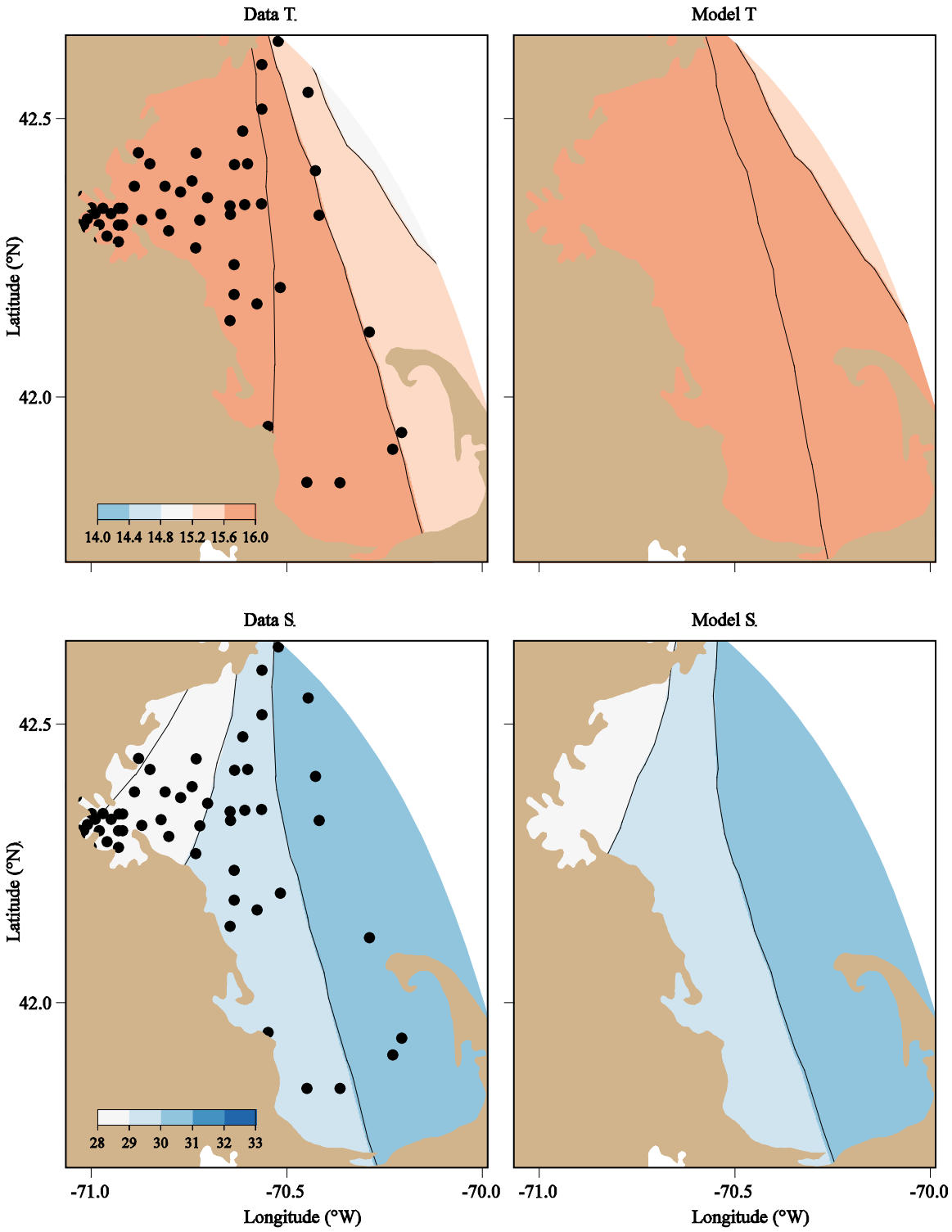

Figure 3. 6 Comparison between observed (left) and model-computed (right) near-surface temperatures (upper panels) and salinities (lower panels) in June 2010.

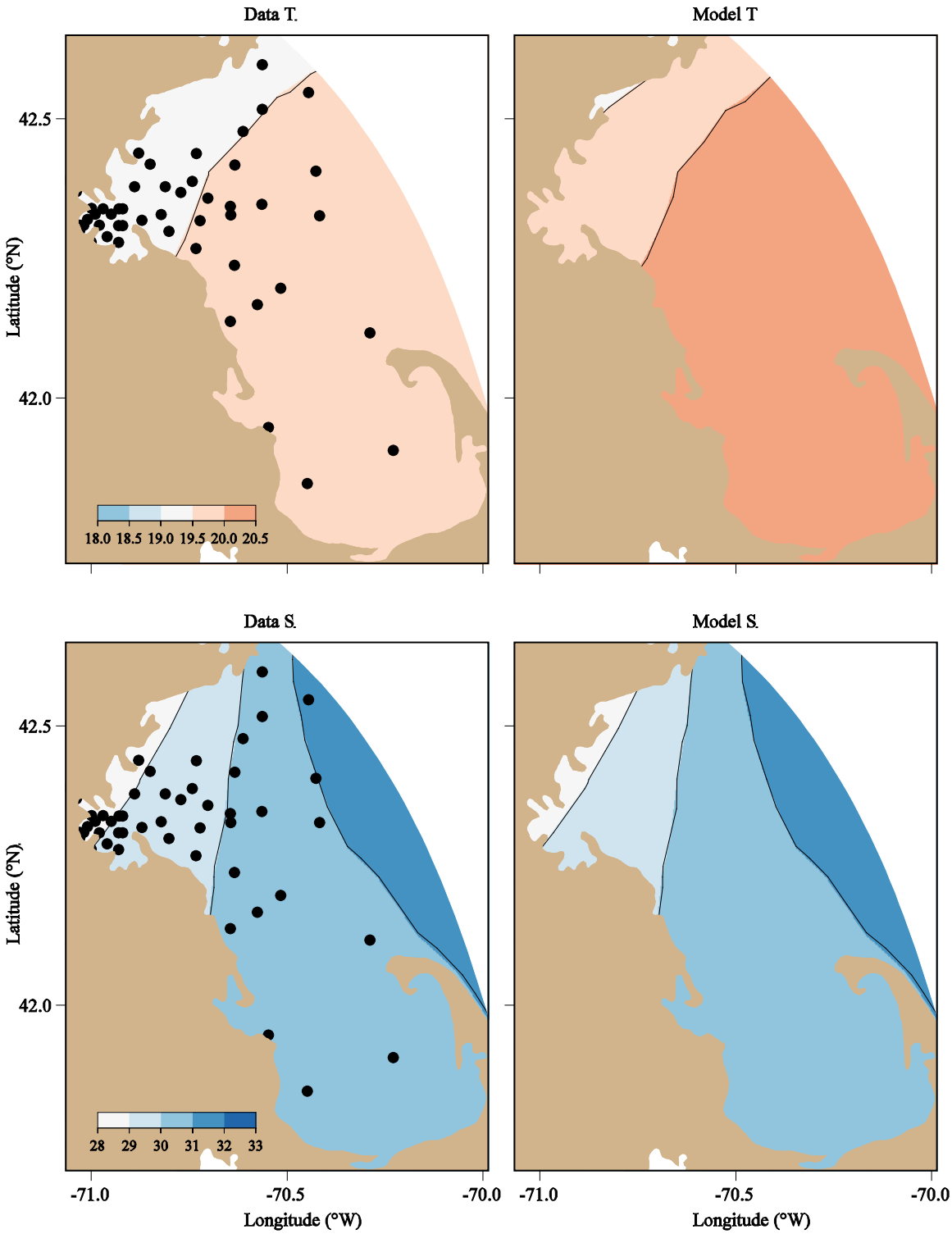

Figure 3. 7 Comparison between observed (left) and model-computed (right) near-surface temperatures (upper panels) and salinities (lower panels) in August 2010.

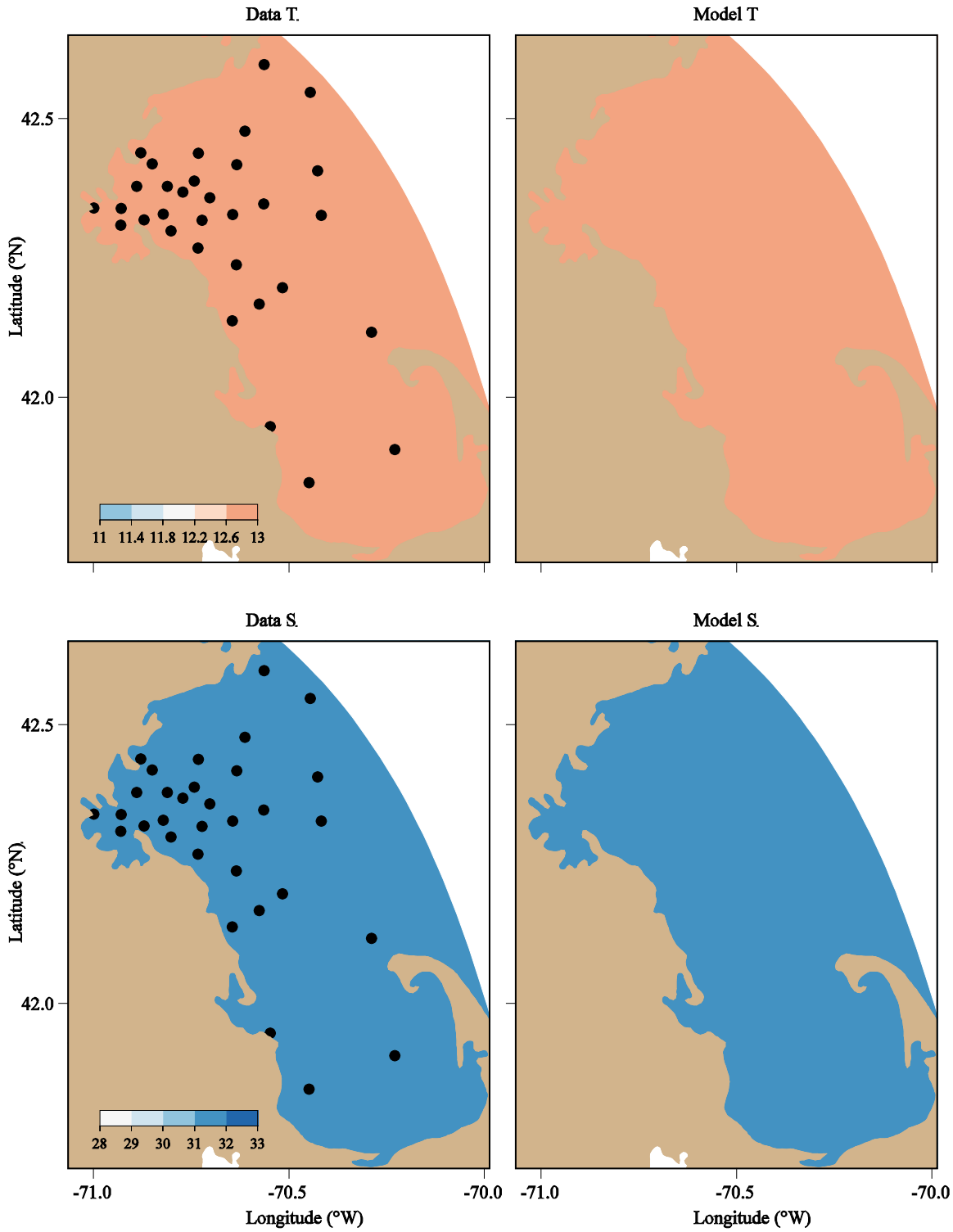

Figure 3. 8 Comparison between observed (left) and model-computed (right) near-surface temperatures (upper panels) and salinities (lower panels) in October 2010.

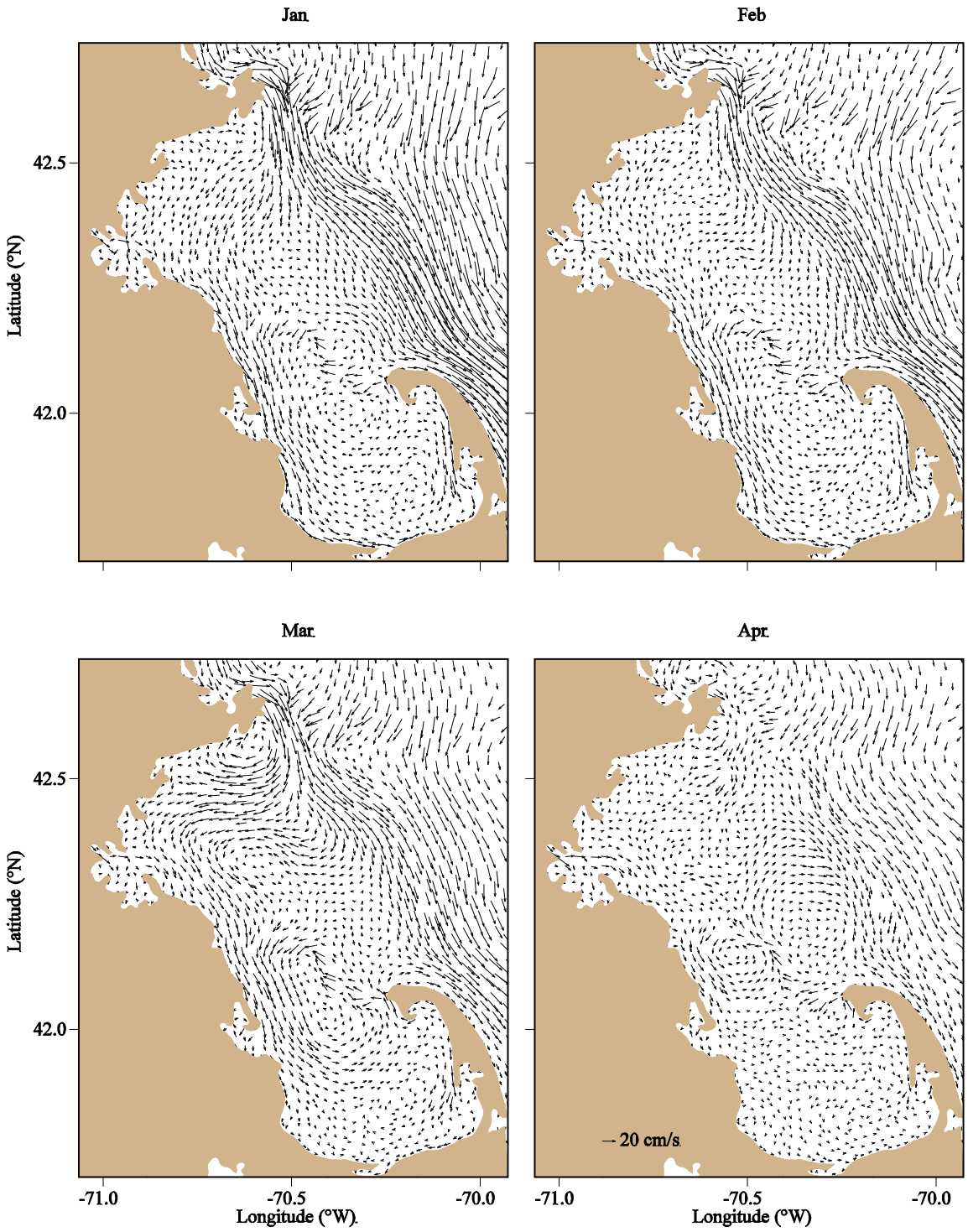

Figure 3. 9 Monthly-averaged surface current from January through April 2010 predicted by FVCOM.

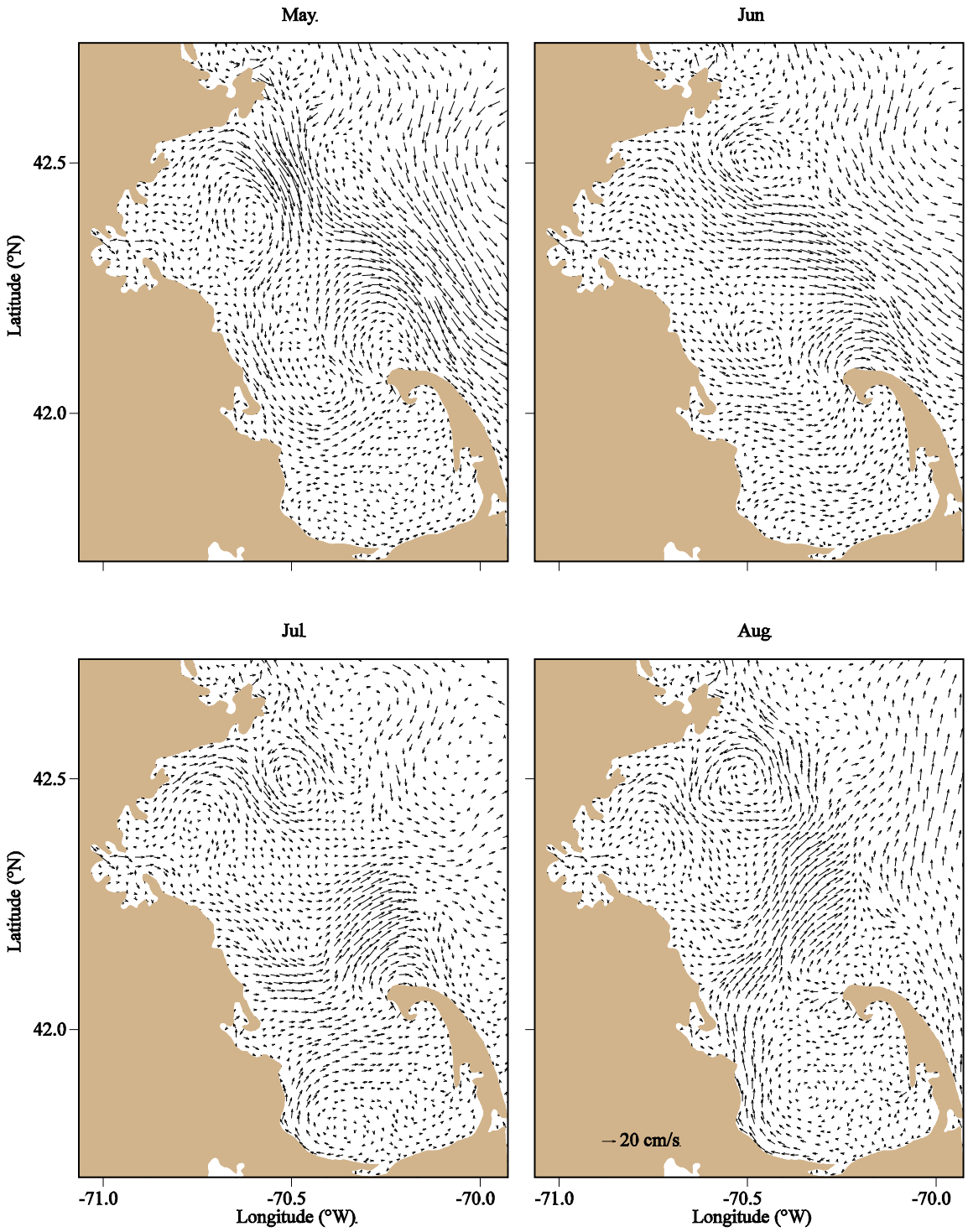

Figure 3. 10 Monthly-averaged surface current from May through August 2010 predicted by FVCOM.

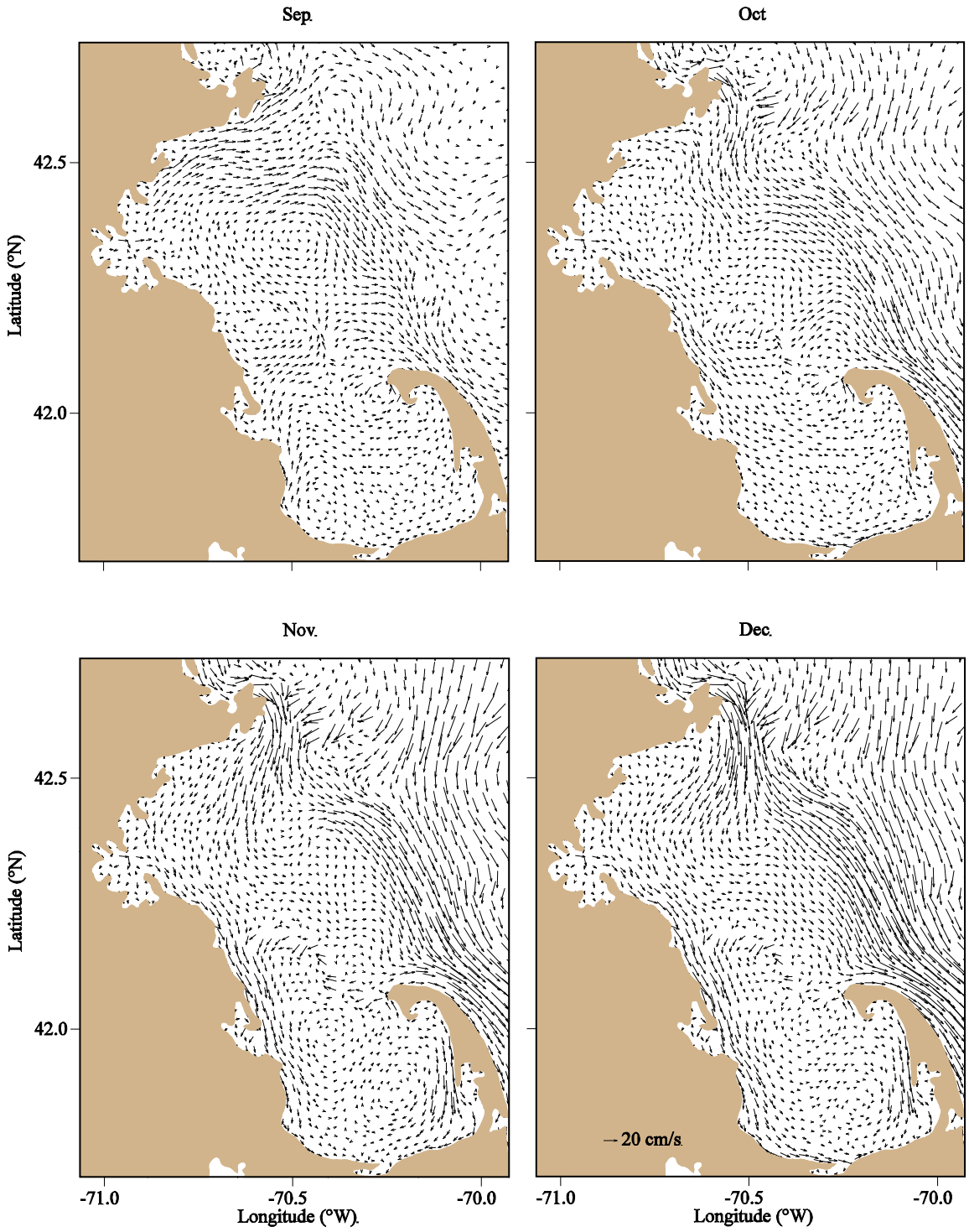

Figure 3. 11 Monthly-averaged surface current from September through December 2010 predicted by FVCOM.

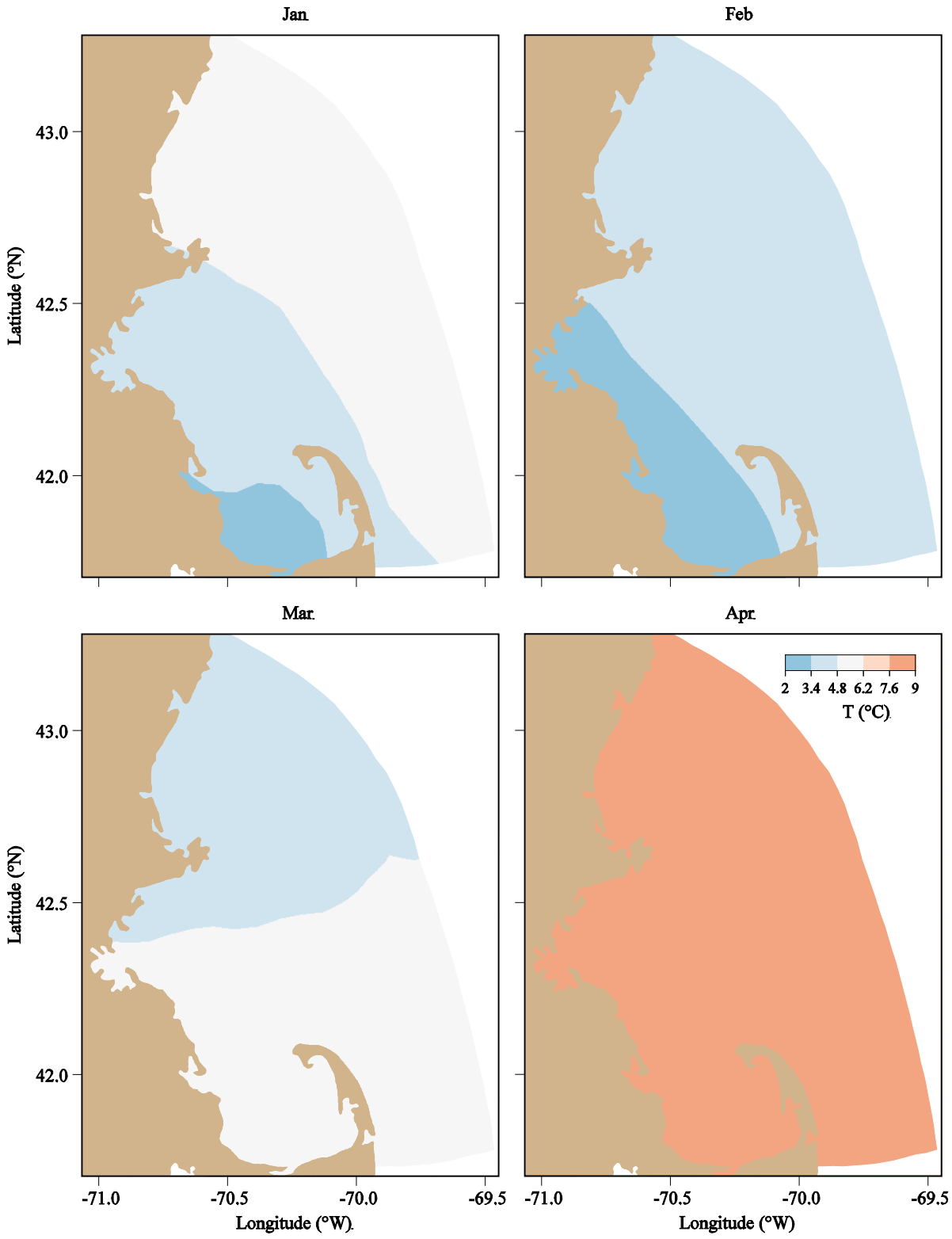

Figure 3. 12 Surface temperature at the end of January, February, March and April, 2010 predicted by FVCOM.

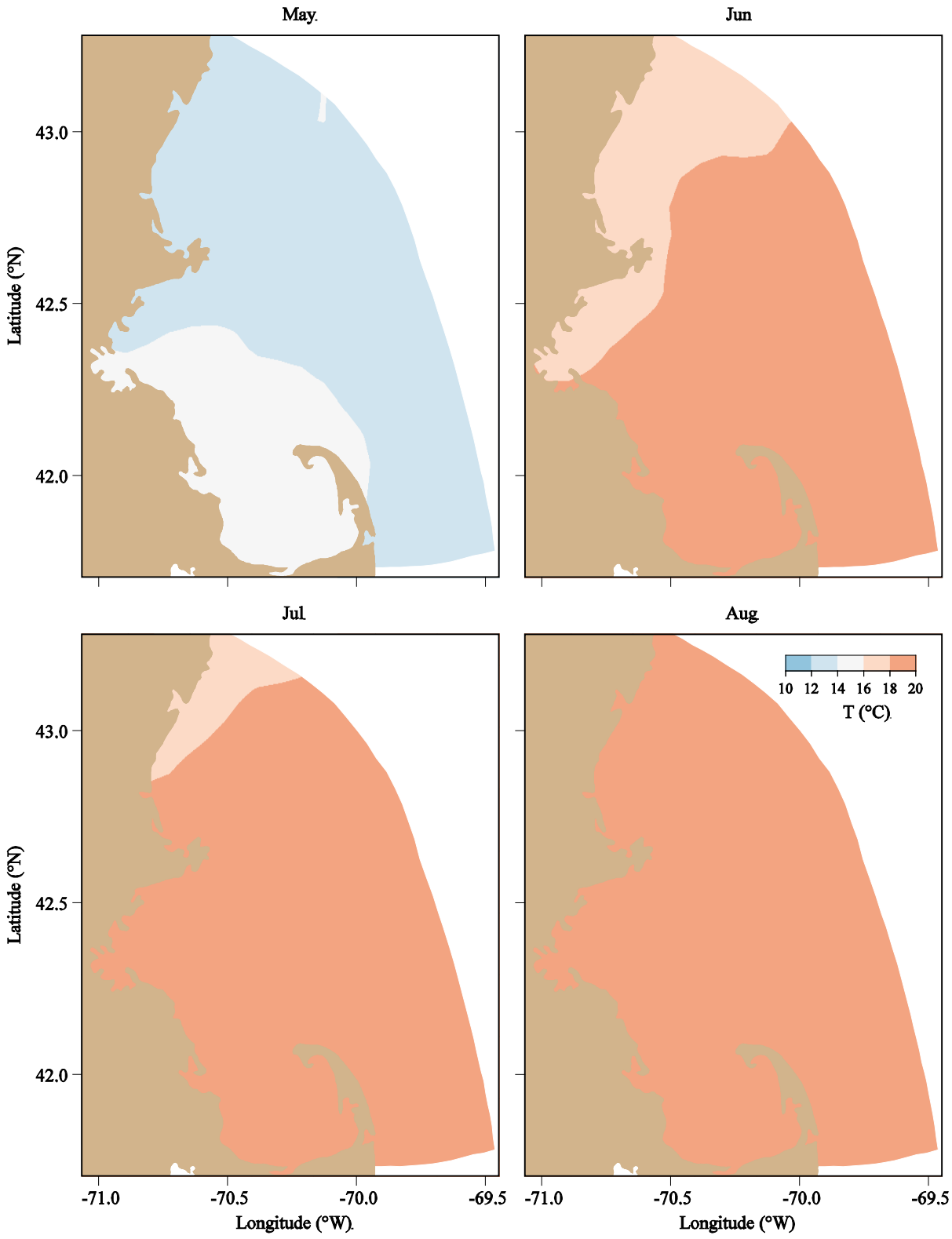

Figure 3. 13 Surface temperature at the end of May, June, July and August, 2010 predicted by FVCOM.

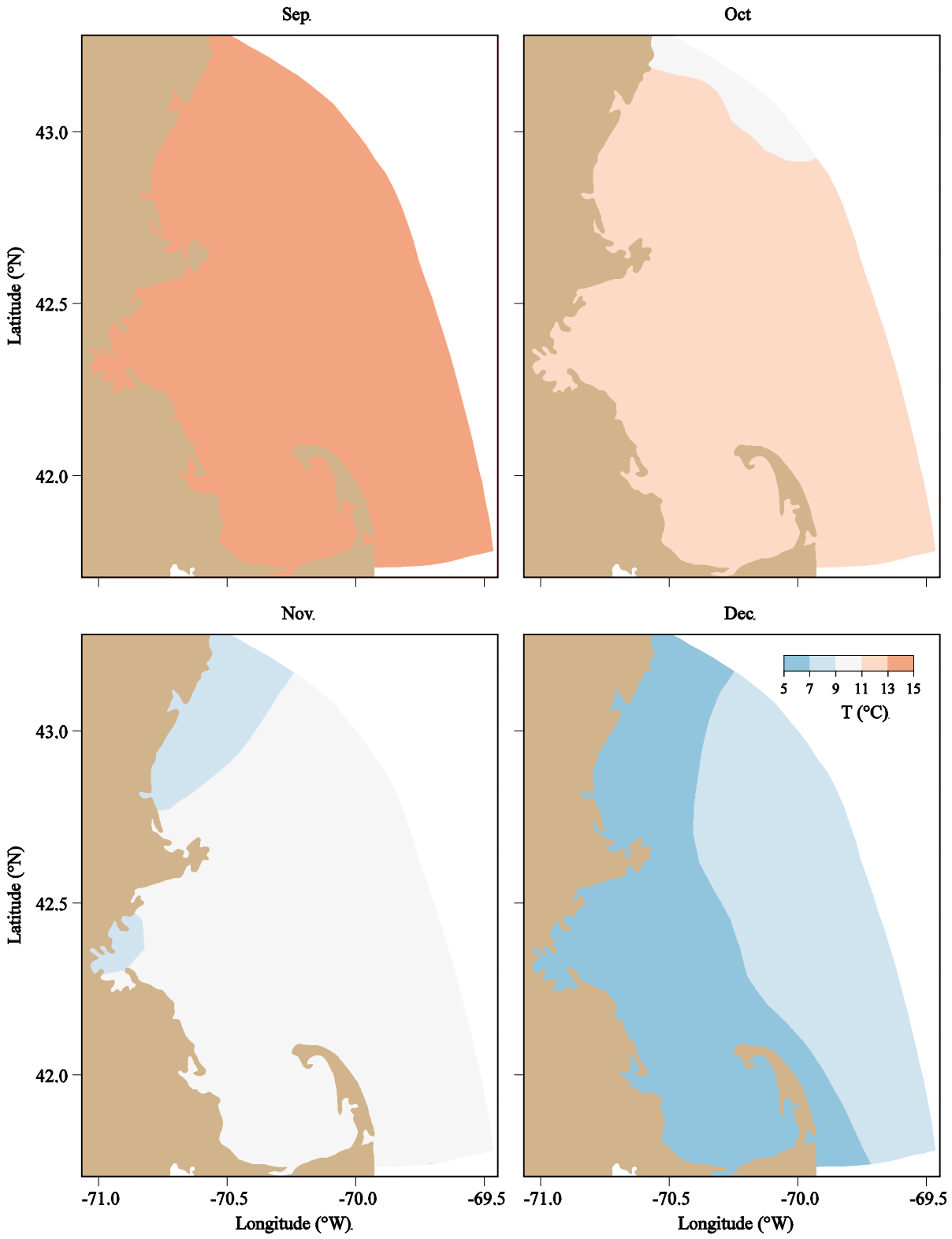

Figure 3. 14 Surface temperature at the end of September, October, November and December, 2010 predicted by FVCOM.

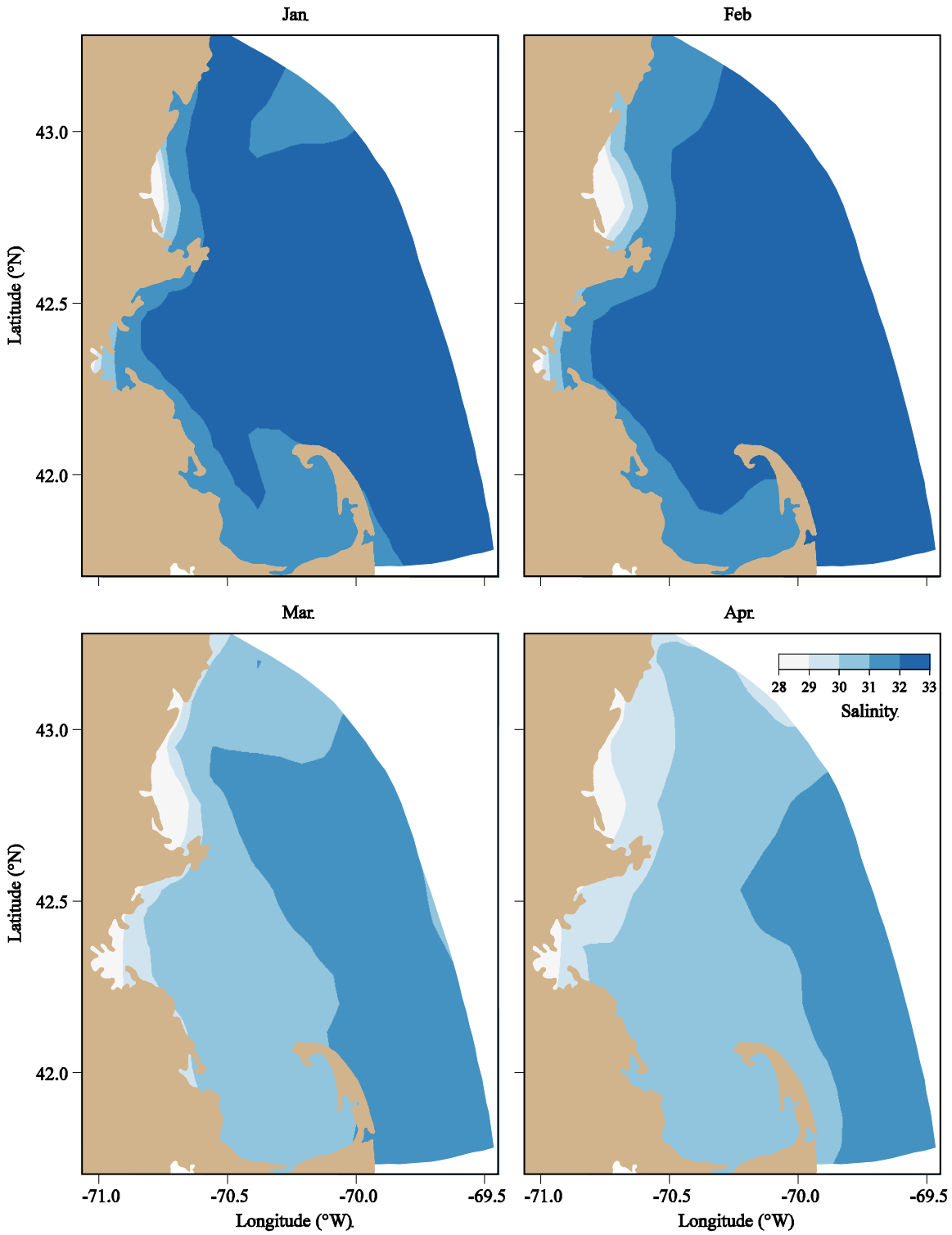

Figure 3. 15 Surface salinity at the end of January, February, March and April, 2010 predicted by FVCOM.

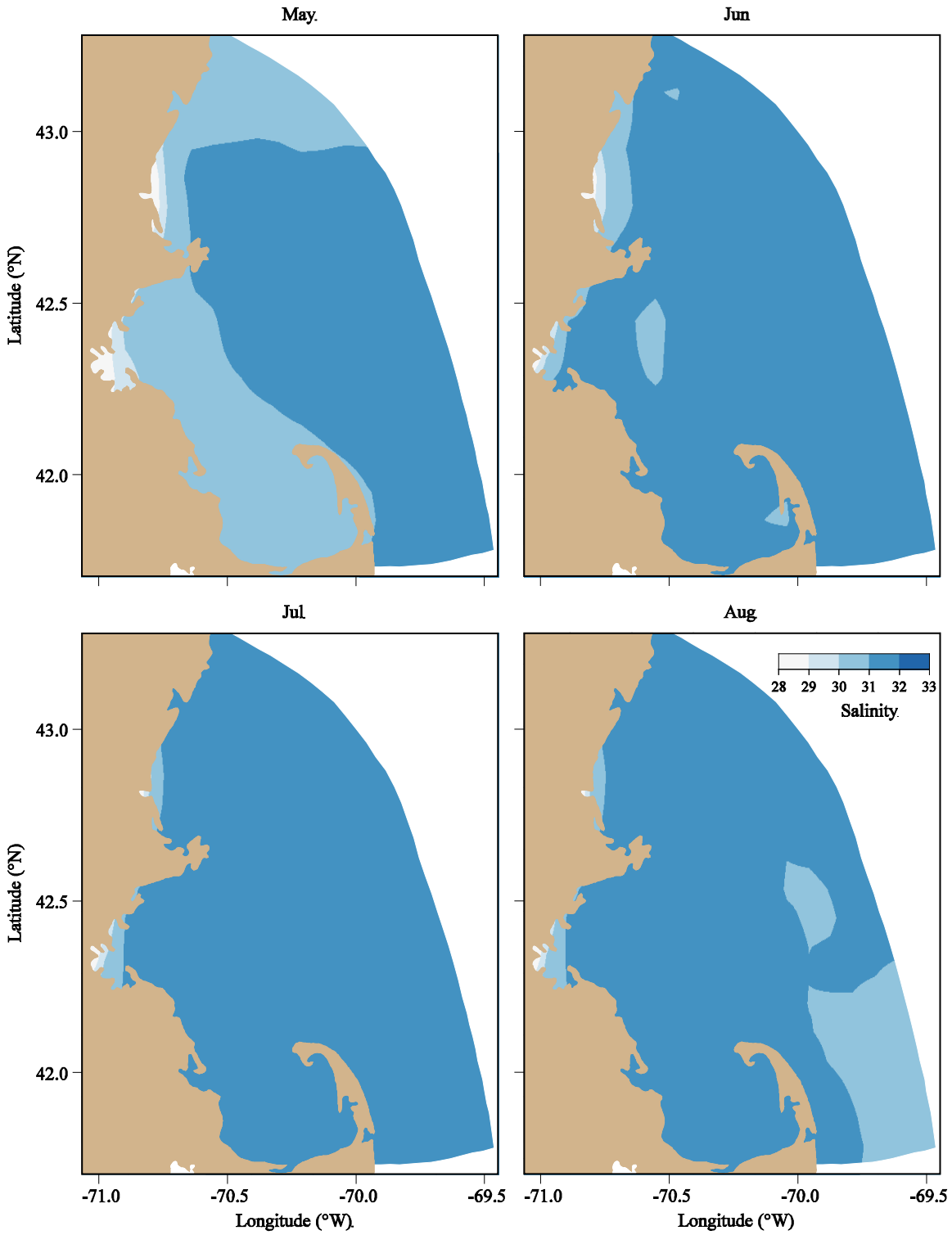

Figure 3. 16 Surface salinity at the end of May, June, July and August, 2010 predicted by FVCOM.

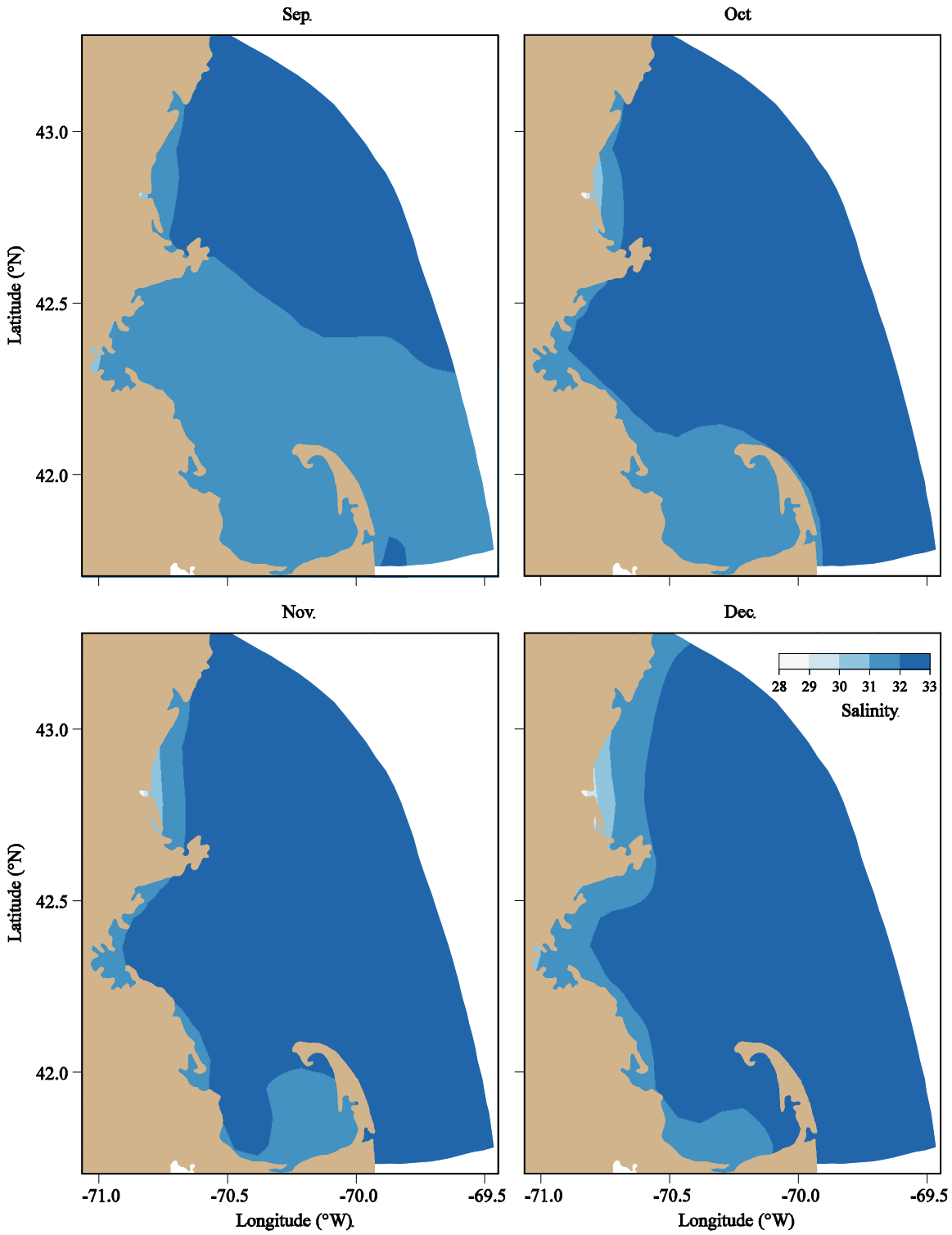

Figure 3. 17 Surface salinity at the end of September, October, November and December, 2010 predicted by FVCOM.

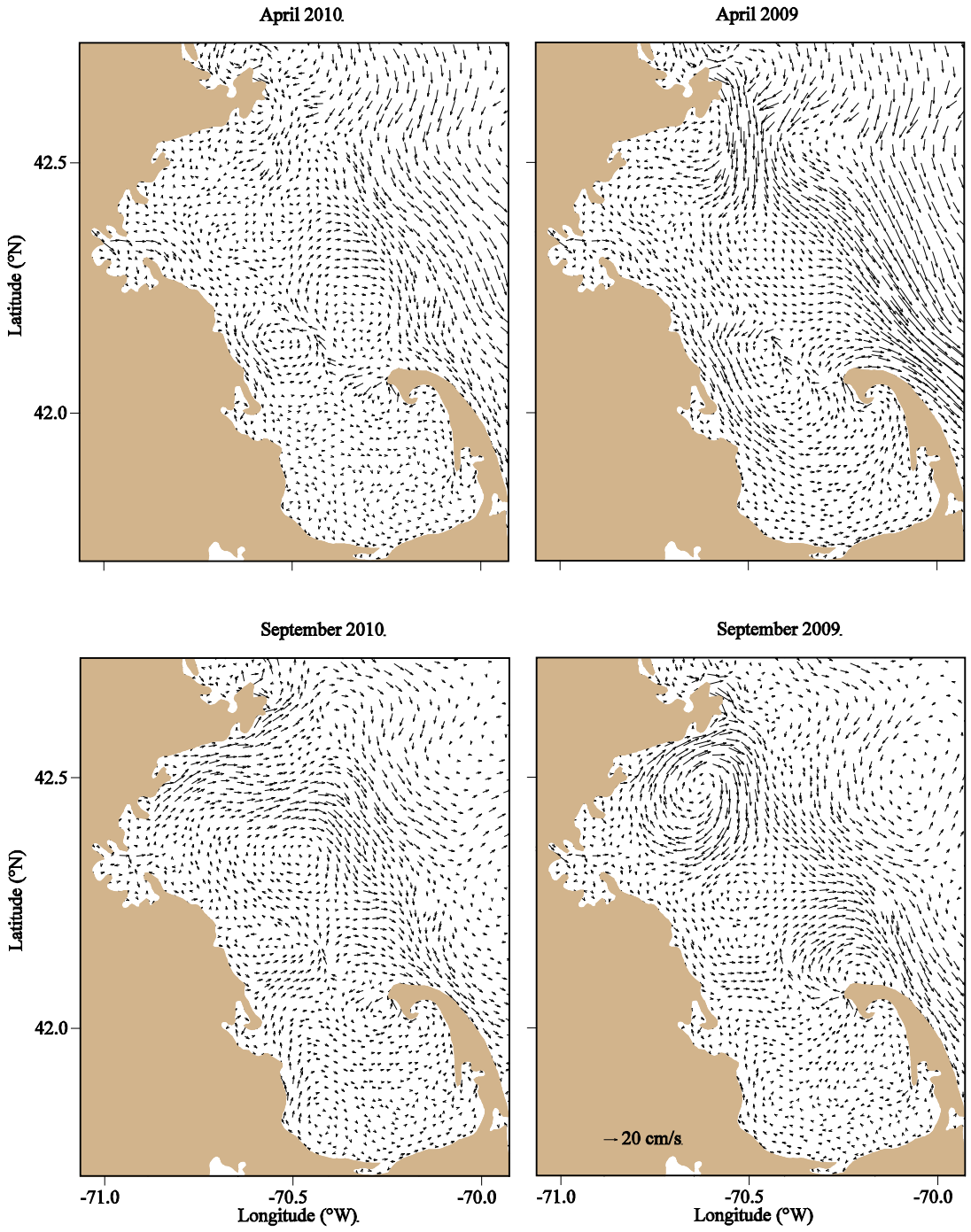

Figure 3. 18. Monthly-averaged surface current of 2010 (left panels) and 2009 (right panels) in April (upper panels) and September (lower panels).

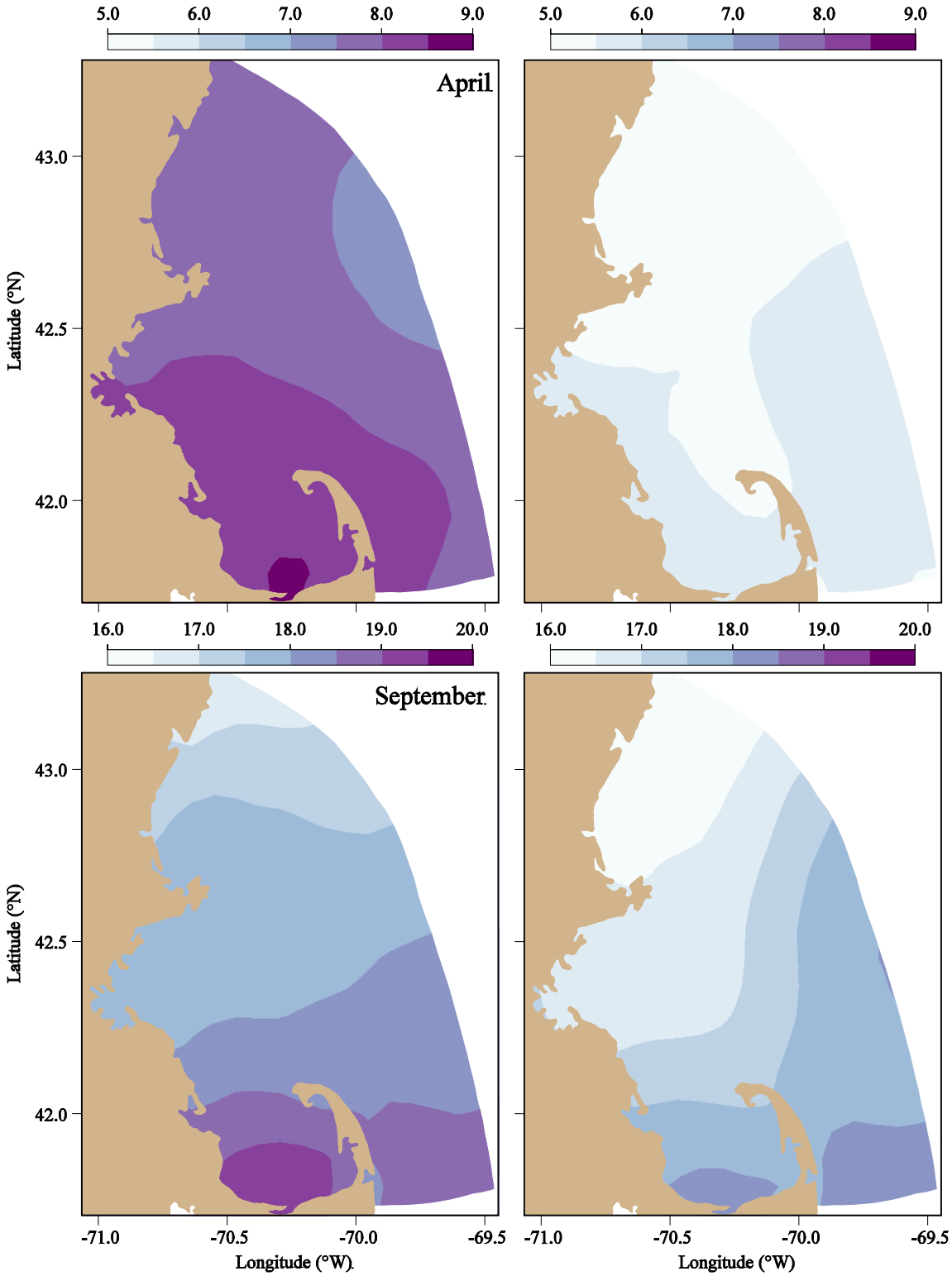

Figure 3. 19. Monthly-averaged surface temperature of 2010 (left panels) and 2009 (right panels) in April (upper panels) and September (lower panels).

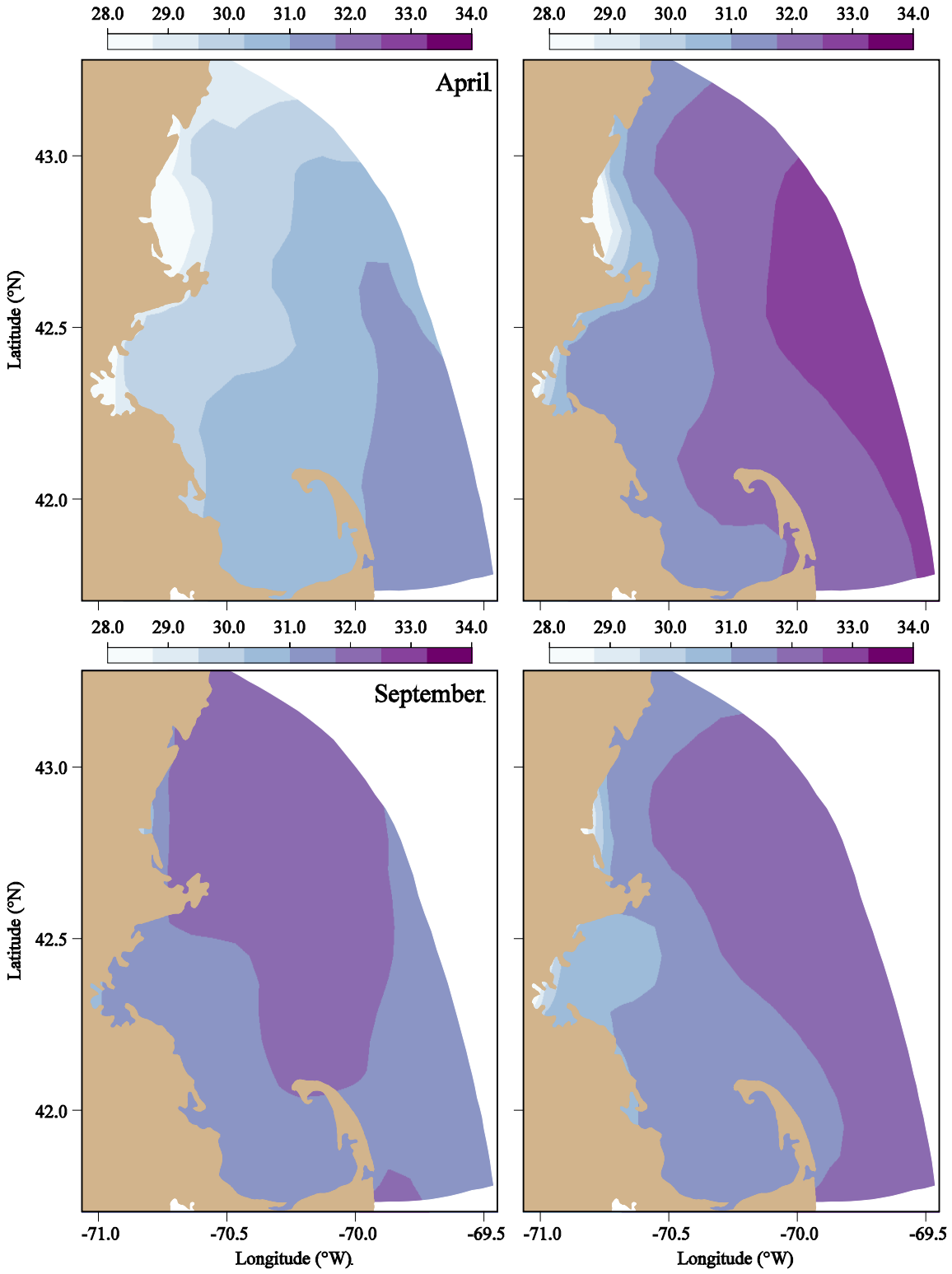

Figure 3. 20. Monthly-averaged surface salinity of 2010 (left panels) and 2009 (right panels) in April (upper panels) and September (lower panels).

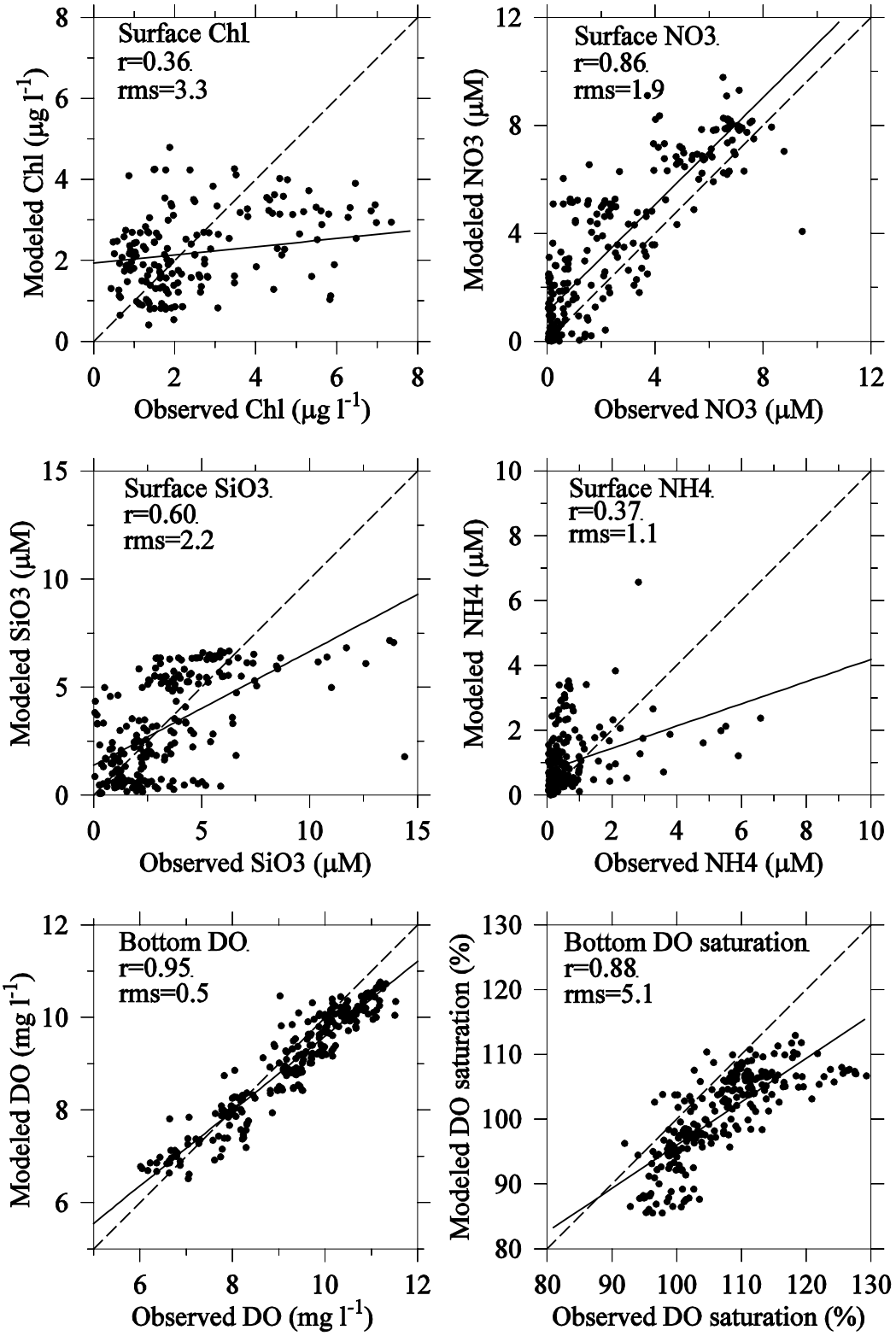

Figure 3. 21 Overall correlation and regression (solid lines) between observed and modeled results of key parameters in 2010. The dashed lines indicate equality between observed and modeled results. All stations are included.

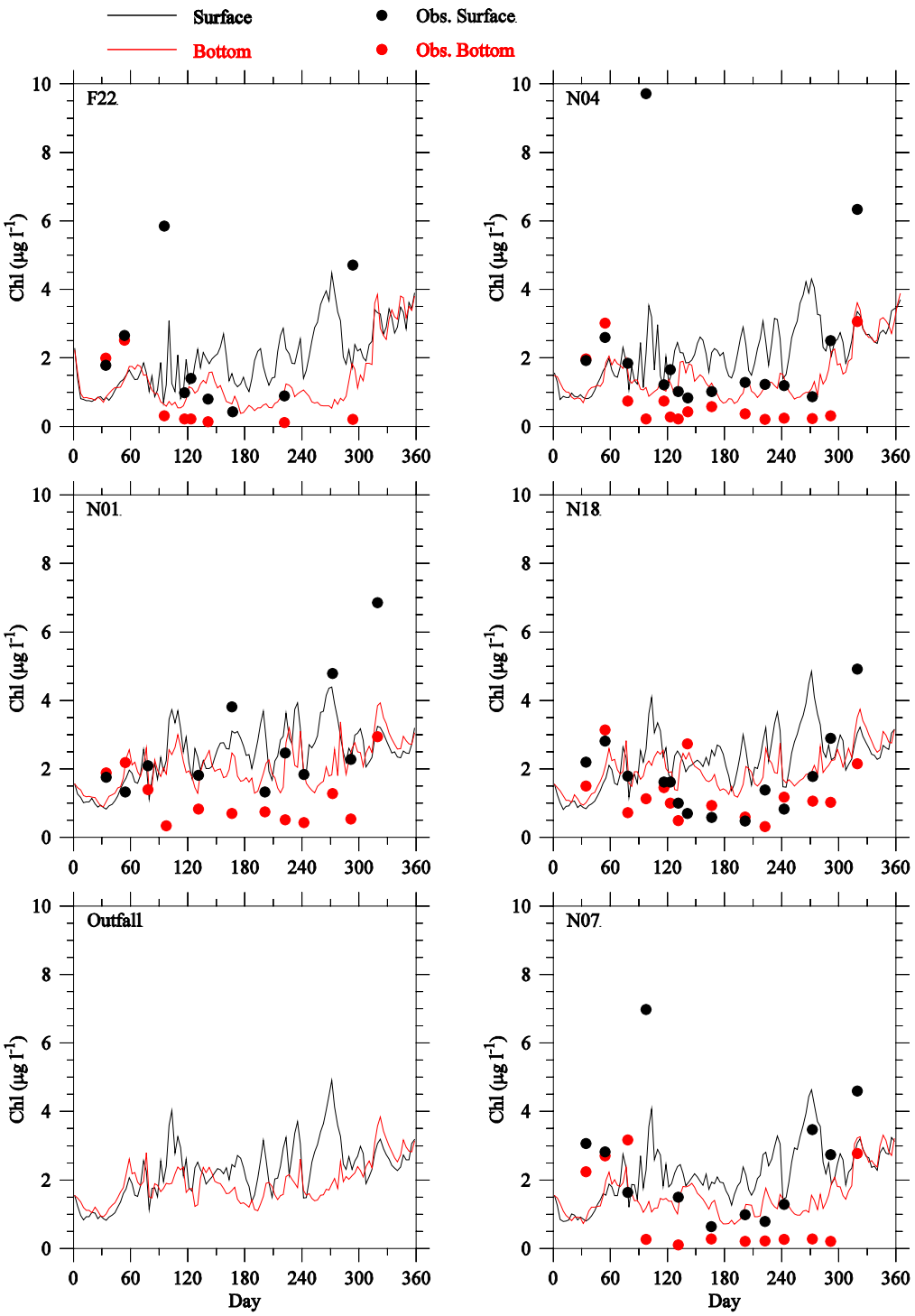

Figure 3. 22 Comparison of chlorophyll observed (dots) and modeled (lines) time-series at the outfall site and selected Massachusetts Bay monitoring stations F22, N04, N01, N18, outfall and N07 for 2010. No chlorophyll data are available at the outfall site.

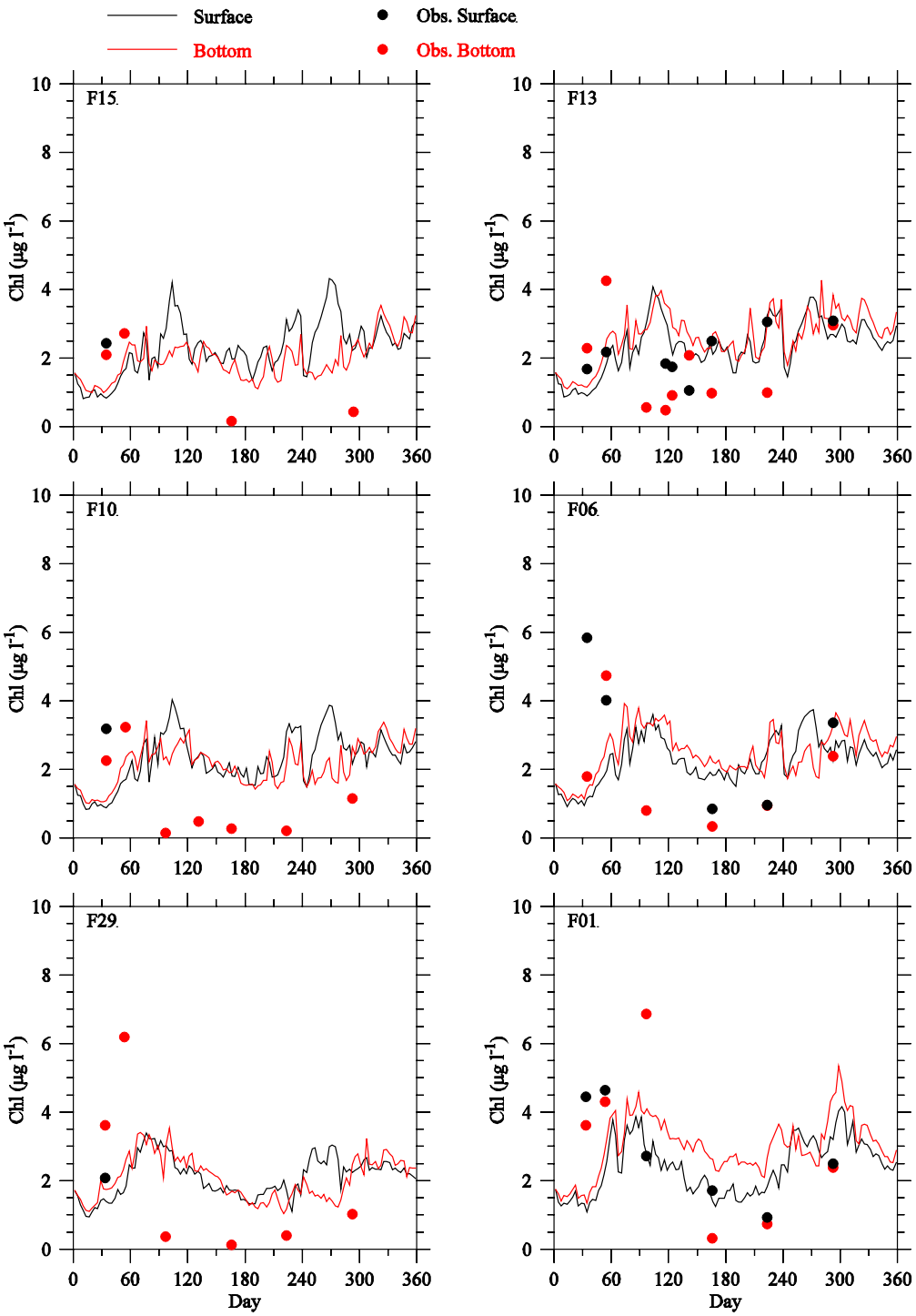

Figure 3. 23 Comparison of chlorophyll observed (dots) and modeled (lines) time-series at selected Massachusetts Bay monitoring stations F15, F13, F10, F06, F29 and F01 for 2010. (Results for stations F15, F10 and F29 are calibrated fluorescence rather than extracted chlorophyll.)

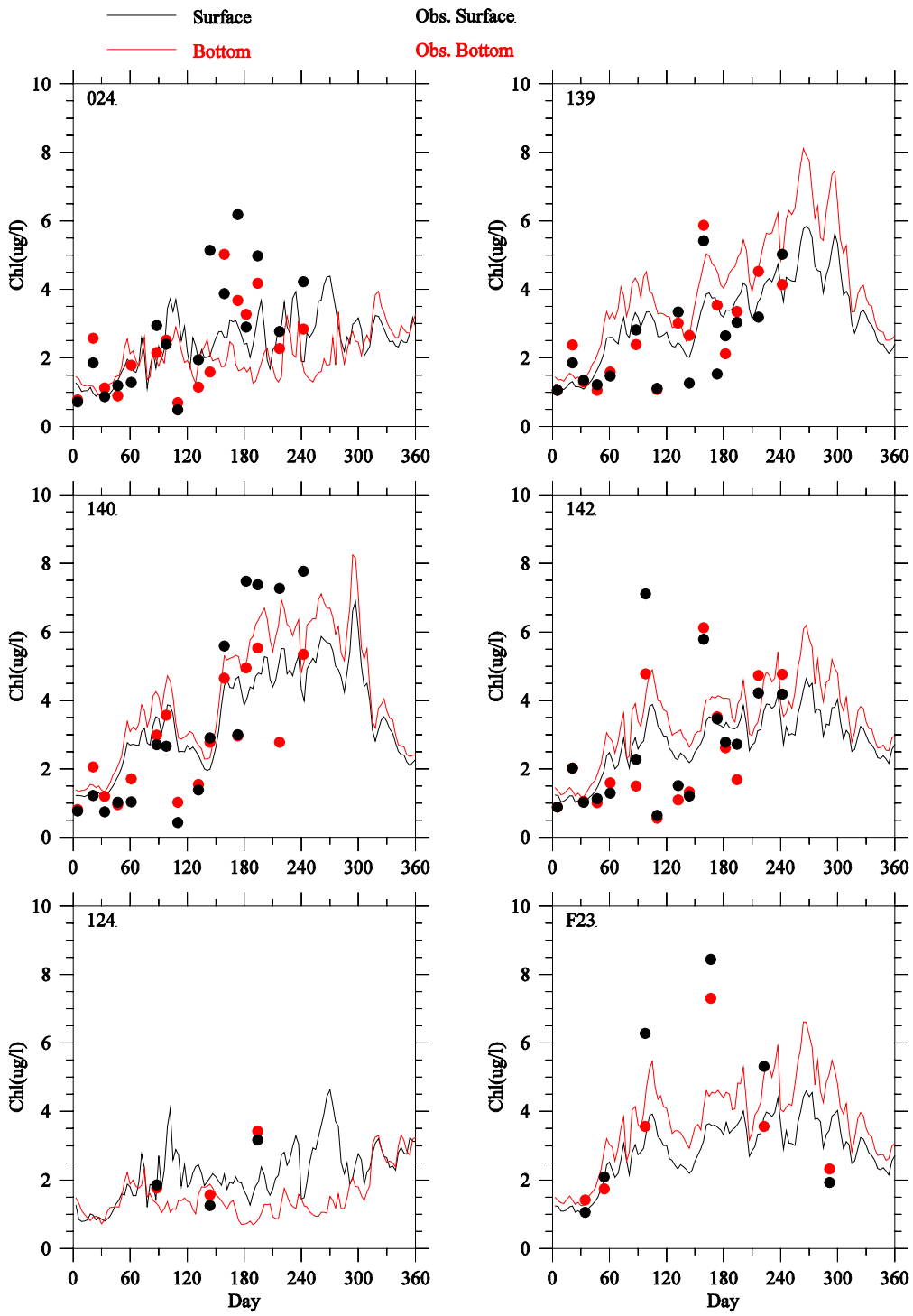

Figure 3. 24 Comparison of chlorophyll observed (dots) and modeled (lines) time-series at selected Boston Harbor stations for 2010.

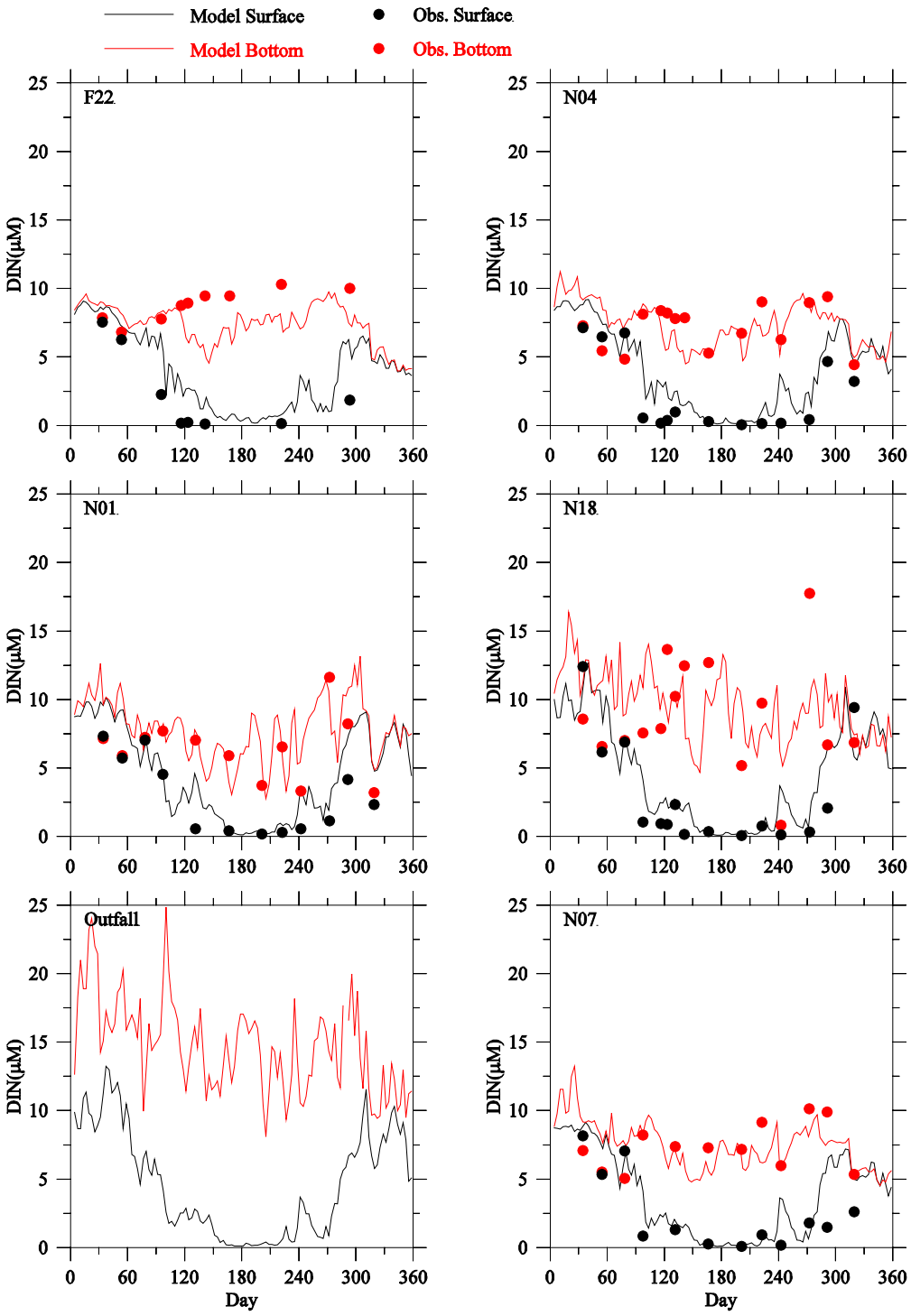

Figure 3. 25 Comparison of DIN observed (dots) and modeled (lines) time-series at the outfall site and selected Massachusetts Bay monitoring stations F22, N04, N01, N18, outfall and N07 for 2010. No DIN data are available at the outfall site.

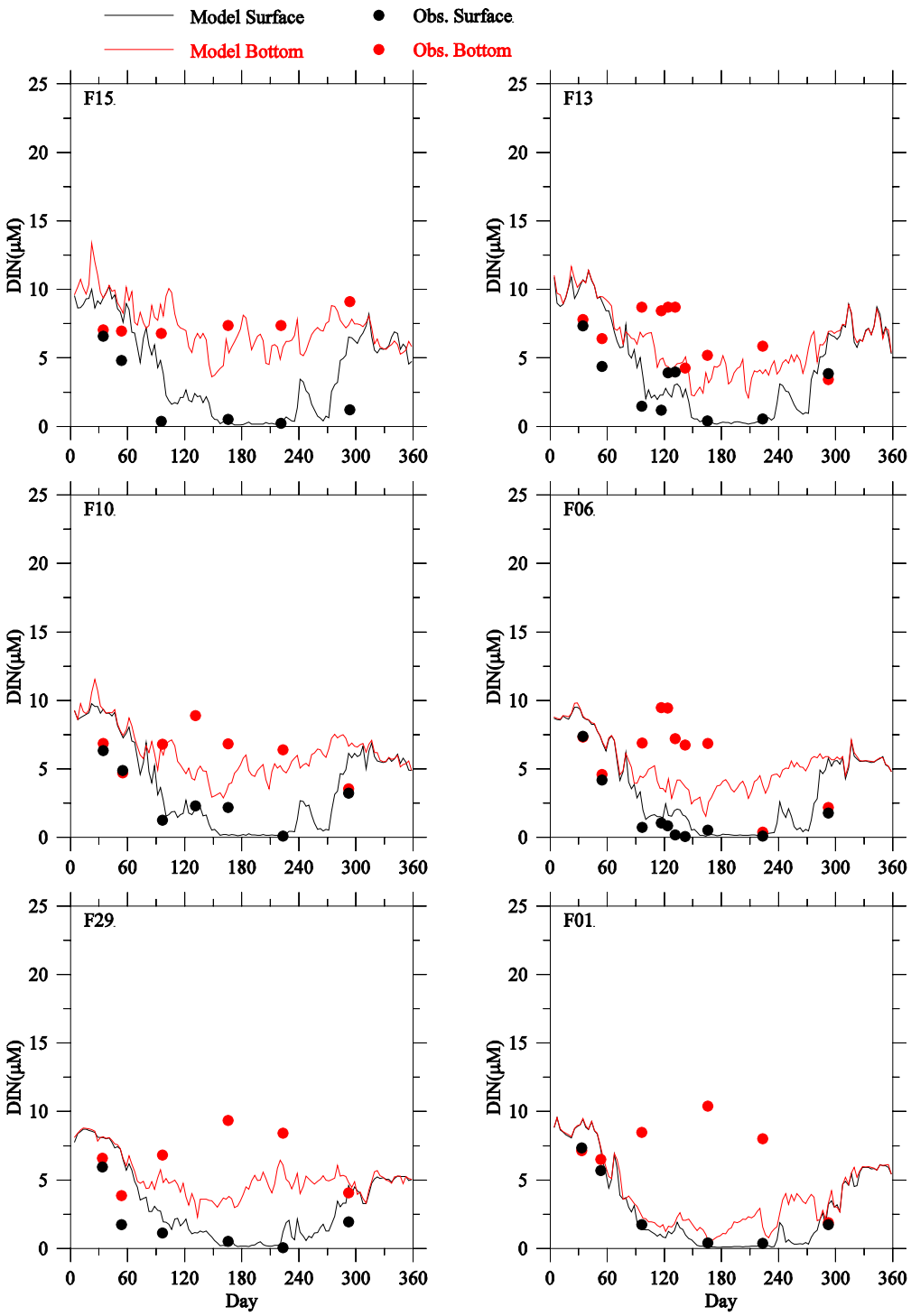

Figure 3. 26 Comparison of DIN observed (dots) and modeled (lines) time-series at selected Massachusetts Bay monitoring stations F15, F13, F10, F06, F29 and F01 for 2010.

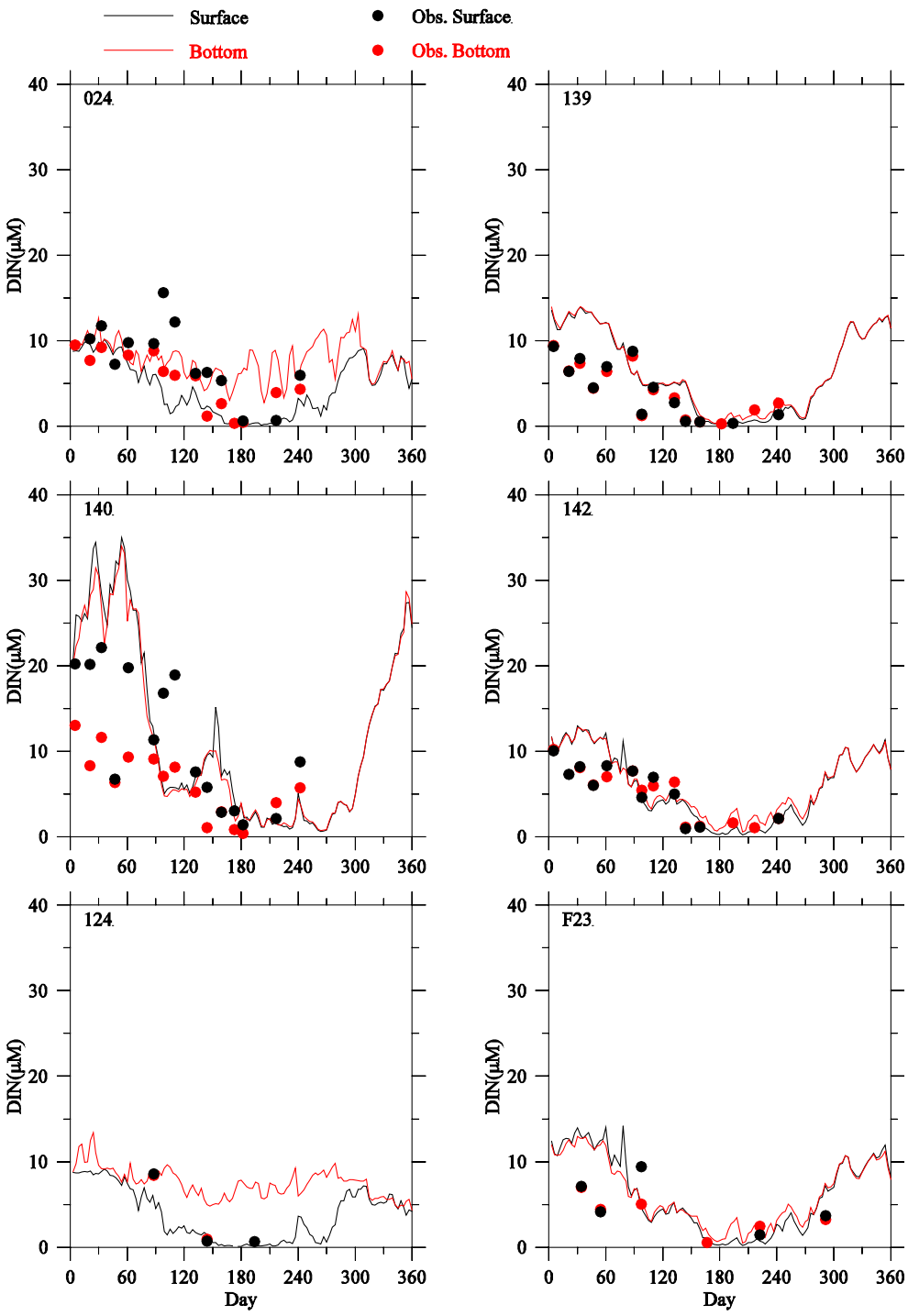

Figure 3. 27 Comparison of DIN observed (dots) and modeled (lines) time-series at selected Boston Harbor stations for 2010.

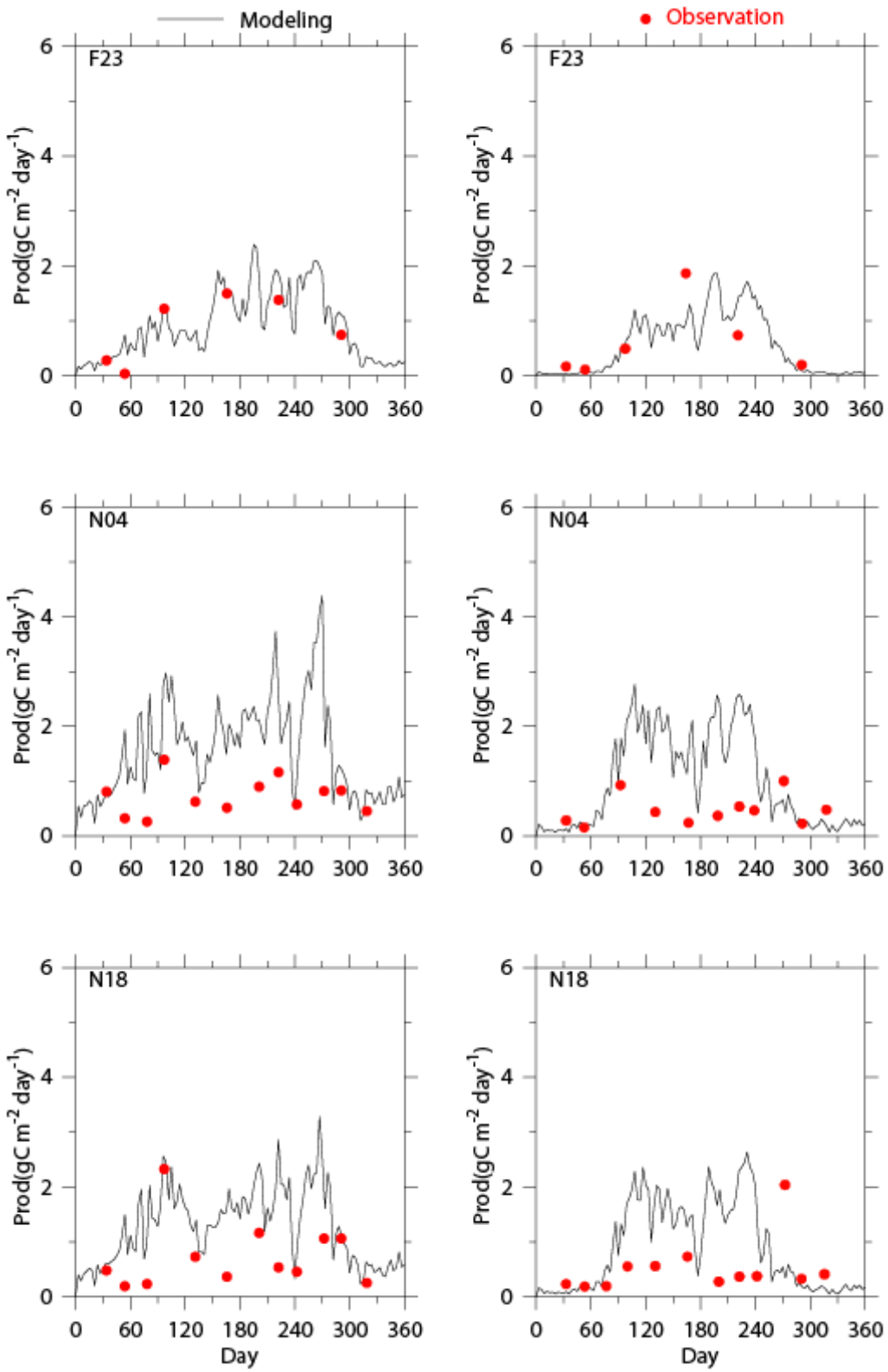

Figure 3. 28 Comparison of vertically integrated primary production observed (dots) and modeled (lines) time series at the MWRA monitoring stations in 2010 (left panels) and 2009 (right panels.)

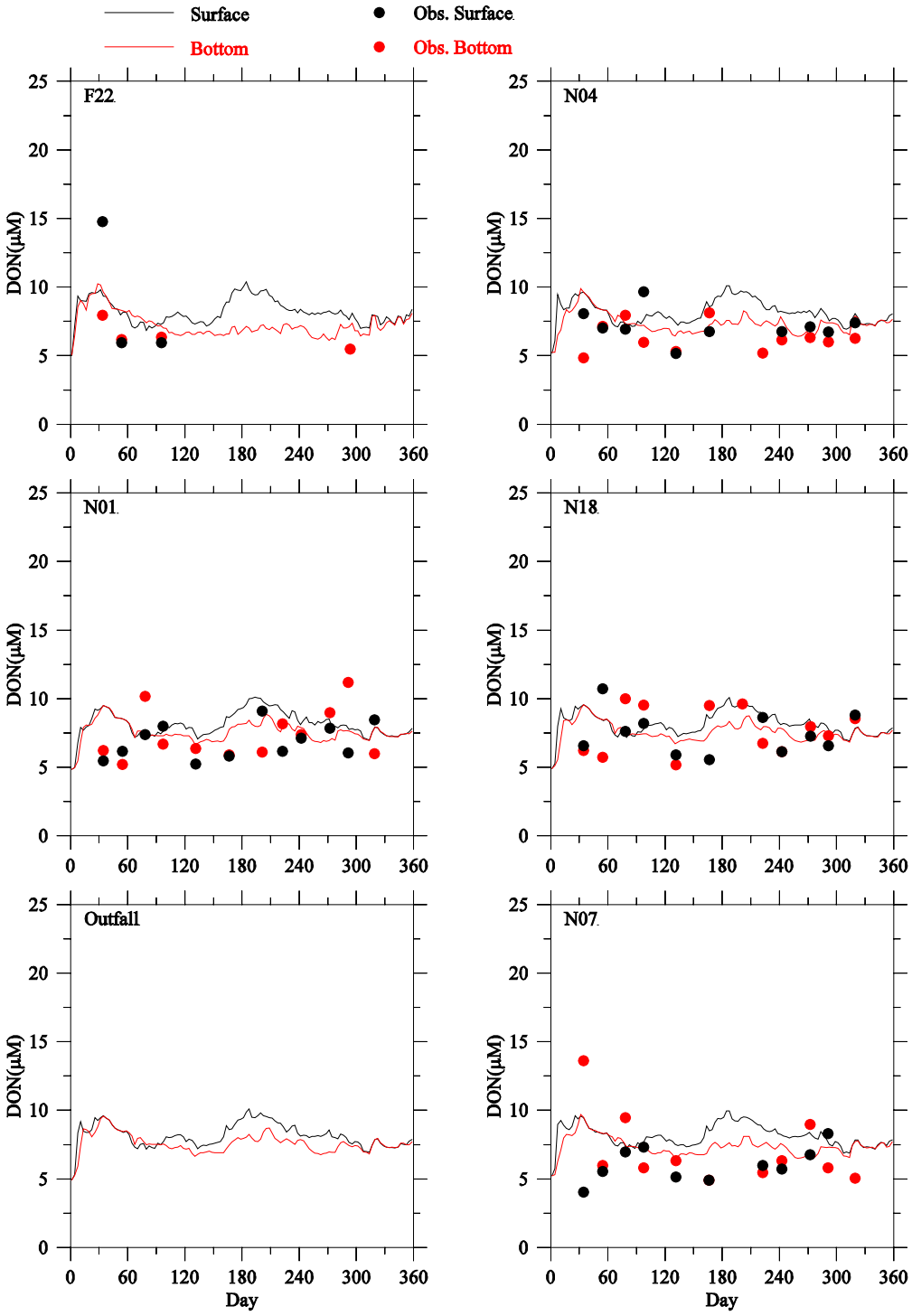

Figure 3. 29 Comparison of DON observed (dots) and modeled (lines) time-series at the outfall site and selected Massachusetts Bay monitoring stations F22, N04, N01, N18, outfall and N07 for 2010. No DON data are available at the outfall site.

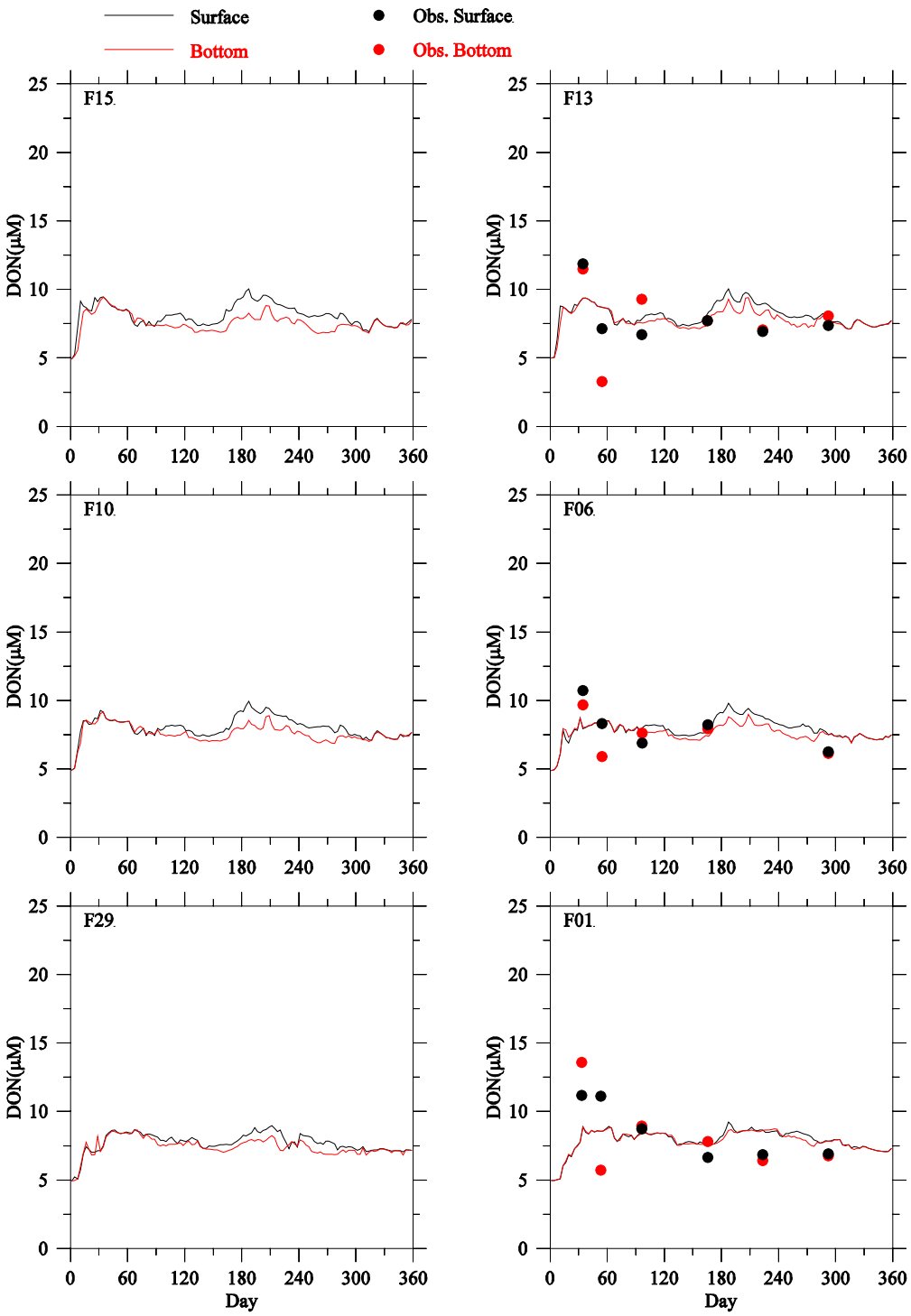

Figure 3. 30 Comparison of DON observed (dots) and modeled (lines) time-series at selected Massachusetts Bay monitoring stations F15, F13, F10, F06, F29 and F01 for 2010. No DON data are available at stations F15, F10 and F29.

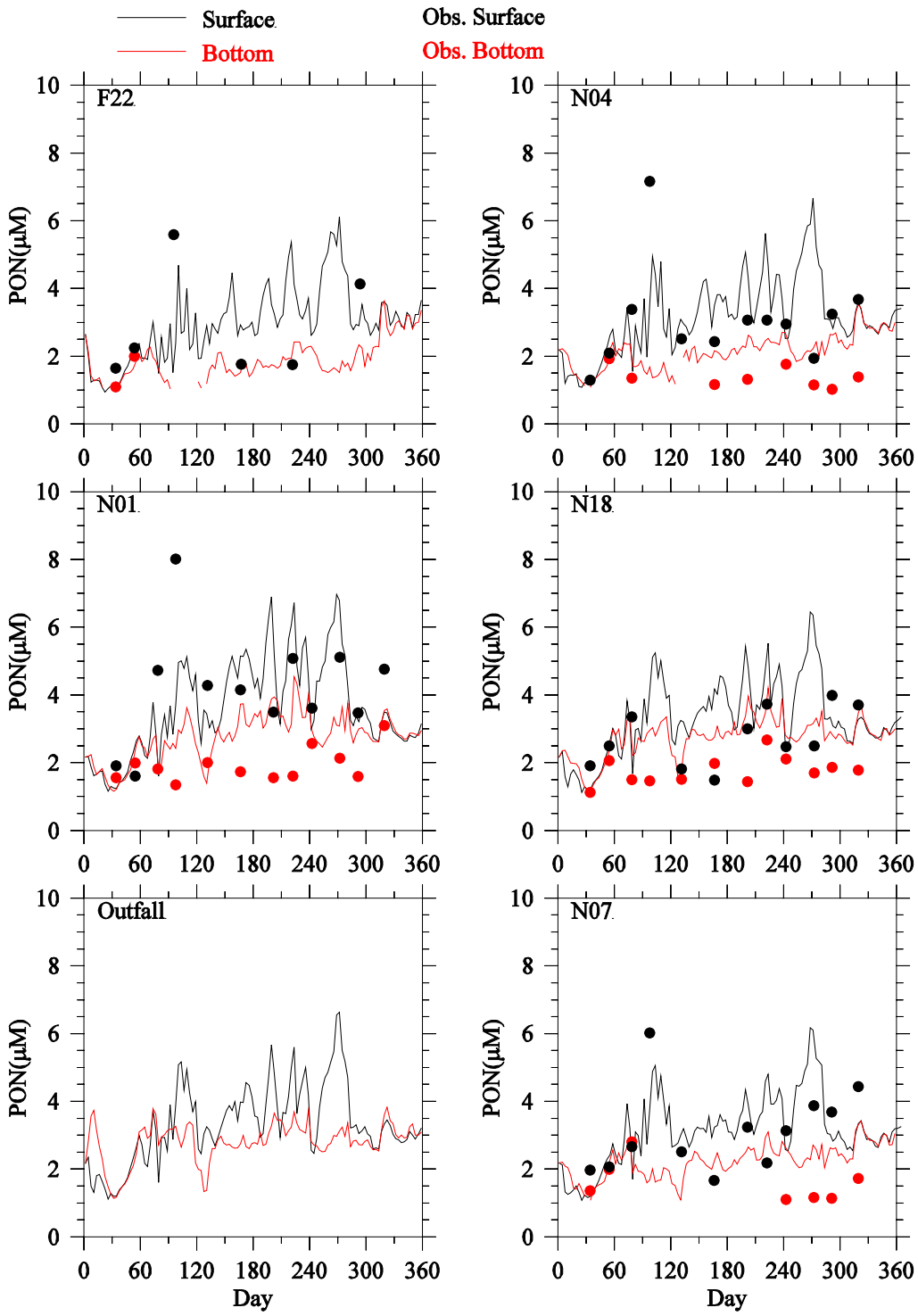

Figure 3. 31 Comparison of PON observed (dots) and modeled (lines) time-series at the outfall site and selected Massachusetts Bay monitoring stations F22, N04, N01, N18, outfall and N07 for 2010. No PON data are available at the outfall site.

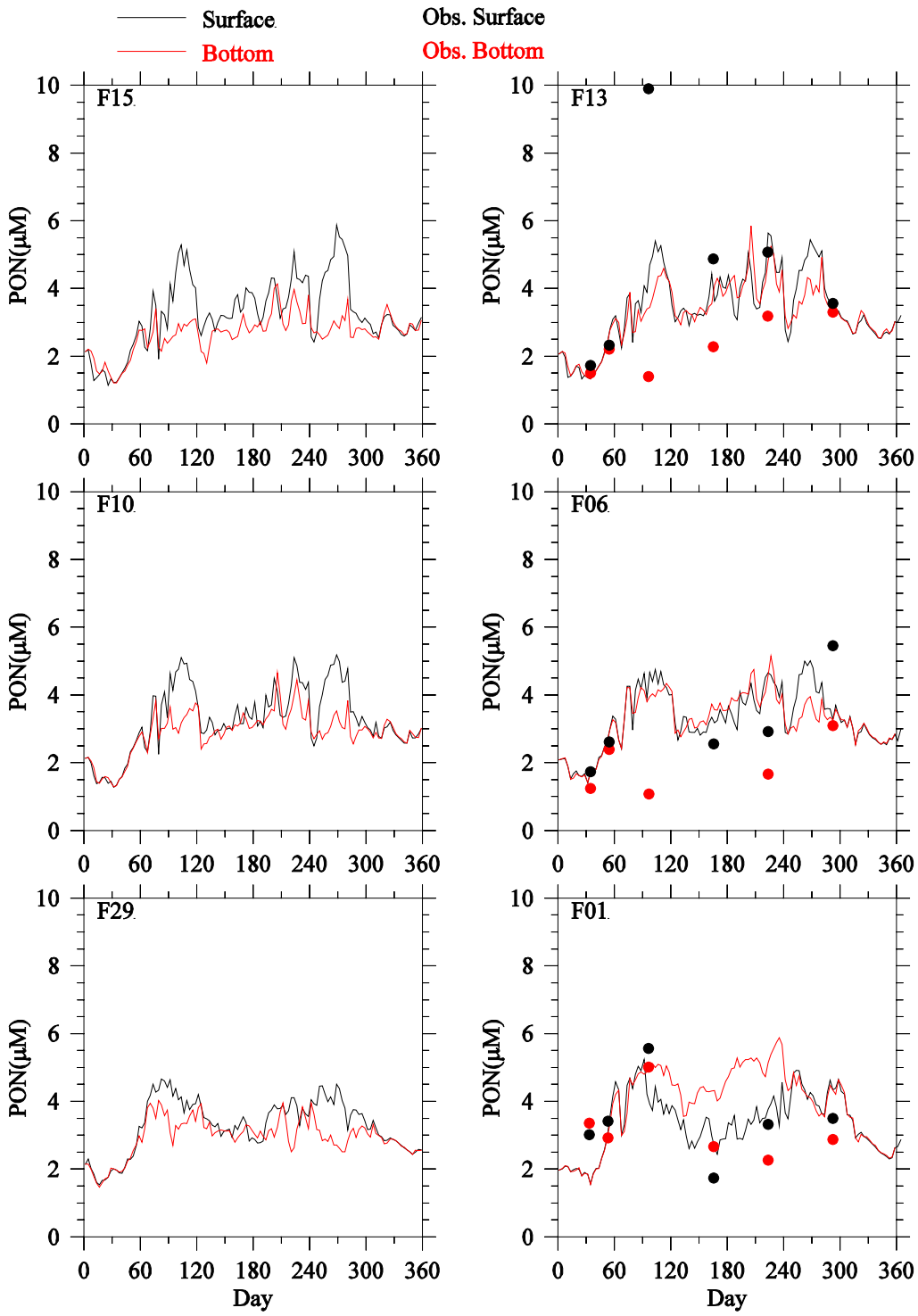

Figure 3. 32 Comparison of PON observed (dots) and modeled (lines) time-series at selected Massachusetts Bay monitoring stations F15, F13, F10, F06, F29 and F01 for 2010. No PON data are available at stations F15, F10 and F29.

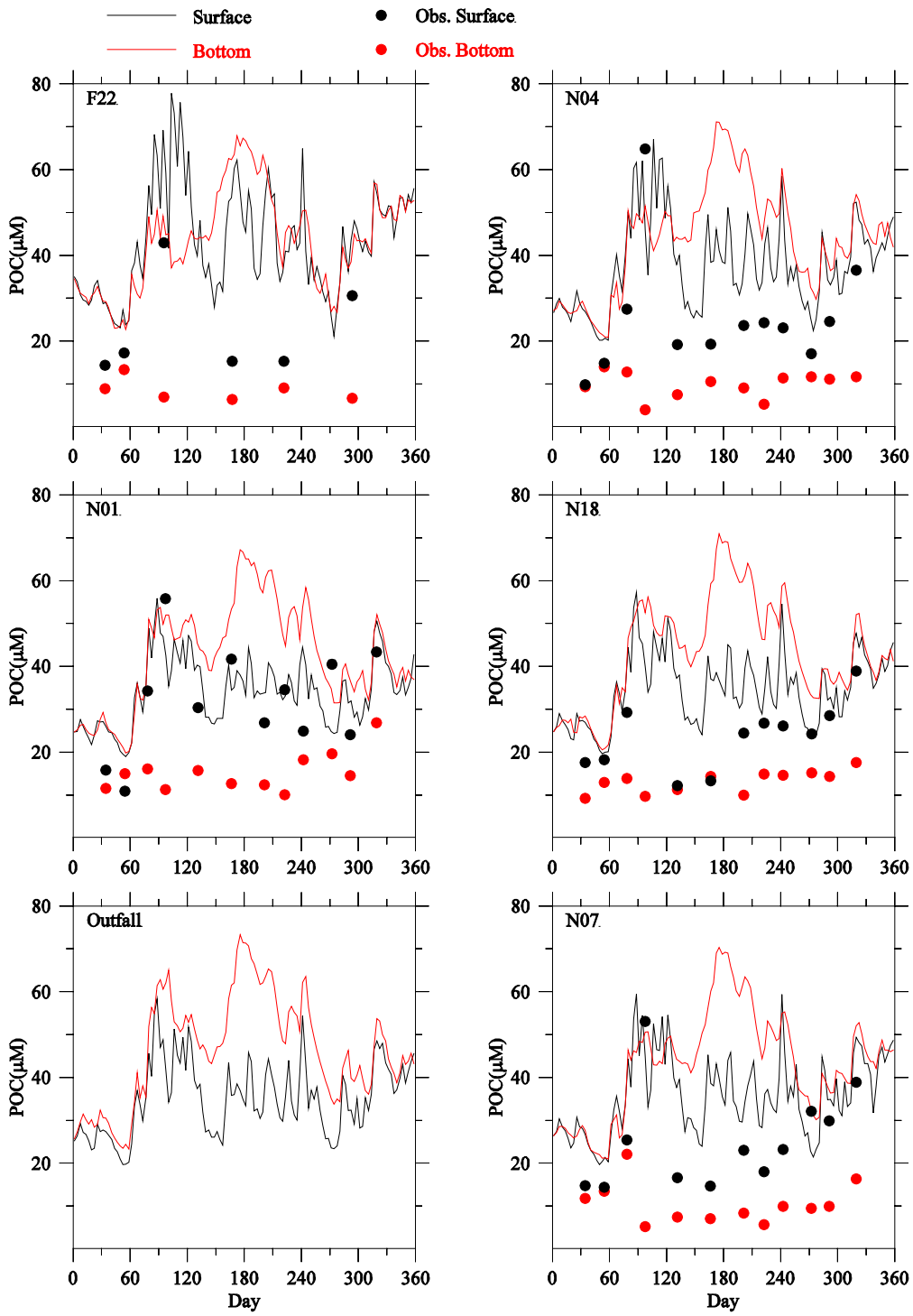

Figure 3. 33 Comparison of POC observed (dots) and modeled (lines) time-series at the outfall site and selected Massachusetts Bay monitoring stations F22, N04, N01, N18, outfall and N07 for 2010. No POC data are available at the outfall site.

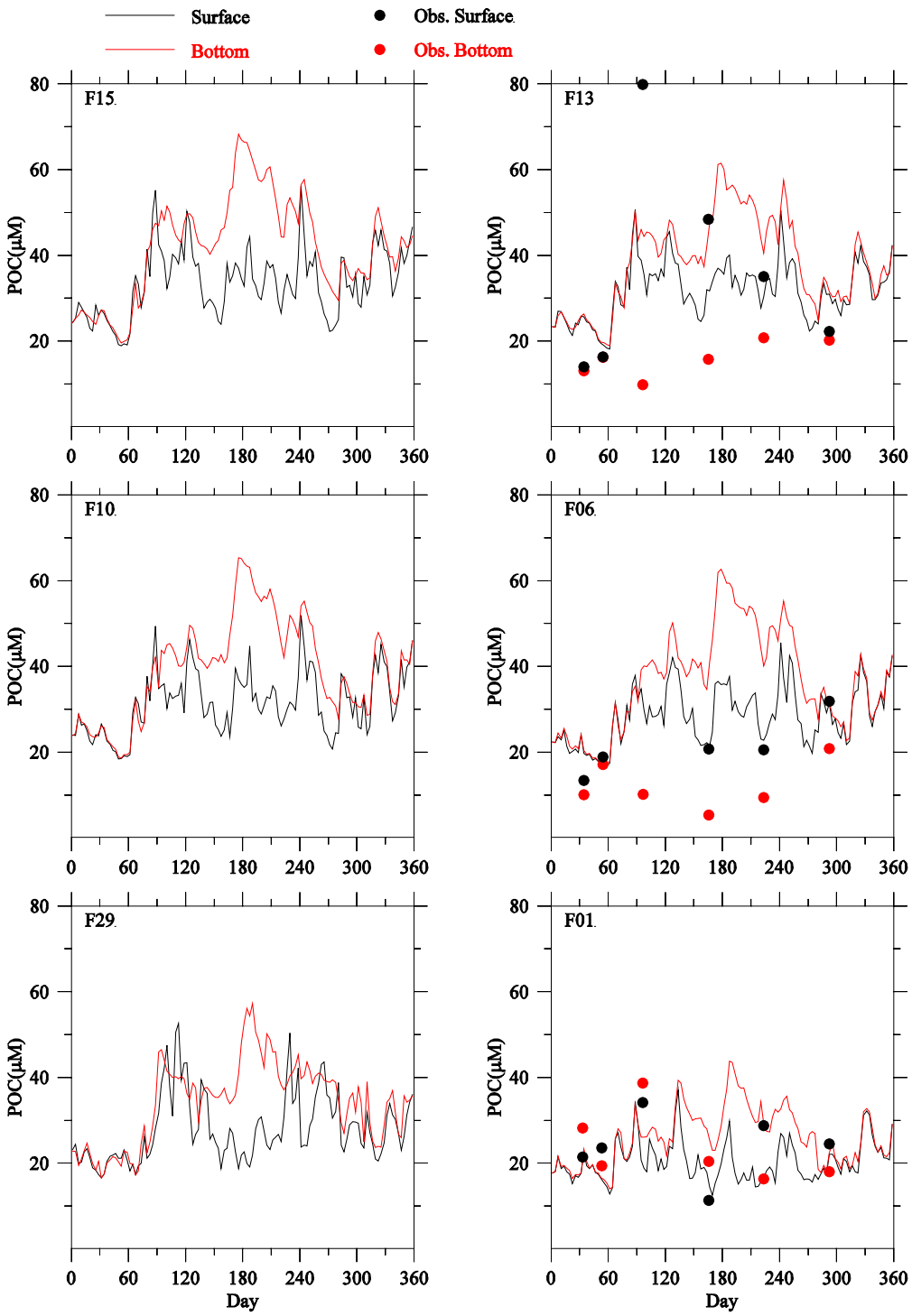

Figure 3. 34 Comparison of POC observed (dots) and modeled (lines) time-series at selected Massachusetts Bay monitoring stations F15, F13, F10, F06, F29 and F01 for 2010. No POC data are available at stations F15, F10 and F29.

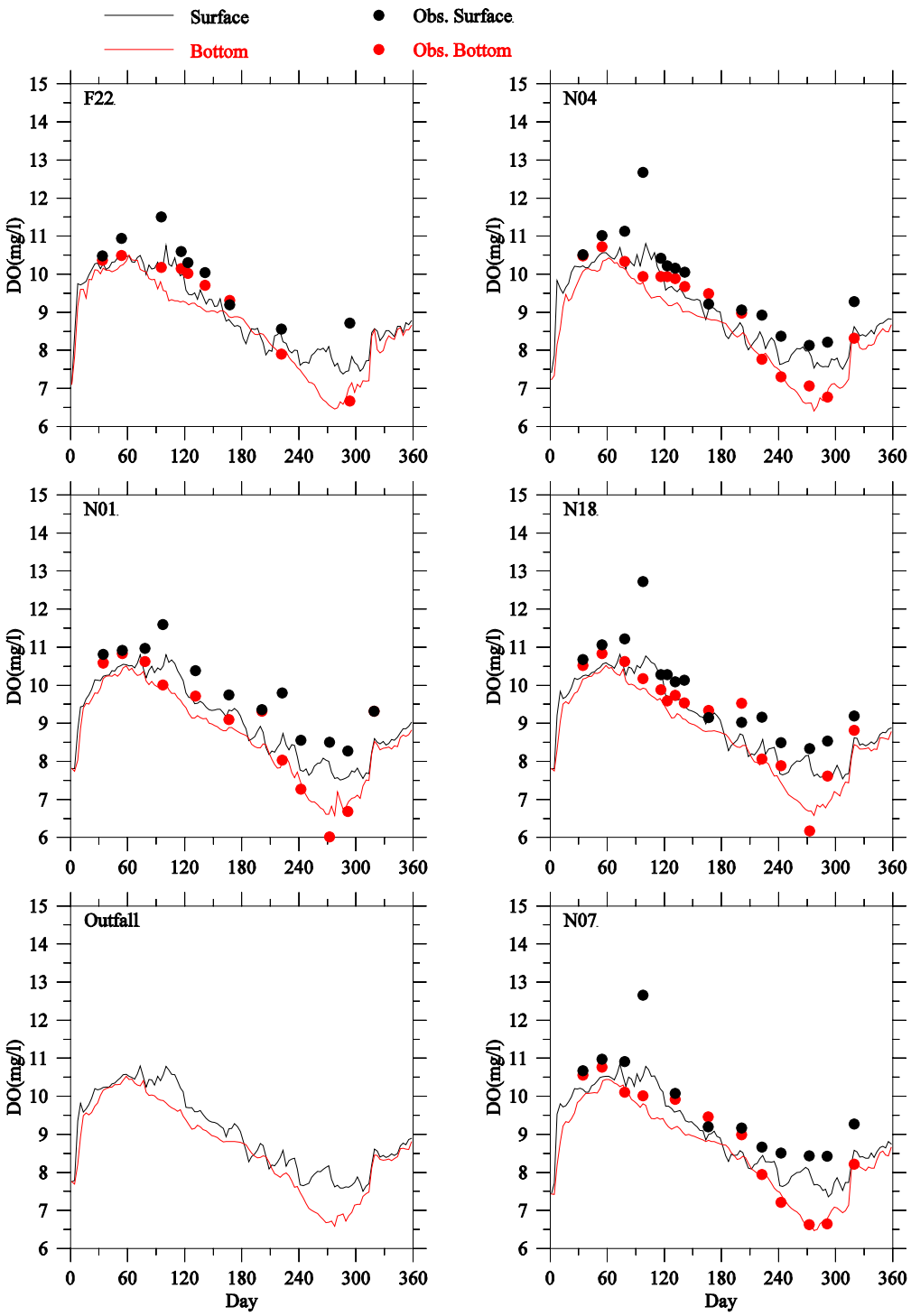

Figure 3. 35 Comparison of DO observed (dots) and modeled (lines) time-series at the outfall site and selected Massachusetts Bay monitoring stations F22, N04, N01, N18, outfall and N07 for 2010. No DO data are available at the outfall site.

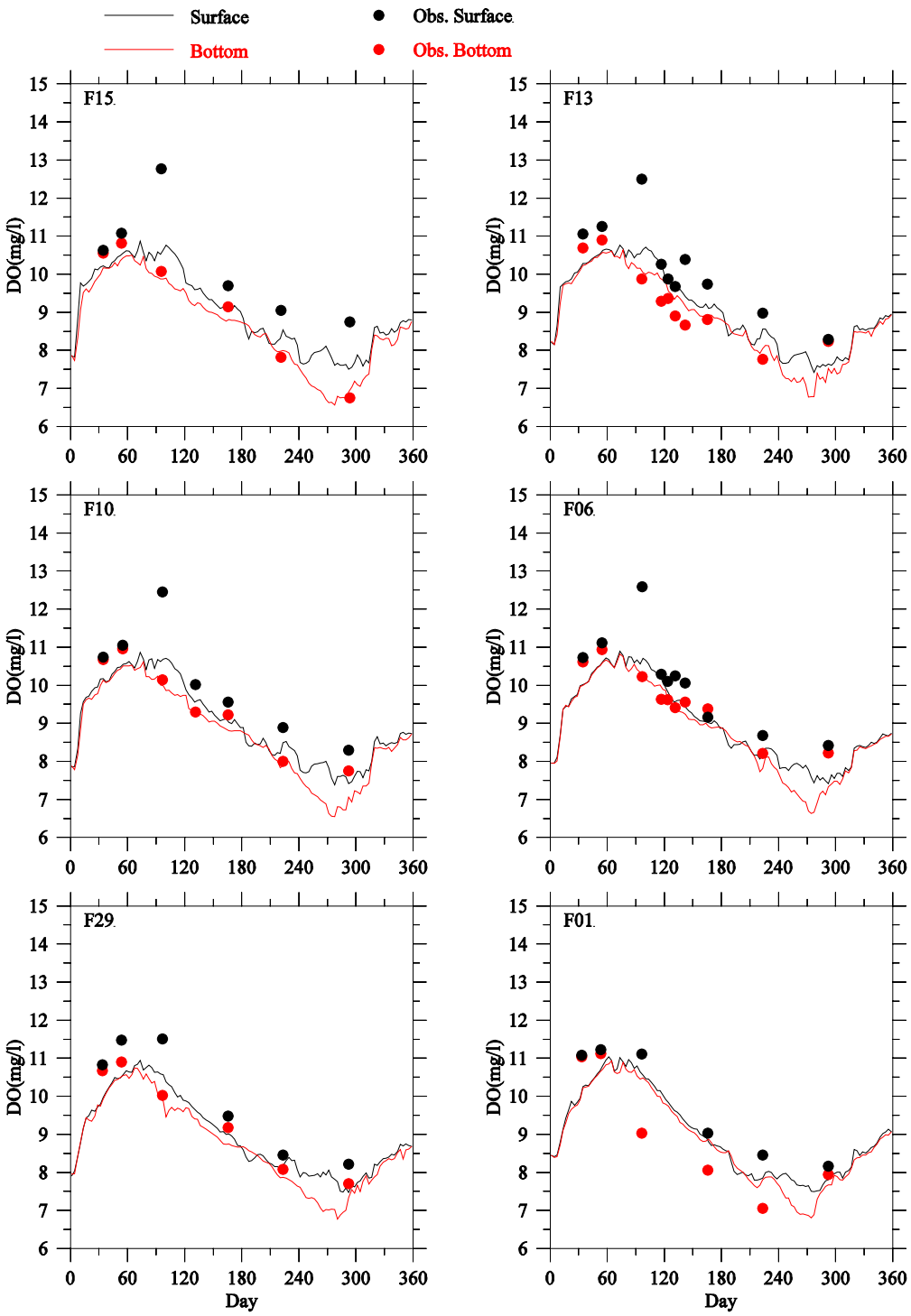

Figure 3. 36 Comparison of DO observed (dots) and modeled (lines) time-series at selected Massachusetts Bay monitoring stations F15, F13, F10, F06, F29 and F01 for 2010.

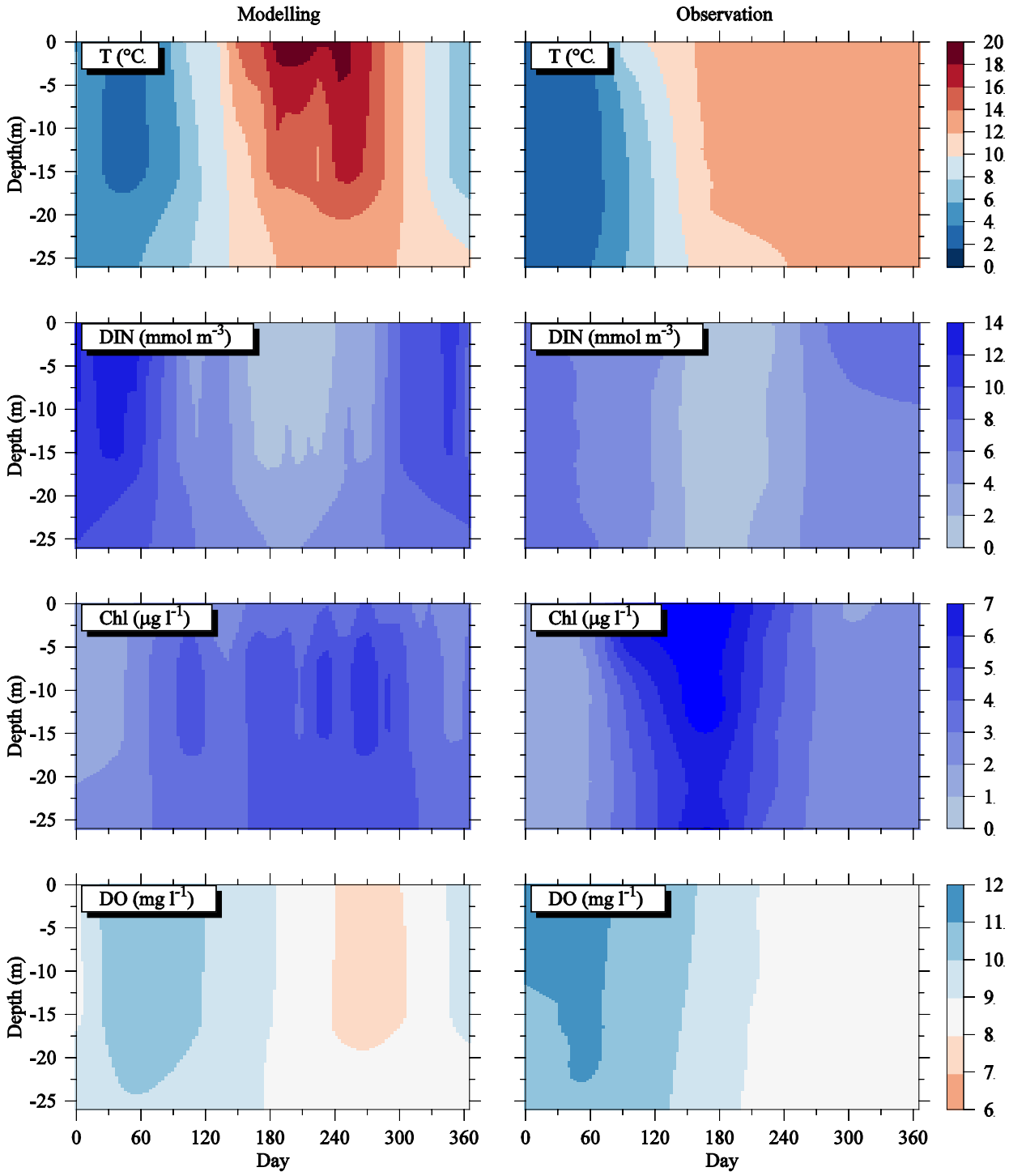

Figure 3. 37 Time-series of vertical distribution of modeled (left panels) and observed (right panels) key parameters (T, DIN, Chl and DO) in the water column at the far-field station F23 in 2010.

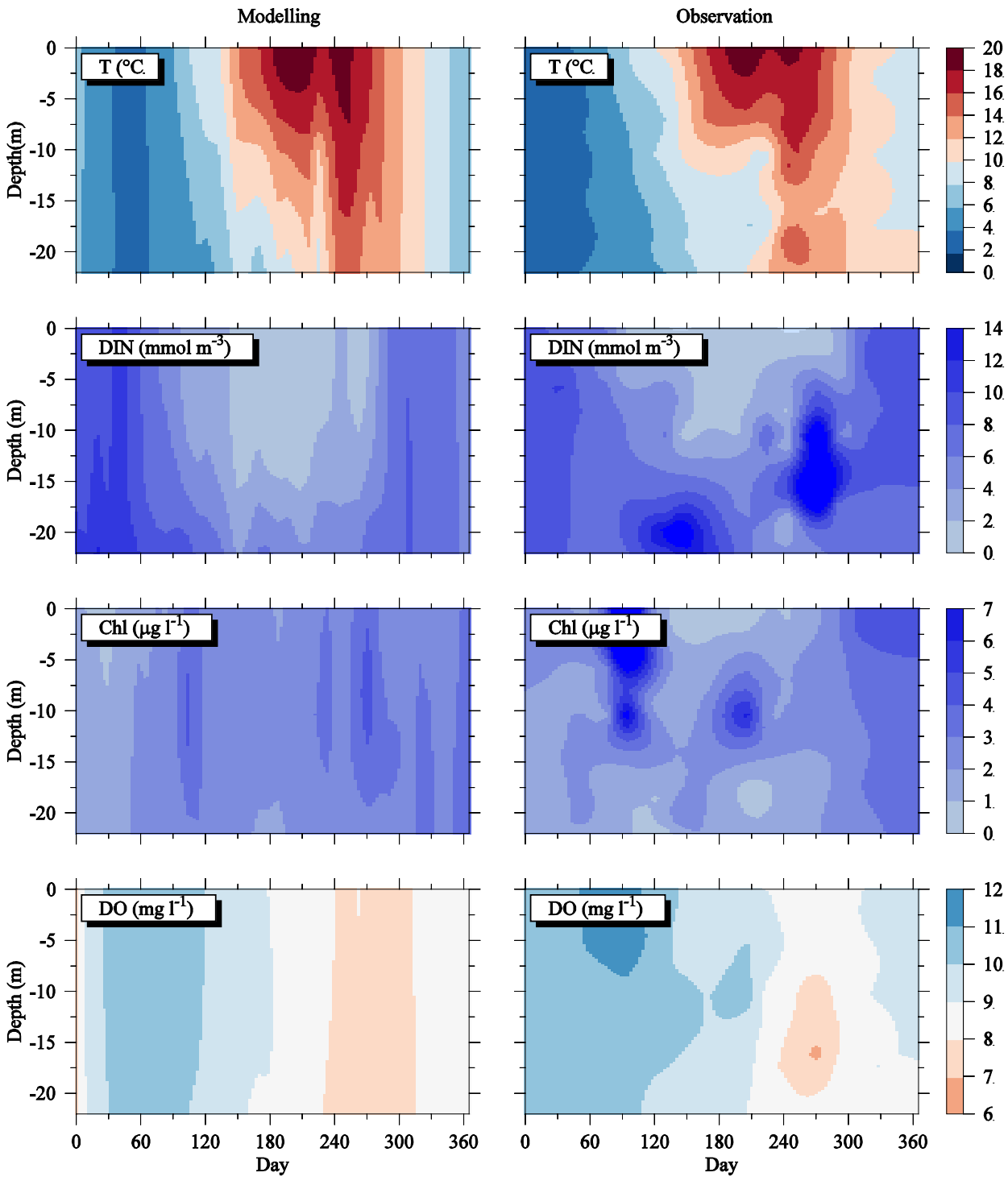

Figure 3. 38 Time-series of vertical distribution of modeled (left panels) and observed (right panels) key parameters (T, DIN, Chl and DO) in the water column at the near-field station N18 in 2010.

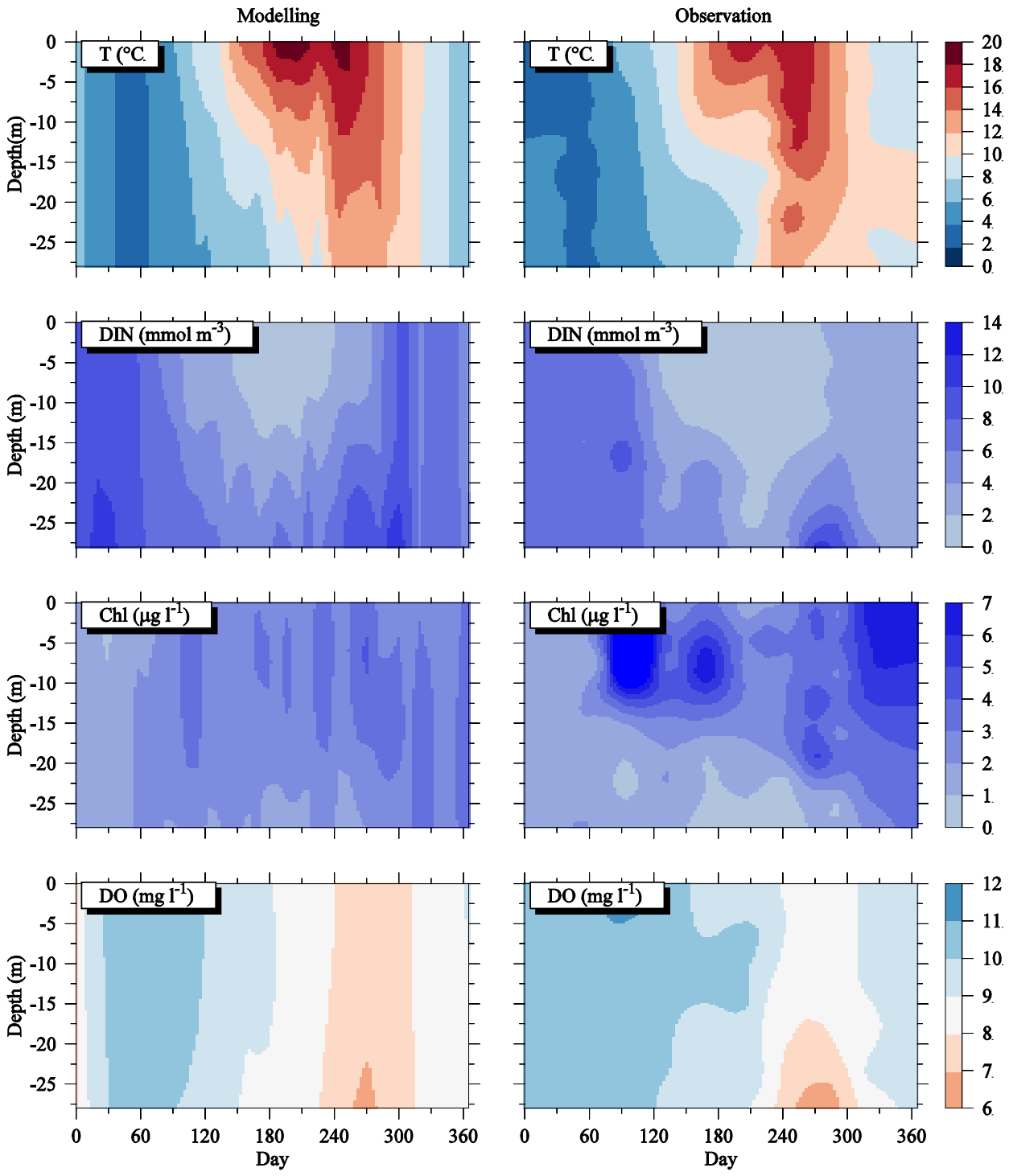

Figure 3. 39 Time-series of vertical distribution of modeled (left panels) and observed (right panels) key parameters (T, DIN, Chl and DO) in the water column at the near-field station N01 in 2010.

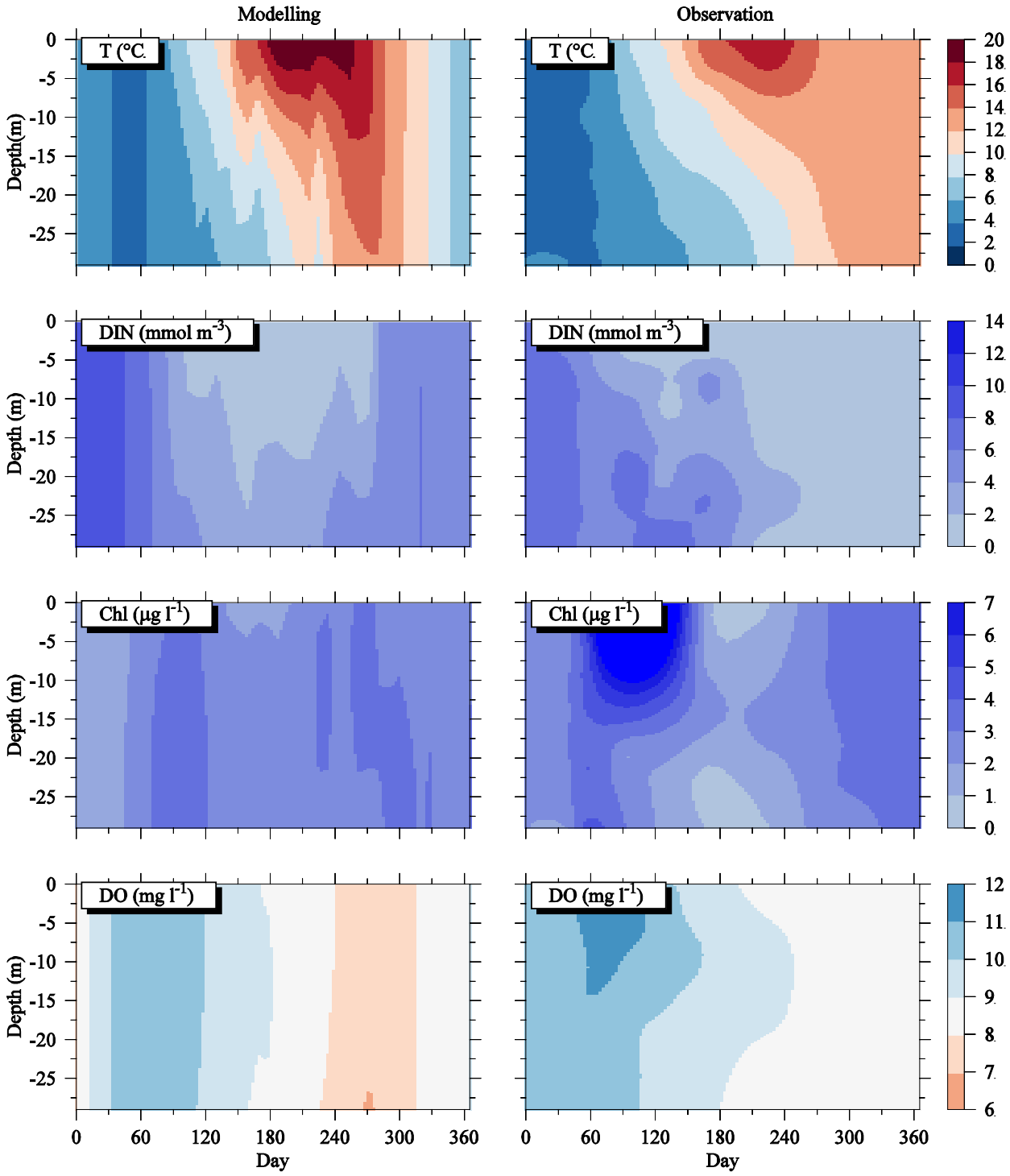

Figure 3. 40 Time-series of vertical distribution of modeled (left panels) and observed (right panels) key parameters (T, DIN, Chl and DO) in the water column at the far-field station F06 in 2010.

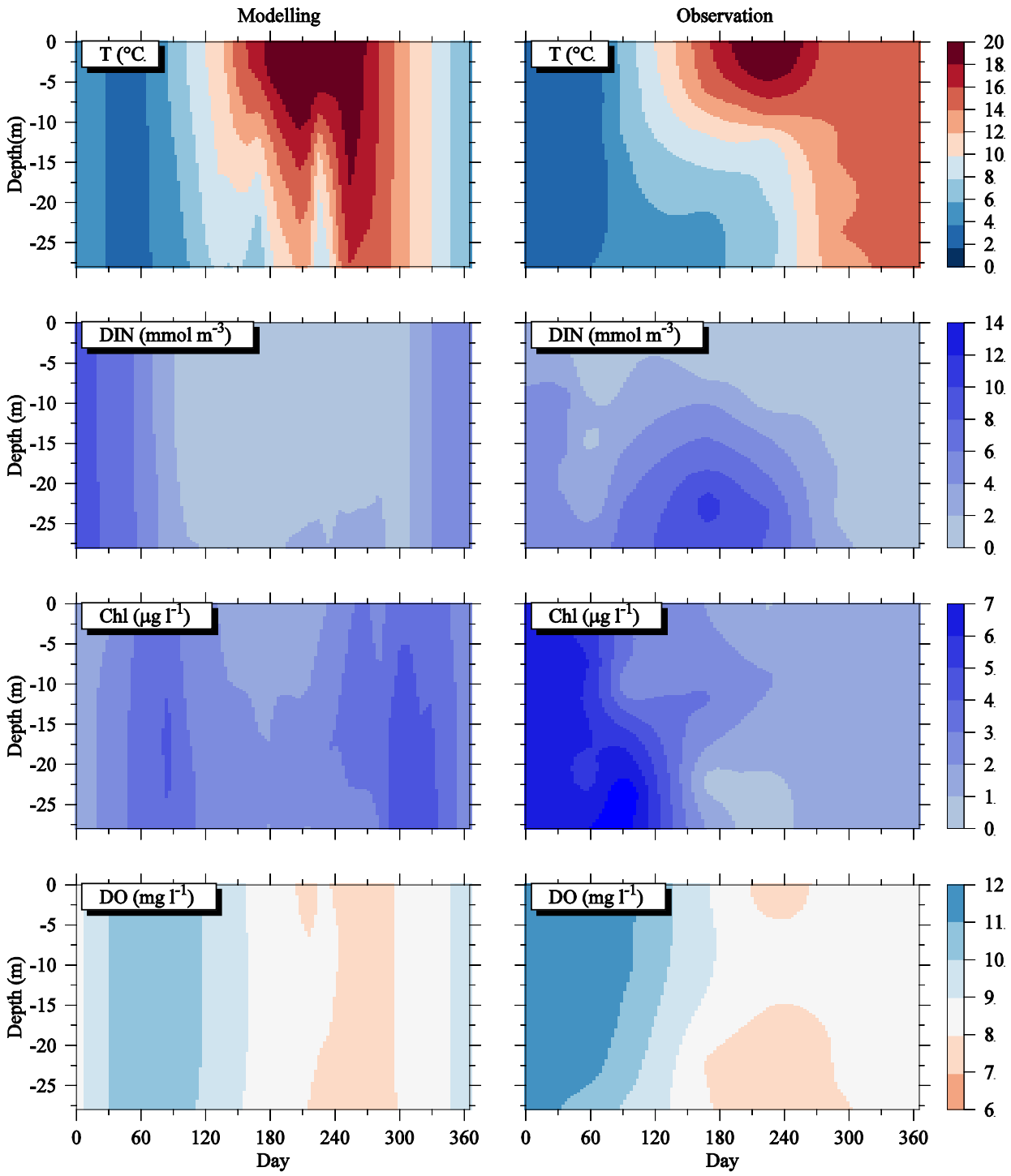

Figure 3. 41 Time-series of vertical distribution of modeled (left panels) and observed (right panels) key parameters (T, DIN, Chl and DO) in the water column at the far-field station F02 in 2010.

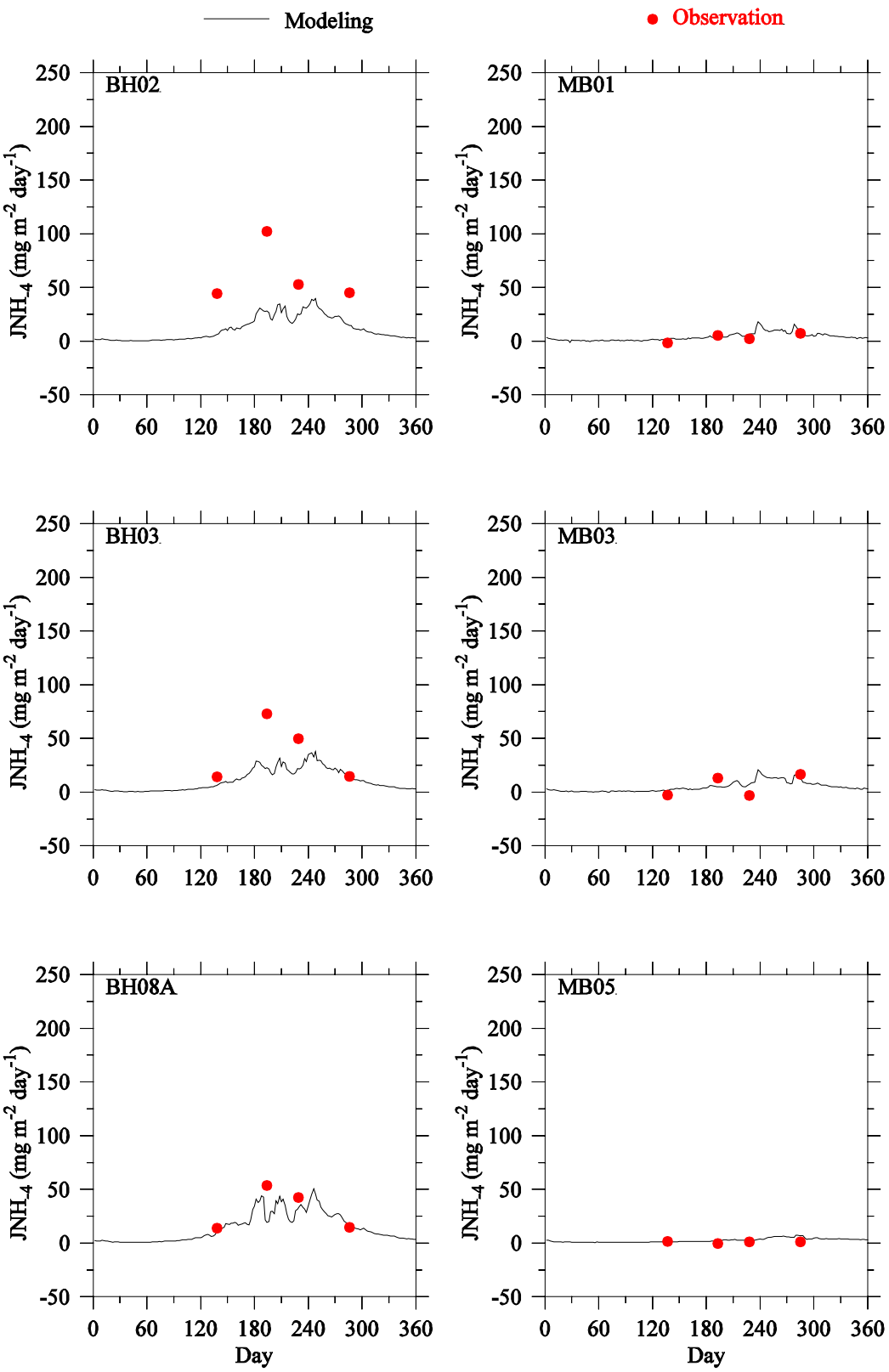

Figure 3. 42 Comparison of sediment NH_4^+ flux observed (dots) and modeled (lines) time-series in 2010.

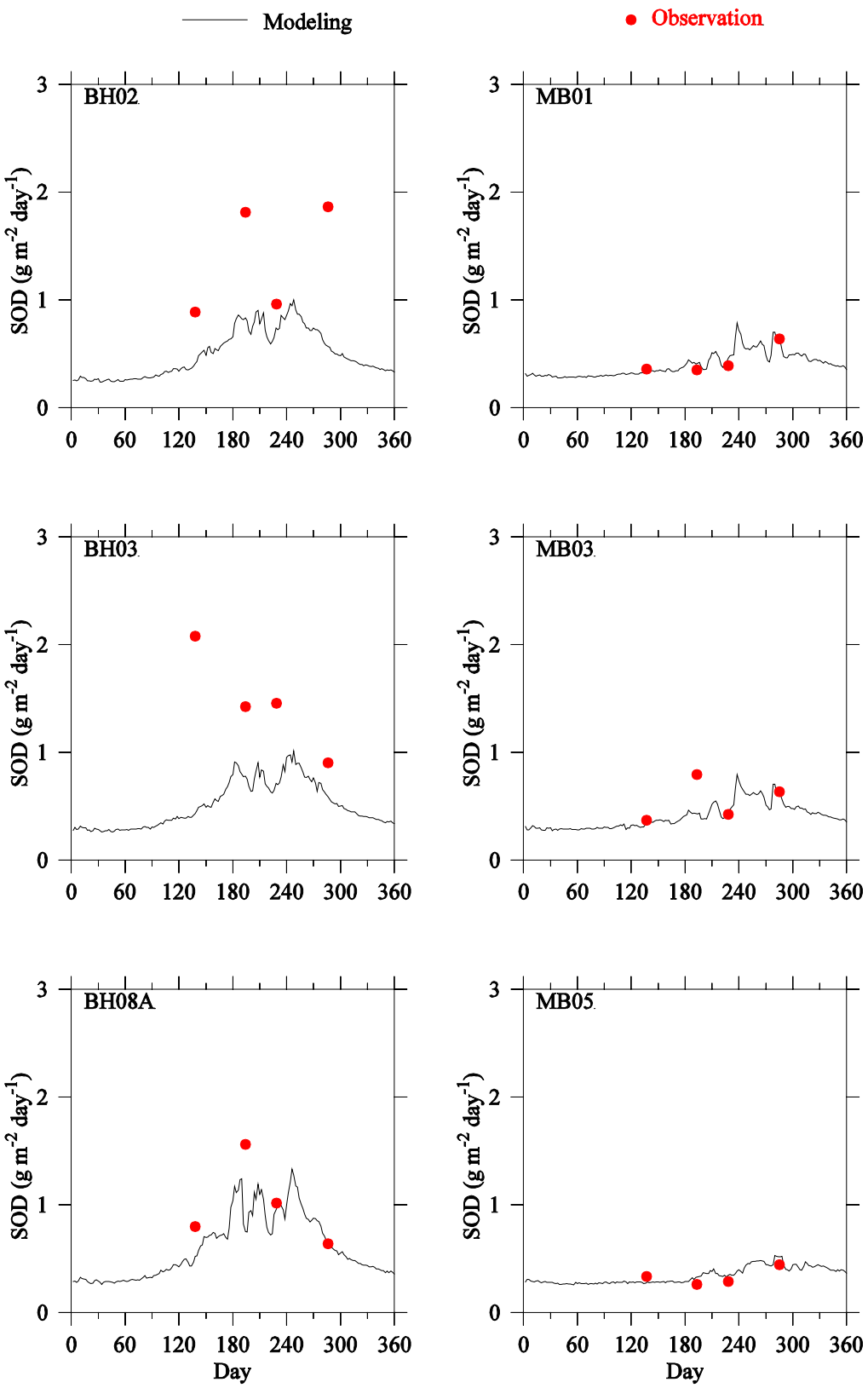

Figure 3. 43 Comparison of sediment oxygen demand observed (dots) and modeled (lines) time-series in 2010.

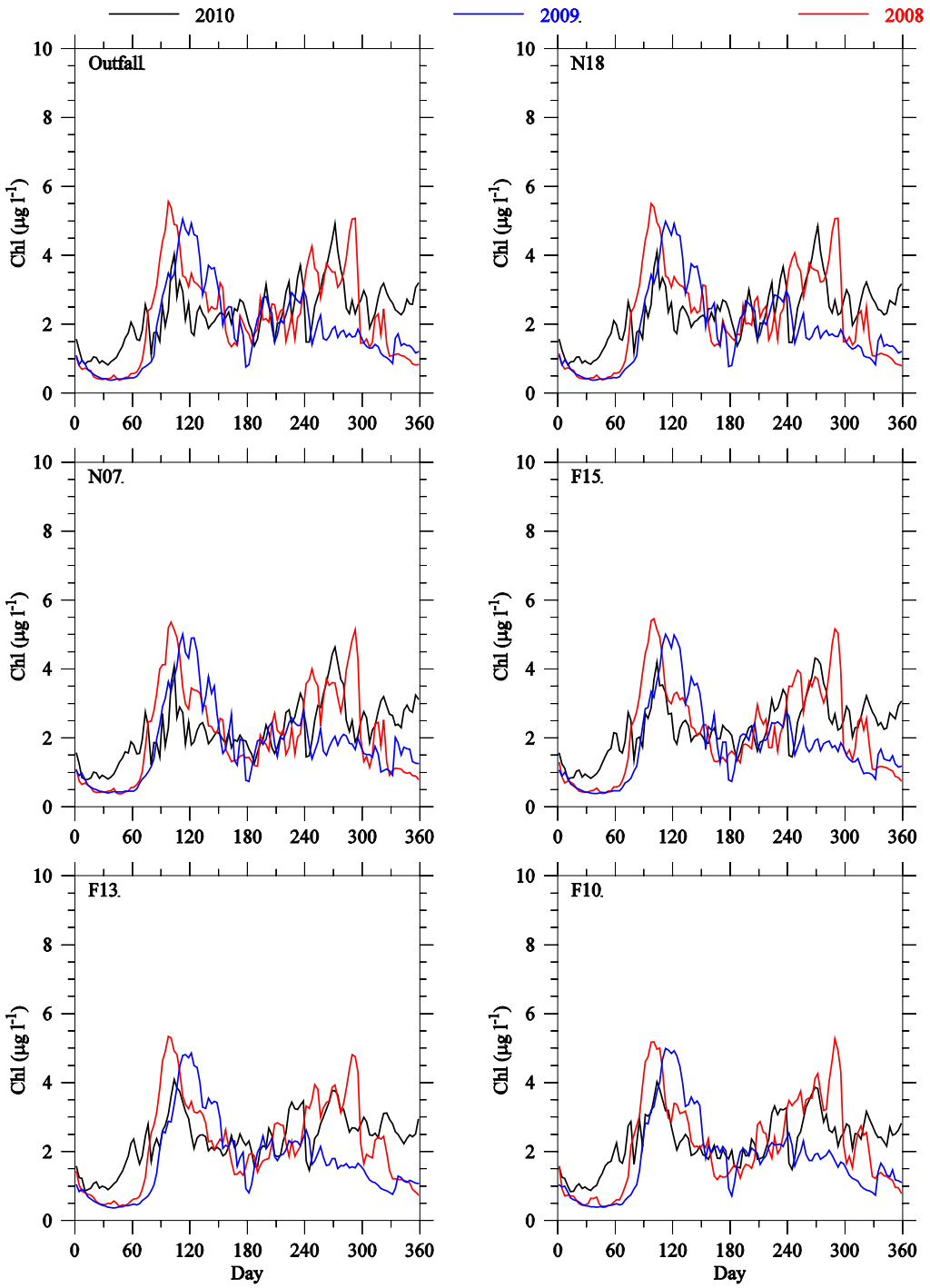

Figure 3. 44 Seasonal and interannual variations in surface chlorophyll concentration at the MWRA outfall site and Stations N18, N07, F15, F13 and F10 computed for 2008 (red lines), 2009 (blue lines) and 2010 (black lines).

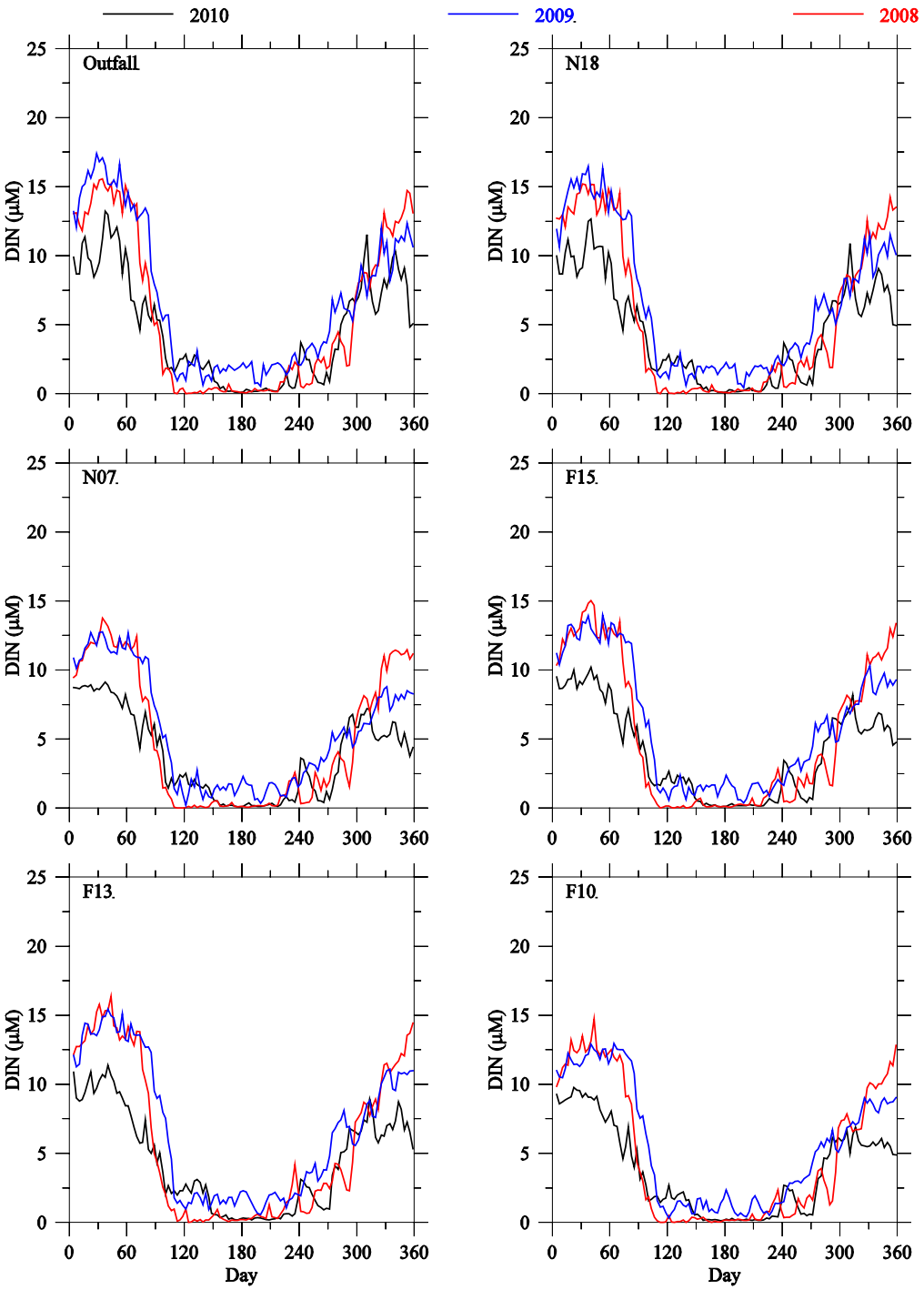

Figure 3. 45 Seasonal and interannual variations in surface DIN concentration at the MWRA outfall site and Stations N18, N07, F15, F13 and F10 computed for 2008 (red lines), 2009 (blue lines) and 2010 (black lines).

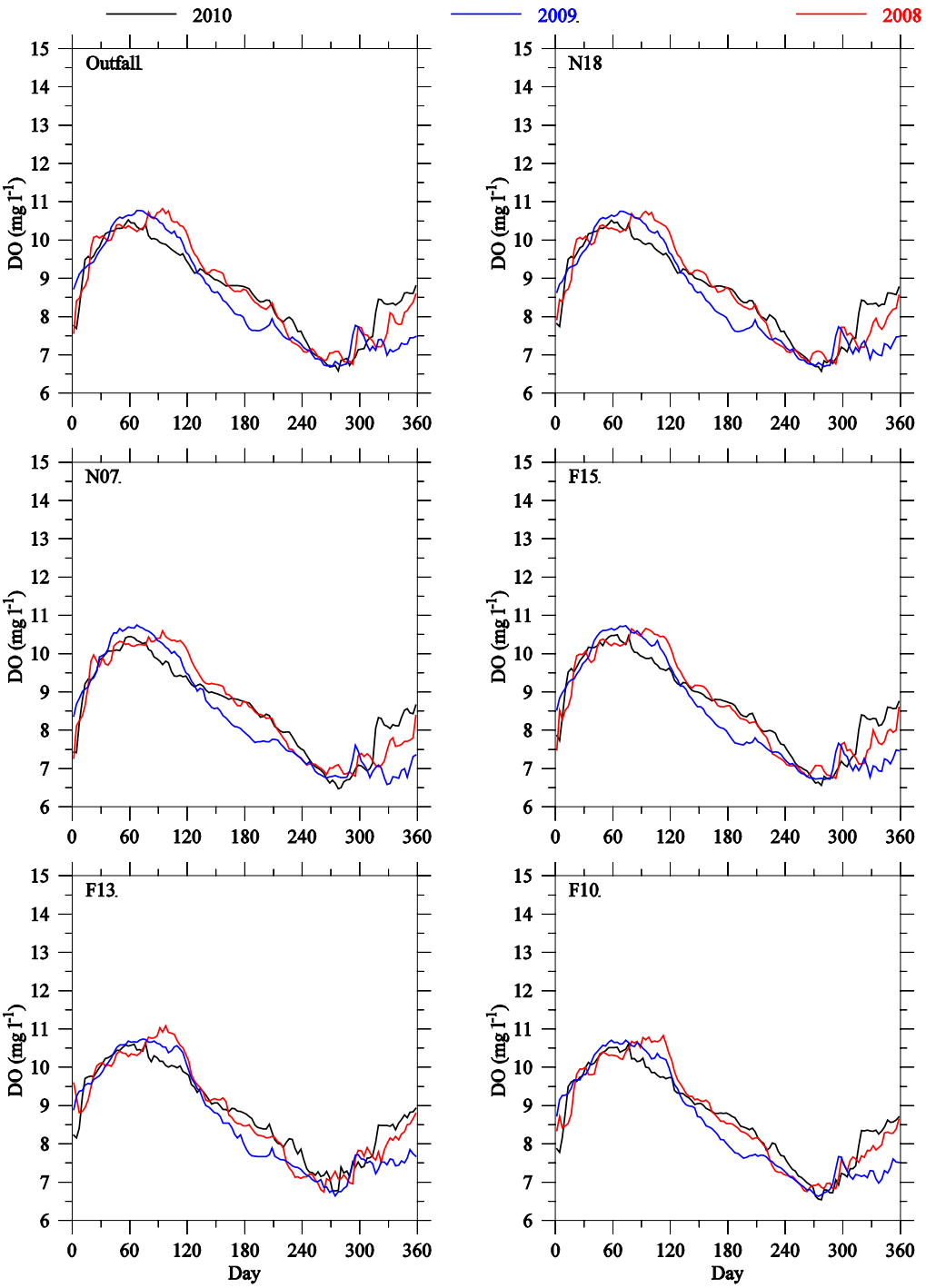

Figure 3. 46 Seasonal and interannual variations in bottom DO concentration at the MWRA outfall site and Stations N18, N07, F15, F13 and F10 computed for 2008 (red lines), 2009 (blue lines) and 2010 (black lines).

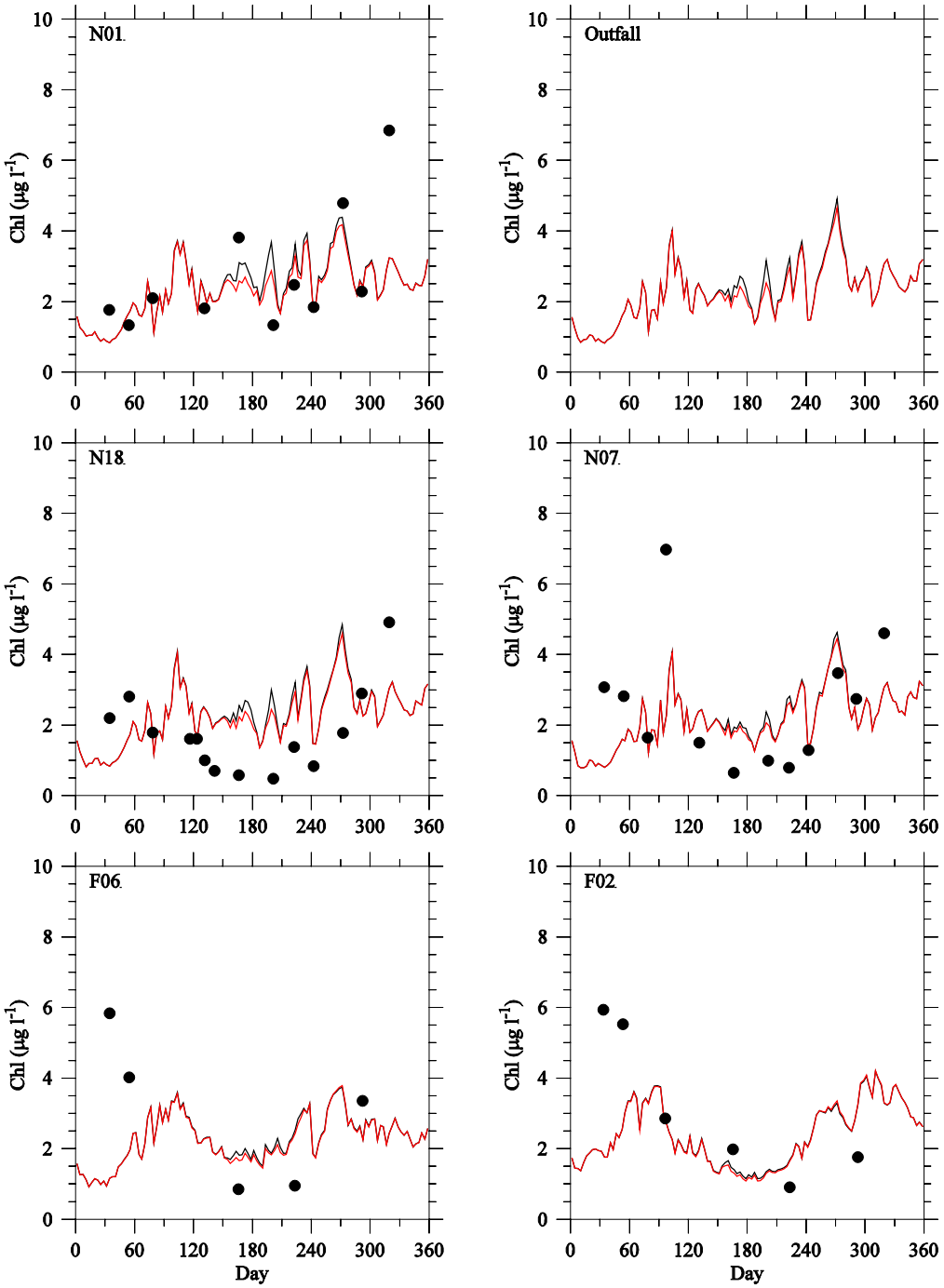

Figure 4. 1 Comparison of surface chlorophyll concentration between the Control (black) and Non-sewage (red) experiments at selected monitoring stations in 2010. Black dots show observed values.

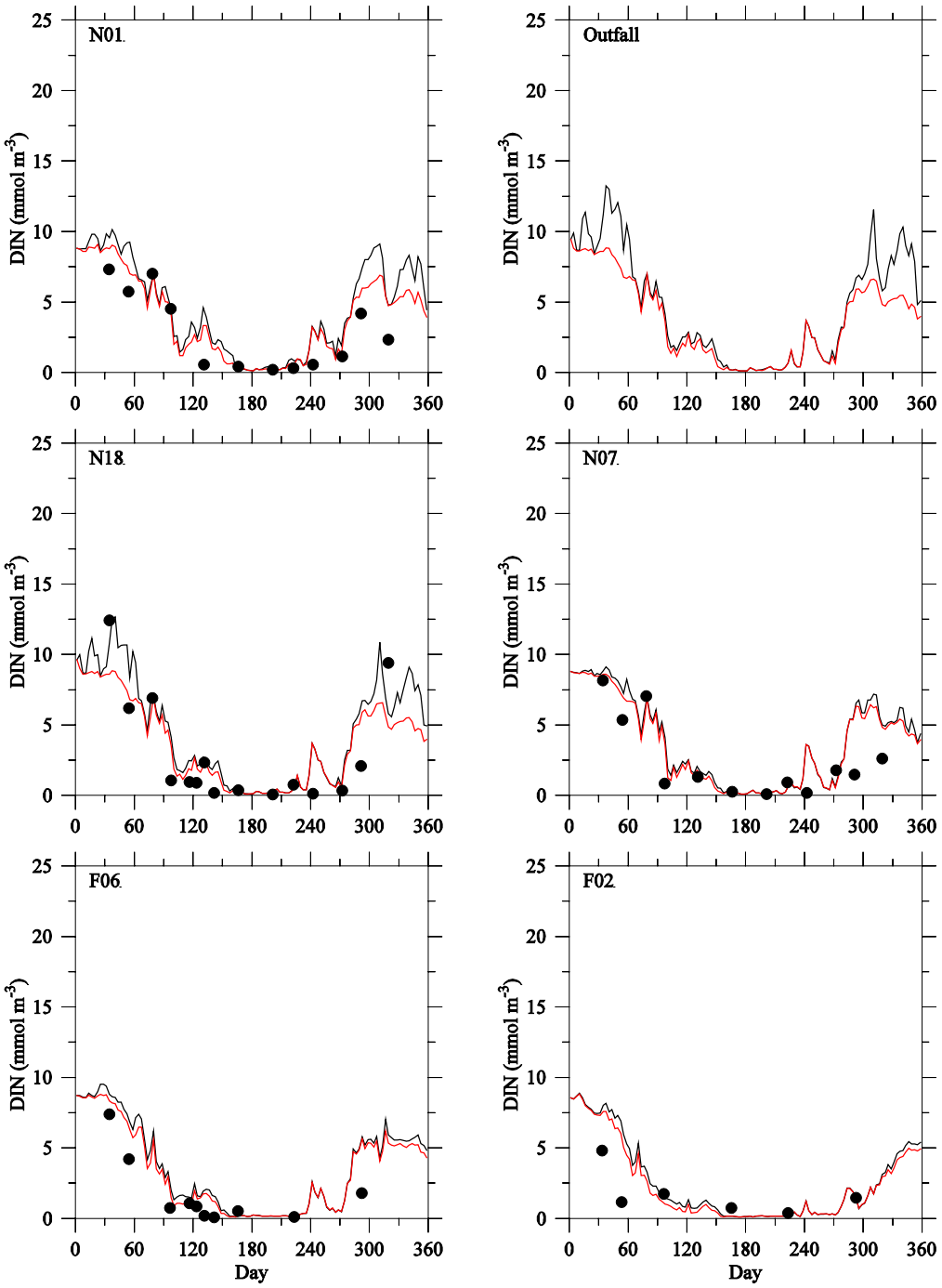

Figure 4. 2 Comparison of surface DIN concentration between the Control (black) and Non-sewage (red) experiments at selected monitoring stations in 2010.

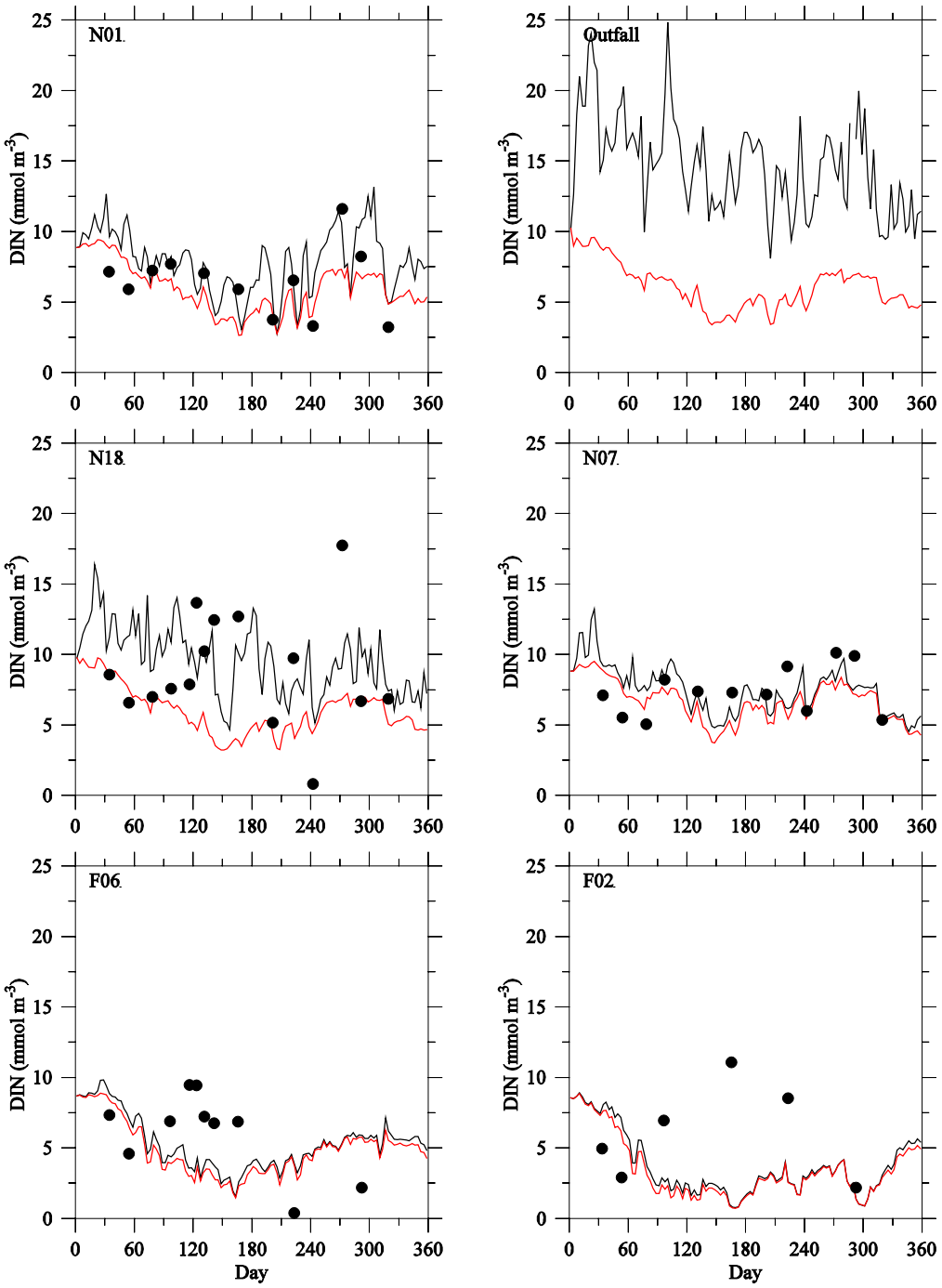

Figure 4. 3 Comparison of bottom DIN concentration between the Control (black) and Non-sewage (red) experiments at selected monitoring stations in 2010.

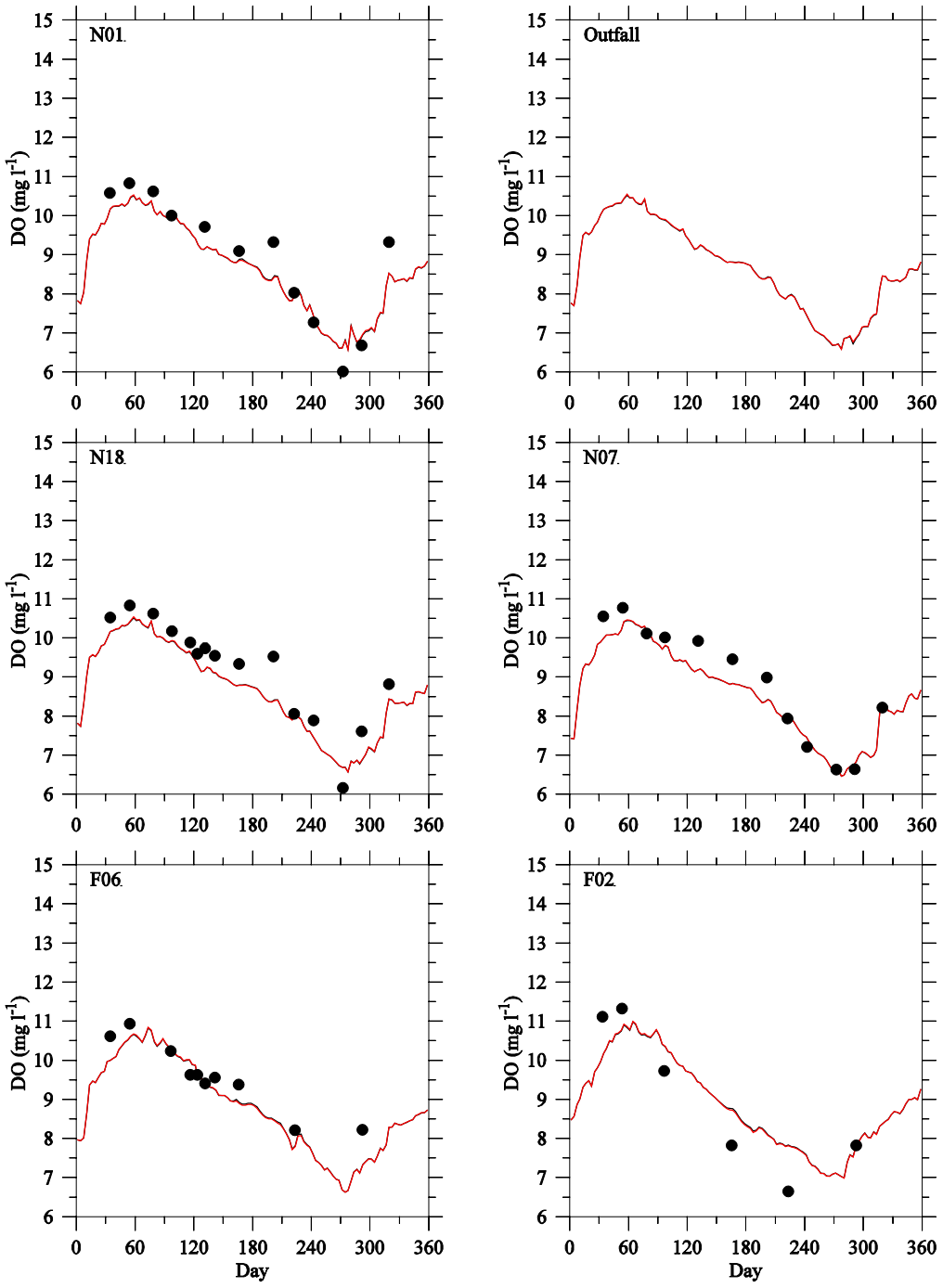

Figure 4. 4 Comparison of bottom dissolved oxygen concentration between the Control (black) and Non-sewage (red) experiments at selected monitoring stations in 2010.

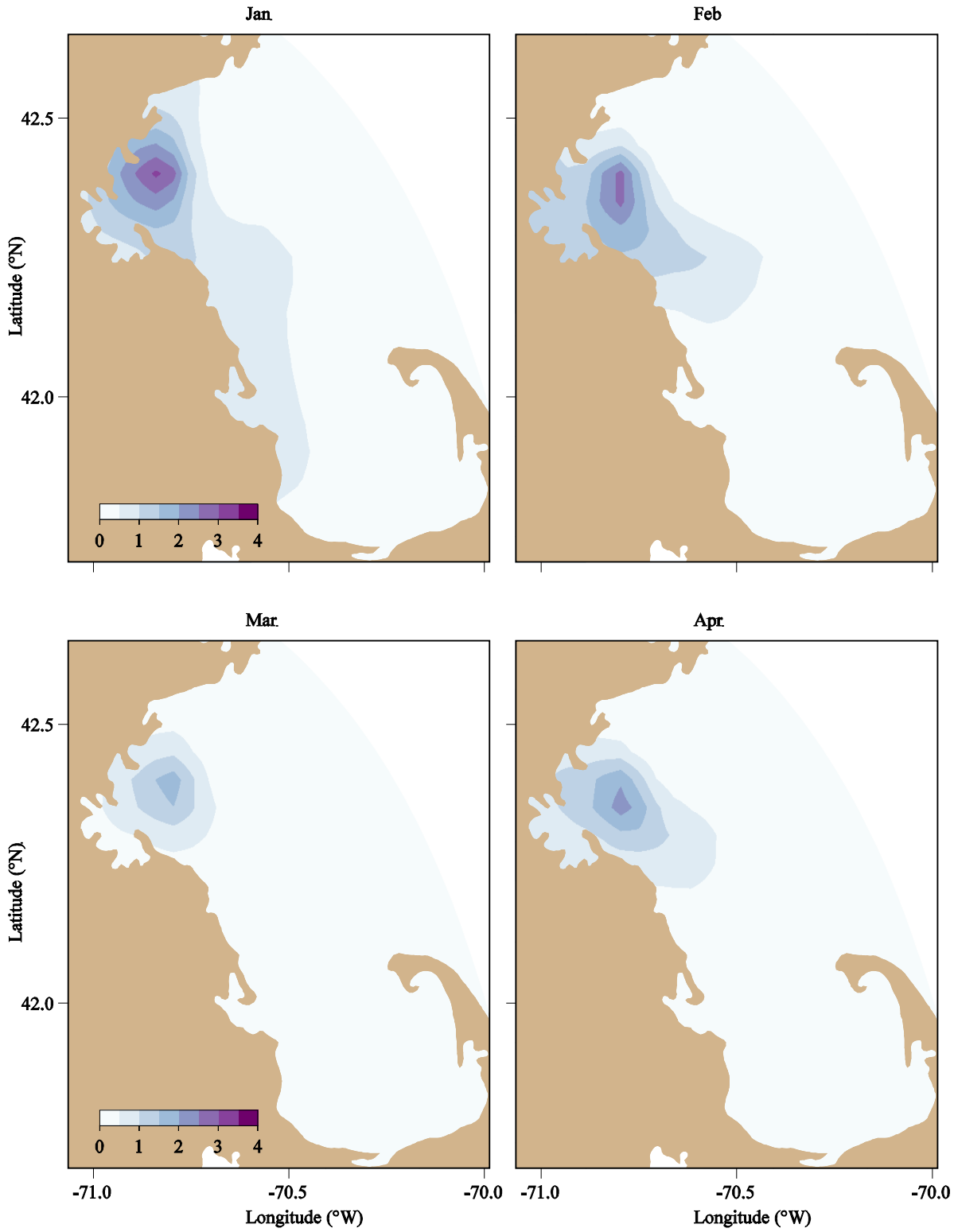

Figure 4. 5 Differences in bottom NH_4^+ concentrations (μM) at the end of January, February, March and April between the Control and Non-sewage experiments in 2010.

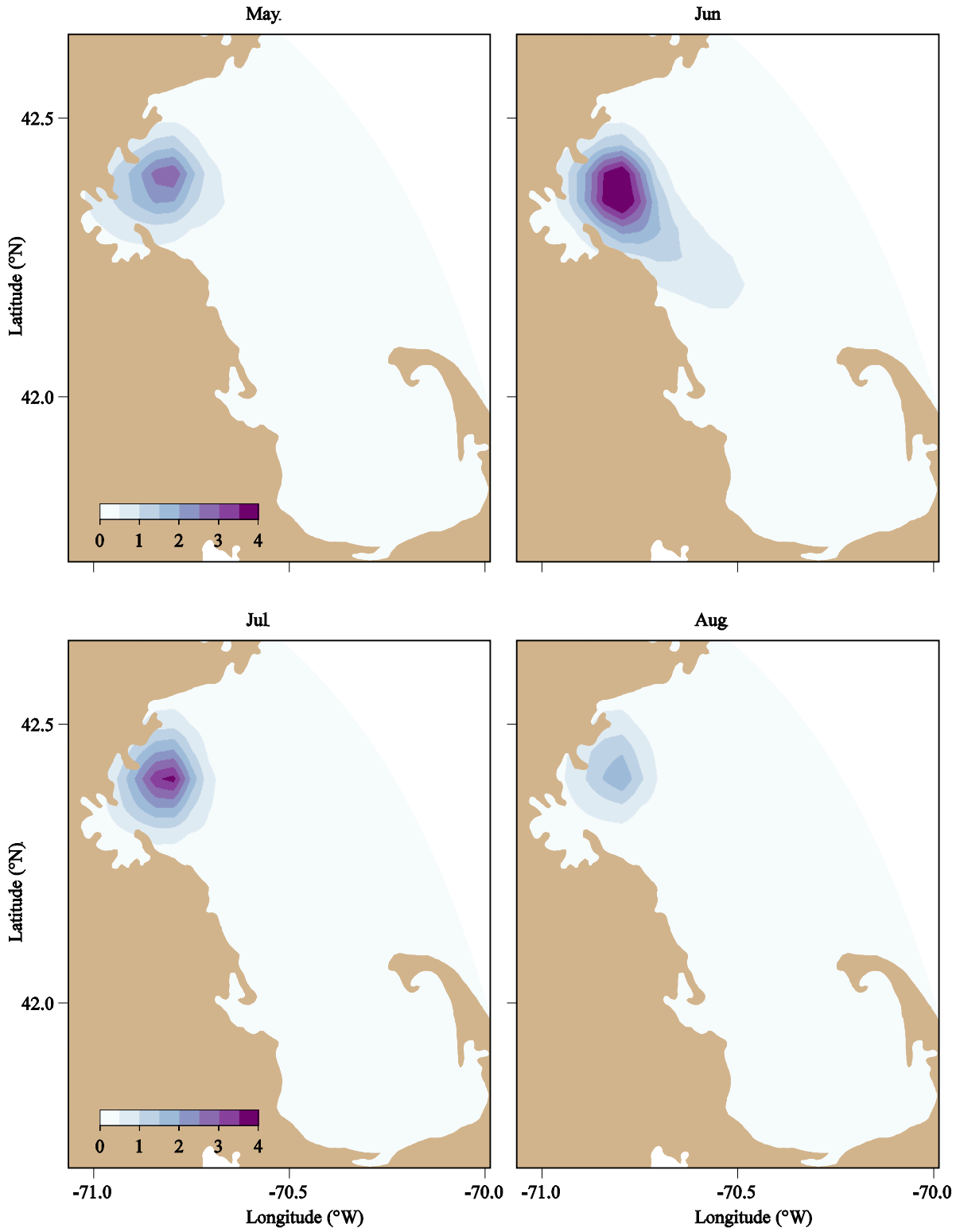

Figure 4. 6 Differences in bottom NH_4^+ concentrations (μM) at the end of May, June, July and August between the Control and Non-sewage experiments in 2010.

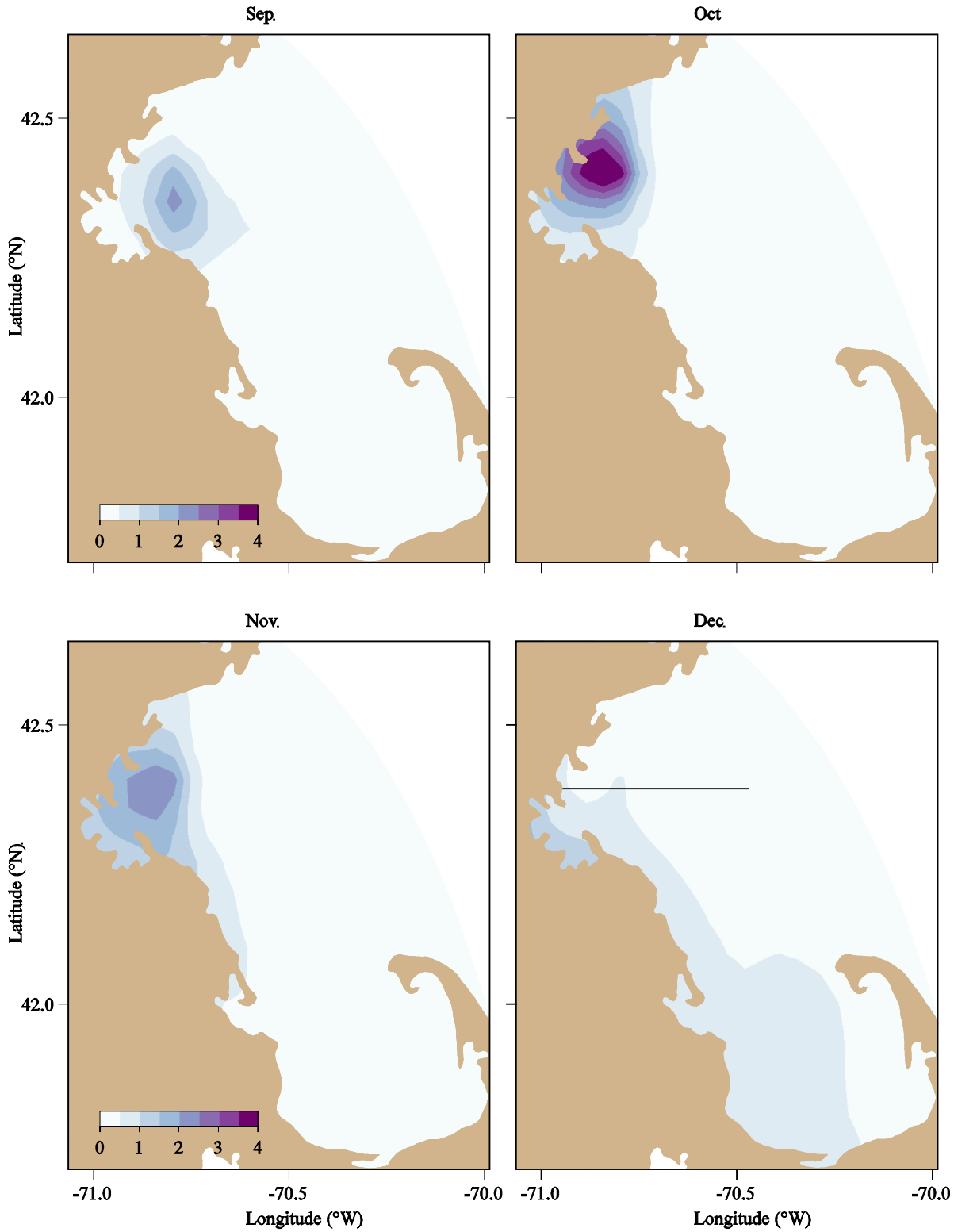

Figure 4. 7 Differences in bottom NH_4^+ concentrations (μM) at the end of September, October, November and December between the Control and Non-sewage experiments in 2010. Black line indicates the transect depicted in the following figures.

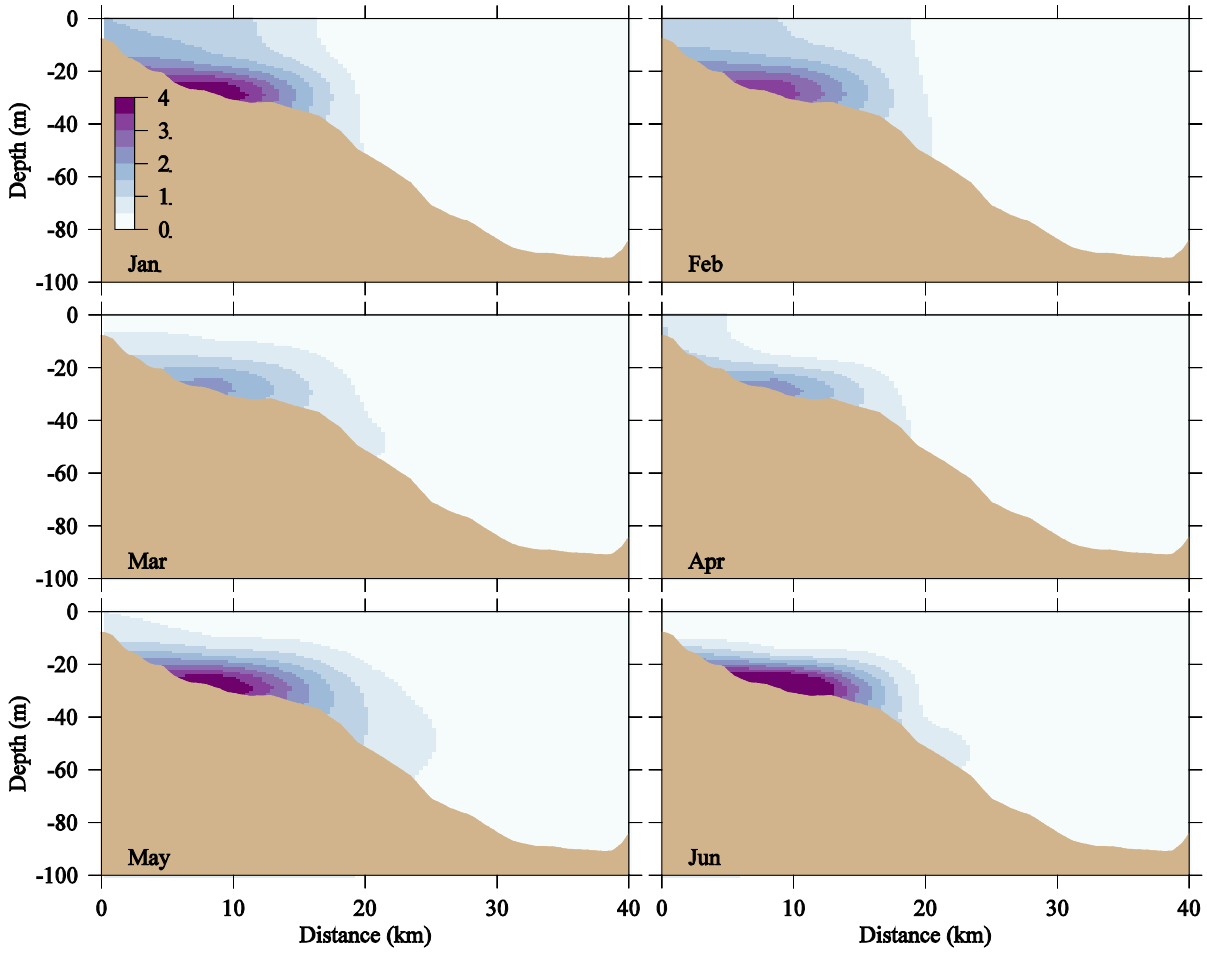

Figure 4. 8 Differences in NH_4^+ concentration (μM) on an east-west transect across the MWRA outfall at the end of each month from January through June between the Control and Non-sewage experiments in 2010.

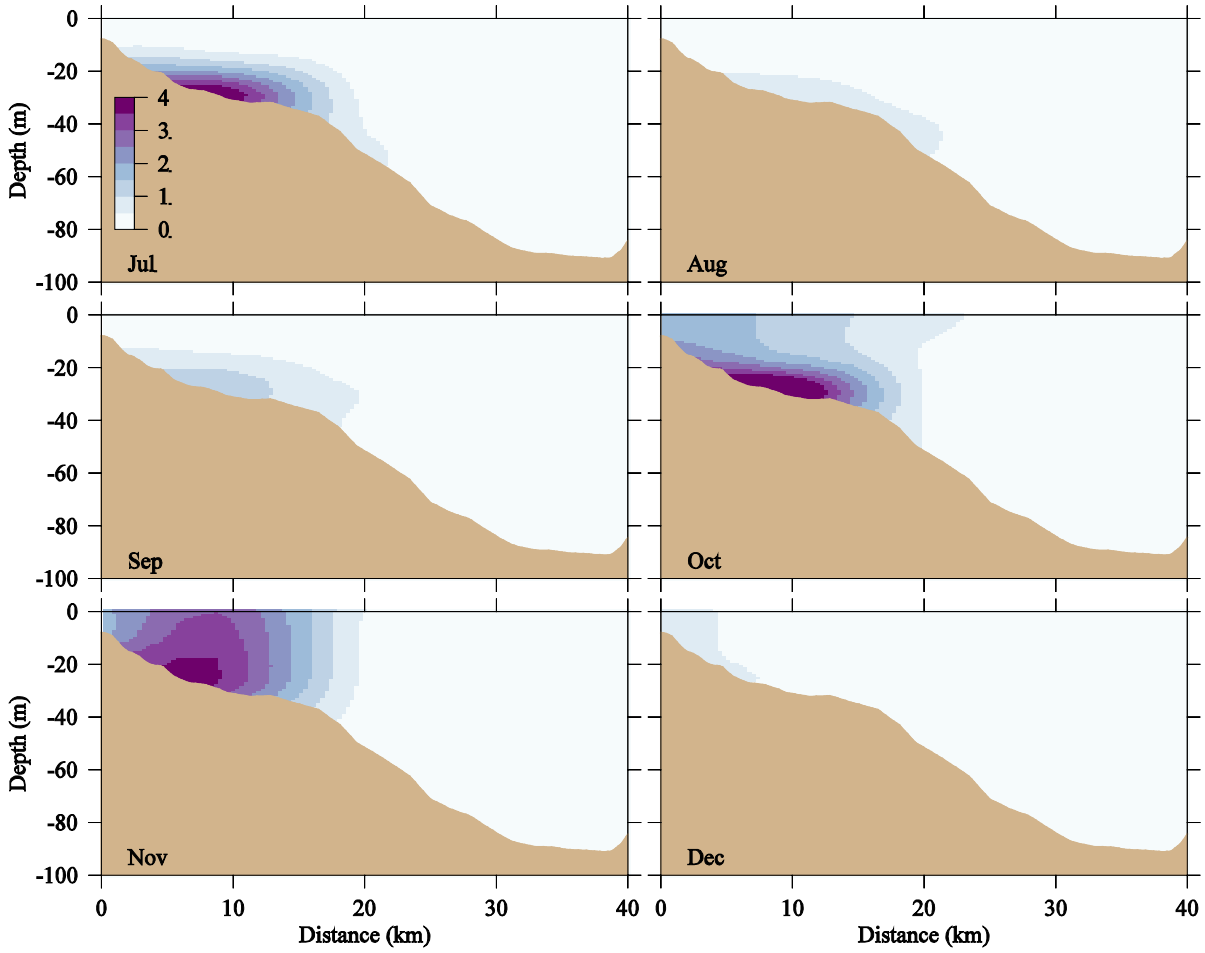

Figure 4. 9 Differences in NH_4^+ concentration (μM) on an east-west transect across the MWRA outfall at the end of each month from July through December between the Control and Non-sewage experiments in 2010.

Massachusetts Water Resources Authority
Charlestown Navy Yard
100 First Avenue
Boston, MA 02129
(617) 242-6000
http://www.mwra.state.ma.us